

Novel Thermal Energy Storage for Electric Power Generation

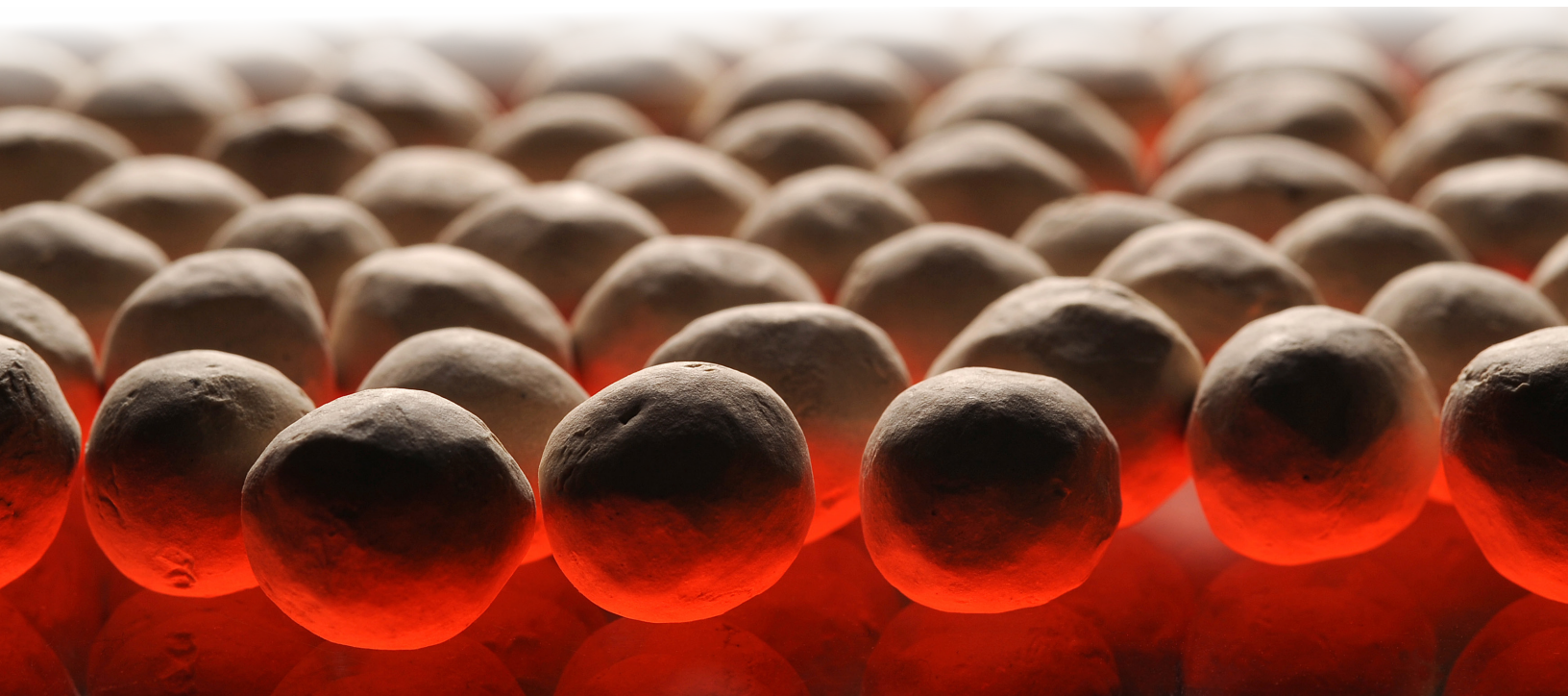
Master Thesis

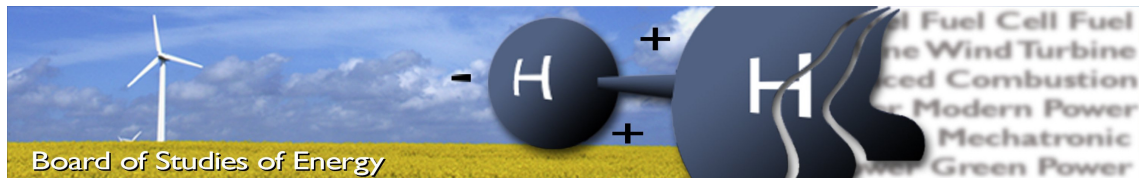
TEPE4-1003: Federico Lo Brutto, Oscar Miralles Pérez

10th Semester: M. Sc. Energy Engineering



AALBORG UNIVERSITY
DENMARK





Title: Novel Thermal Energy Storage for Electric Power Generation

Semester: 10nd Semester, Spring 2017

Project period: 02.02.2017 to 01.06.2017

ECTS: 30

Supervisors: Mads Pagh Nielsen & Søren Knudsen Kær

Project group: TEPE4-1003

Federico Lo Brutto

Oscar Miralles Pérez

SYNOPSIS:

This thesis investigates the feasibility of packed bed thermal energy storage charged by a heat pump, a high temperature electric heater, or a combination of the previous two. Two independent models are developed: one simulating the performance of charging and discharging unit, the other regarding the thermal storage. The system model is quasi-steady state and describes the different thermodynamic cycles occurring in the system. The storage model is a dynamic one-dimension two-phase heat transfer model with variable properties for the solid and the fluid phases. The simulation tool is exploited to evaluate the effect of different design parameters which affect the system operation. Segmentation of the storage and cycling effect are analysed. Finally, five possible configurations of the system with different settings and charging strategies are proposed and discussed.

Submission form: Electronic submission

Pages, total: 101

Supplements: Data (submitted together with report in Zip-folder)

By signing this document, each member of the group confirms that all group members have participated in the project work, and thereby all members are collectively liable for the contents of the report. Furthermore, all group members confirm that the report does not include plagiarism.

Preface

Novel thermal energy storage for electric power generation was developed between February 2017 and June 2017 by group TEPE4-1003 as a Master's thesis during the 10th semester of the study program of "*Thermal Energy and Process Engineering*" conducted at Aalborg University.

The softwares used for modelling and graphical data presentation are MATLAB R2016a and REFPROP. Attached files; MATLAB scripts and a PDF version of the report can be found for those of interest.

Sections, figures, equations and tables are referenced by chapter# .index# , e.g. section 5.2, figure 5.2, equation (5.2) and table 5.2.

The Harvard author-date referencing system has been used in the paper and the report. All the references used can be found in the bibliography.

The cover figure was published under (CC BY 3.0) licence "Photo: DLR, CC-BY 3.0", accessible at the website: <http://www.dlr.de/dlr/en/desktopdefault.aspx/tabid-10629#gallery/9256>

Reader Guidelines

Ahead of the report a nomenclature is given alphabetically. The nomenclature is divided into abbreviations, symbols and subscripts.

Throughout the report literary references are made using the Harvard method, so the sources are referred to as [Author, Year]. The used sources are listed alphabetically in the back of the report. All sources are listed by author, year and title. Additionally, edition and publisher are given for books, journals for papers and URLs for web pages. Furthermore, lists of figures and tables are given after the bibliography.

Equations, tables and figures are numbered related to the current chapter and in order of appearance.

Acknowledgements

Acknowledgements are addressed to supervisors Associate Professor Mads Pagh Nielsen and Professor Søren Knudsen Kær for their helpful supervision and advices.

Summary

The aim of this thesis is to investigate the feasibility of packed bed thermal energy storage charged by a heat pump, a high temperature electric heater, or a combination of the previous two.

In chapter 1, motivation to the thesis has been explained together with an introduction to the field and a brief explanation of the alternative storage technologies. The chapter is concluded with the problem formulation, limitations and methodology followed during this work.

Chapter 2 contains an exhaustive explanation of the TES system studied in this thesis. The system is divided into 3 essential parts, the charging unit, the storage itself and the discharging unit. The second part of the chapter lists the three main configurations explored during this work with their own peculiarities: HP-TES (heat pump only), EH-TS (electric heater) and HPEH-TES (combination of the previous).

In chapter 3 the simulation tool developed during the work is explained. In this chapter it is presented the system model with its assumptions for each configuration, which consists of the different charging units, the discharging unit, and all the links between them and the storage. The chapter is concluded by the block diagram representing the system model. After that, the core part of the simulation tool, the thermal storage model, is introduced and explained in chapter 4. The storage model is a dynamic one-dimension two-phase heat transfer model with variable properties for the solid and the fluid phases. First, a review of the main publication within the topic is presented, then all the main assumptions are introduced and discussed. After that, all the equations of the model are explained and the numerical strategy is exposed. The chapter is concluded again by the block diagram representing the storage model.

In chapter 5 the analysis of the obtained results from the simulation is carried out. First it is explained how the geometry of the TES is determined, then the parametric analysis of the complete system is presented. It is important to remember that all the figures shown in chapters 5 and 6 are referring only to the first configuration for the sake of brevity.

Chapter 6 contains the main results obtained from the simulation. Once again, it has been decided to differentiate the charging process from the discharging process. Subsequently, the investigation on the cycling effect and the segmented storage by means of the Sliding flow method are illustrated. After that, the results for each one of the three initial configurations are presented. Two additional options for the HPEH-TES configuration are discussed, for a total of five final configurations for the system.

Finally the thesis reaches its conclusion in chapter 7. The technological feasibility of the system has been proven thanks to the results obtained from the different simulations.

In chapter 8 the possibilities of an eventual future work are exposed.

Nomenclature

		Symbols
A	Surface/ cross section area	$[m^2]$
Bi	Biot number	[-]
c_p	Heat capacity of air at constant pressure	$[J\ kg^{-1}\ K^{-1}]$
c_s	Heat capacity of the solid	$[J\ kg^{-1}\ K^{-1}]$
D	Diameter of the storage	$[m]$
d	Particle diameter	$[m]$
E	Energy	$[J]$
f	fraction of energy flow	[-]
G	Mass flow rate per unit cross section	$[kg/m^2\ s]$
h_f	Specific enthalpy of the fluid	$[J/kg]$
h_p	Particle convective heat transfer coefficient	$[W/m^2\ K]$
h_v	Volumetric convective heat transfer coefficient	$[W/m^3\ K]$
h_{rv}	Void to void radiative heat transfer coefficient	$[W/m^2\ K]$
h_{rs}	Solid to solid radiative heat transfer coefficient	$[W/m^2\ K]$
k	Heat capacity ratio	[-]
k	Thermal conductivity	$[W/m\ K]$
k_{20}	Thermal conductivity at ambient temperature	$[W/m\ K]$
m	Mass	[kg]
\dot{m}	Mass flow rate	$[kg/s]$
L	Length of the storage	$[m]$
Nu	Nusselt number	[-]
p	Pressure	[Pa]
Pr	Prandtl number	[-]
Q	Heat	[J]
\dot{Q}	Heat rate	[W]
r	Radius	$[m]$

		Symbols
Re	Reynolds number	[-]
S	Entropy	[J/kgK]
T	Temperature	[K]
t	Time	[s]
U	Overall heat transfer coefficient	[W/m^2K]
u	Specific internal energy	[J/kg]
v	Interstitial fluid velocity	[m/s]
V	Volume	[m^3]
W	Power	[W]
x	Axial coordinate	[m]

Greek Symbols

α	Convective heat transfer coefficient	W/m^2K
β	Ratio of the average length between two close particles and the particle diameter	-
β	Function of tortuosity in Ergun-Wu's correlation	-
χ	Vapour quality	-
ε	Void fraction	-
ϵ	Emissivity	-
η	Efficiency	-
γ	Function of void fraction in Pfeffer's correlation	-
γ	Ratio of heat capacities	-
κ	Ratio of solid to fluid thermal conductivity	-
μ	Dynamic viscosity	kg/ms
ν	Poisson ratio	-
ϕ	Measure of the effective thickness of the fluid film	-
ρ	Density	[kg/m^3]
σ	Stefan-Boltzmann constant	W/m^2K^4
ϱ	Density	[kg/m^3]
τ	Tortuosity	-

			Subscripts
<i>comp</i>	Compressor		[-]
<i>comp, sys</i>	Compressor system		[-]
<i>el, el</i>	Electricity to electricity		[-]
<i>eff</i>	Effective		
<i>f</i>	Fluid		[-]
<i>id</i>	Ideal		[-]
<i>in</i>	Inlet		[-]
<i>isen</i>	Isentropic		[-]
<i>out</i>	Outlet		[-]
<i>p</i>	Particle		[-]
<i>Rk</i>	Rankine		[-]
<i>RT</i>	Round-trip		[-]
<i>poly</i>	Polytropic		[-]
<i>s</i>	Solid		[-]
<i>t</i>	Turbine		[-]
<i>Th</i>	Thermal		[-]
<i>tot</i>	Total		[-]
∞	Surrounding		[-]

Abbreviations

<i>ACAES</i>	Adiabatic Compressed Air Energy Storage
<i>CAES</i>	Compressed air energy storage
<i>CCGT</i>	Combined-Cycle Gas Turbines
<i>CES</i>	Cryogenic Energy Storage
<i>CFL</i>	Courant-Friedrichs-Lewy
<i>COP</i>	Coefficient Of Performance
<i>CSP</i>	Concentrated Solar Power
<i>DC</i>	District Cooling
<i>DH</i>	District Heating
<i>EH</i>	Electric Heater
<i>EH – TES</i>	Electric Heater-Thermal Energy Storage
<i>FDM</i>	Finite Difference Method
<i>HP</i>	Heat Pump
<i>HP – TES</i>	Heat Pump-Thermal Energy Storage
<i>HPEH – TES</i>	Heat Pump Electric Heater-Thermal Energy Storage
<i>HRSG</i>	Heat Recovery Steam Generator
<i>LMTD</i>	Log Mean Temperature Difference
<i>NTU</i>	Number of Transfer Units
<i>ORC</i>	Organic Rankine Cycle
<i>PCM</i>	Phase change materials
<i>PHS</i>	Pumped Hydroelectric Storage
<i>RE</i>	Renewable Energies
<i>RK</i>	Rankine Cycle
<i>SFM</i>	Sliding Flow Method
<i>SHS</i>	Sensible heat storage
<i>SMES</i>	Superconducting Magnetic Energy Storage
<i>TES</i>	Thermal Energy Storage
<i>TCS</i>	Thermochemical heat storage

Contents

1	Introduction	3
1.1	Motivation	3
1.1.1	Energy Storage Technologies	5
1.1.2	Role of the Energy Storage	6
1.2	Thermal energy storage (TES)	8
1.2.1	High Temperature Energy Storage (HT-TES)	9
1.3	Problem Statement	11
1.4	Methodology	12
1.5	Limitations	12
2	System Description	13
2.1	HT-TES System Description	13
2.1.1	Charging Unit	13
2.1.2	Discharging Unit	15
2.1.3	Thermal Energy Storage Unit	16
2.2	System Configurations	21
2.2.1	Configuration 1: HP-TES	21
2.2.2	Configuration 2: EH-TES	23
2.2.3	Configuration 3: HPEH-TES	24
3	System Modelling	27
3.1	Configuration 1: HP-TES	28
3.1.1	General Assumptions	28
3.1.2	Charging Unit: equations	28
3.1.3	Discharge Unit: equations	30
3.2	Configuration 2: EH-TES	35
3.2.1	Specific Assumptions	35
3.2.2	Charging Unit equations	35
3.3	Configuration 3: HPEH-TES	37
3.3.1	Specific Assumptions	37
3.4	System model: Block Diagram	39
4	Thermal Storage Model	41
4.1	Literature Review	41
4.2	Model assumptions	42
4.3	Mathematical equations	42
4.3.1	Heat transfer model and boundary conditions	42
4.3.2	Numerical resolution	45
4.3.3	Thermophysical properties	48
4.3.4	Physical correlations	50
4.4	Numeric assumptions	55

4.5	TES model: Block Diagram	56
4.6	TES model validation	58
4.6.1	Grid independence	60
4.6.2	Time resolution	62
4.6.3	Energy balance	62
4.6.4	Optimization of the computational time	63
5	Analysis and optimisation	65
5.1	Geometry of the TES	65
5.1.1	TES limitations	65
5.1.2	Particle size effect	68
5.1.3	Void fraction effect	68
5.1.4	TES cross section effect	69
5.2	System: Parametric Analysis	71
5.2.1	Charging unit maximum temperature	71
5.2.2	Discharging unit maximum temperature	73
5.2.3	Steam quality at the turbine outlet	75
6	Results and Discussion	77
6.1	Charging process	78
6.2	Discharging process	84
6.3	Cycling effect	89
6.4	Segmentation	91
6.5	Configuration results	95
6.5.1	Results HP-TES	95
6.5.2	Results EH-TES	95
6.5.3	Results HPEH-TES	96
6.6	Summary of the results	98
7	Conclusions	99
8	Future work	101
A	Appendix:A	103
A.1	The Effectiveness–NTU Method	103
A.2	Steam Rankine Cycle	104
A.3	Balanced HPEH-TES configuration	107
A.4	Quick-charge HPEH-TES configuration	109
	Bibliography	109
	List of Figures	114
	List of Tables	116

become 100% fossil free by 2050 [Renewable Energy Policy Network for the 21st Century (REN21), 2015].

In order to achieve a higher integration of RE in the energy mix, it is essential that suitable energy storage technologies are implemented, enabling the storage in case of excess of production and releasing it when needed. Thus, a grid storage system would reduce the loss of potential energy produced by renewable energies that could not be possible to make use of due to the mismatch between production and consumption. Grid-scale energy storage is widely believed to have the potential to provide this added flexibility [A.Castillo and Gayme, 2014]. Furthermore, the buffer of energy could reduce the maximum daily energy peak which only last for a reduced number of hours. Traditional power plants were designed to achieve that high power production which led to over-sized systems, designed to operate at a steady state and characterised by a low operational flexibility. The energy storage could offer an increased efficiency working closer to the design operating point with a lower production fluctuation [T.N.Cong et al., 2009].

From the market point of view, the high variability of the renewable production combined with the low flexibility of the large power plants could be responsible of price fluctuations in the spot market. For example, in the Danish Elspot area, the prices were negative respectively for 39 and 30 hours in 2013 for the two price areas, due to a very high wind power production. That production fluctuation can produce the opposite effect, as happened for two hours on June 7th where reached the technical maximum curtailment price on Nord Pool Spot of 2000 euro/MWh, as coincidence of the revision on power plants, the grid maintenance and low wind power production [E.Larsson et al., 2014].

The energy storage technologies can be classified into two main categories as function of the technical services that they can provide, power and energy services, based on the time-frame of supply [A.Castillo and Gayme, 2014]. For short term services, energy storage systems could increase the grid performance including grid stabilisation, grid operational support, stable power quality, reliability and load shifting [A.Evans et al., 2012]. When it is referred to energy services, the main objective is to provide bulk energy for prolonged periods [A.Castillo and Gayme, 2014]. Despite that some energy storage technologies can reach high powers on the range of tens of megawatts, the only technologies that have been able to deliver high power during extended number of hours are hydroelectric energy and compressed air energy storage. The other technologies have as main purpose to reinforce the grid stability and thus are operating mainly during short periods of time [M.Morandin et al., 2011]. Until 2009 the total storage capacity was basically concentrated in four main technologies (sodium sulphur batteries, pumped hydro energy storage, compressed air energy storage, and thermal energy storage) with a total installed capacity of 100MW [P.Denholt et al., 2010].

1.1.1 Energy Storage Technologies

The different energy storage technologies can be classified as function of the physical or chemical working principle [P.Taylor et al., 2012]:

- **Mechanical:**

- **Pumped Hydroelectric Storage (PHS):** Technology based on storing potential energy by operating a turbine or a generator in reversed mode to pump water from the lower reservoir to the higher one taking advantage of low-energy cost. Water is later released in order to generate back electricity to the grid passing through the turbine. In the United States, the installation capacity power ranges stand between 50MW to 2100MW with a total installed capacity around 20GW. The PHS plants can achieve a round-trip efficiency greater than 75%, and a discharge period longer than 20 hours [P.Denholm et al., 2010].
- **Compressed Air Energy Storage (CAES):** This technology is based on the storage of energy as compressed air into a airtight underground cavern by the use a electric-driven compressor. In order to recover the energy, the air is expanded through a turbine and heated up by an additional combustion. CAES system is considered an hybrid system since requires the use of supplementary combustion to perform the discharging. The energy ratio of the system ranges between 60-80% [P.Denholm et al., 2010].
- **Flywheel:** System consisting of a motor/generator attached to a large rotating mass. When there is an excess of energy it is stored as kinetic energy by increasing the spinning velocity, and extracted by working as a generator [P.Denholm et al., 2010].

- **Electromechanical:**

- **Batteries(Nickel, Lithium-Ion, lead-acid, metal-air and sodium-sulphur chemistries):** Technology based on chemical reactions for the electrical energy storage. They are designed to be able to provide a very fast response. This technology is limited to low power applications which make it suitable for short term grid services. The main disadvantage is the short system lifetime with a limited number of cycles [P.Taylor et al., 2012].
- **Flow Batteries:** Differs form batteries as the chemical reaction takes place in a reaction chamber and the electrolyte is stored in external tanks. In that case, power and energy are independent variables, which enables modular systems. Different chemistries are under development e.g. vanadium redox and zinc-bromine [P.Taylor et al., 2012].
- **Fuel Cells:** Technology based on hydrogen as storage vector. Different stages of the hydrogen production and conversion to electricity are under development [P.Taylor et al., 2012].

- **Electrical:**

- **Superconducting Magnetic Energy Storage (SMES):** Stores energy in a superconducting coil in the form of a magnetic field. This technology is characterised by a fast response, which makes it suitable for grid stabilisation [P.Taylor et al., 2012].
- **Electric-double Layer Capacitors (Supercapacitors):** This system is able to store electricity in an electric charge. This technology have the fastest

time response of any store technology, therefore it is used in power quality applications [P.Denholm et al., 2010].

- **Thermal:**

- **Cryogenic Energy Storage (CES):** New technology based on liquefying air or nitrogen at low temperatures to be recovered afterwards by expansion through a turbine. This technology is under developments, and is meant to provide off-peak applications [P.Taylor et al., 2012].
- **Thermal energy storage(TES):** This category includes different technologies according to the application. For heating services such as low temperature storage in water tanks, or high temperature molten salts for thermal storage in Concentrated Solar Power (CSP). The technology is based on the store of energy as heat taking advantage of low-cost materials. It can be used afterwards directly for heat supply or to be converted into electricity by a thermodynamic cycle [Al.S.Pedersen et al., 2014].

1.1.2 Role of the Energy Storage

The different storage technologies can offer various services according to the power and energy storage capacity [P.Denholm et al., 2010]. Thus, each of the them can provide diverse operating features to the system operation. They can mainly be classified in three different applications as function of the length of discharge as shown in figure 1.2:

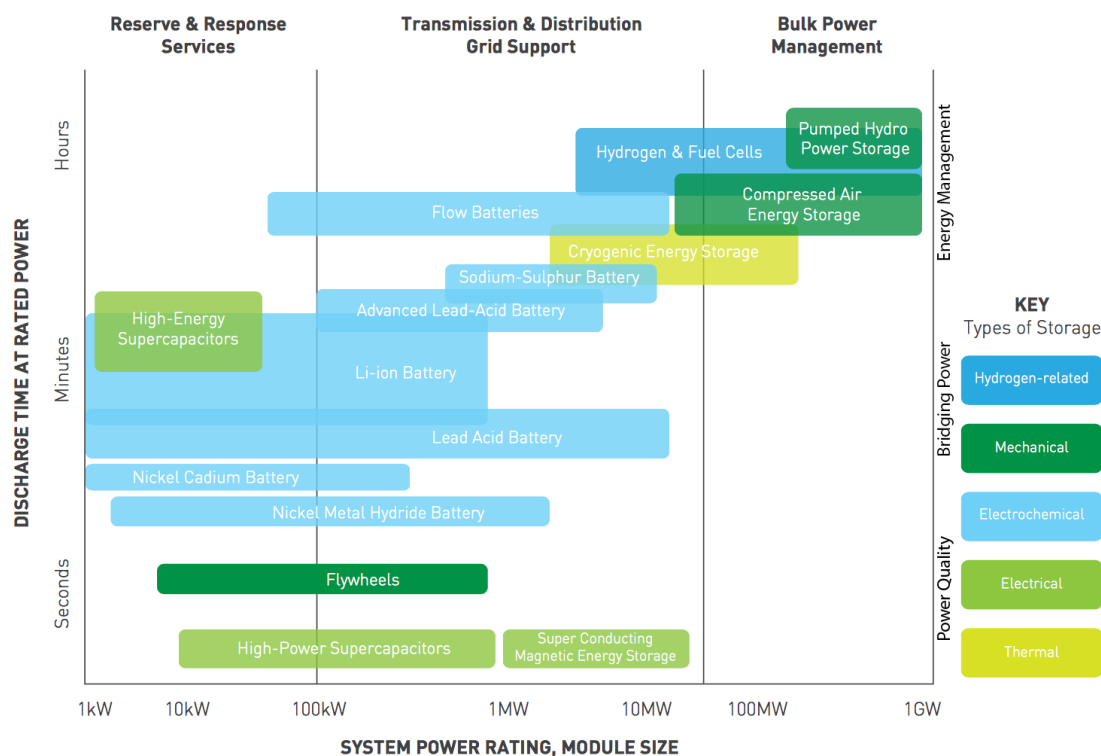


Figure 1.2. Energy storage technologies comparison (modified) [P.Taylor et al., 2012]

- **Power quality:** The main application is the transient stabilization and the frequency control. The discharge time ranges between seconds to minutes.

- **Bridging Power:** The objective is to provide contingency reserves and ramping. The required discharge time is in the order of minutes to 1 hour.
- **Energy management:** Requires larger capacities, operating for load levelling, firm capacity and T&D deferral. In that case, the discharge time required is in the order of hours.

The grid-scale energy storage can be classified in seventeen different grid applications, which can be grouped in five main services, according to [J.Eyer and G.Corey, 2010]:

- **Electricity supply:** One of the most remunerative applications is time-shifting, which is based on the acquisition of energy at low price, to charge the storage plant so the energy can be sold again when the price is higher. This technology can supply energy for peak demands avoiding others traditional peak plants installation.
- **Ancillary services:** In order to be able to maintain the grid stability, the electrical production and consumption has to be matched locally and globally as well. Therefore, the grid has to be controlled in order to ensure the proper grid operation. The main functions are load following, area regulation, electric supply reserve capacity and voltage support. In particular for area regulation, the energy storage systems can play a key role. The most suitable technology to offer ancillary services are those which are able to supply power instantaneously for short periods of time.
- **Grid system:** Equivalently, the implementation of a storage system can offer support to the Transmission and Distribution network, reducing the load and buffering the energy transmission when the system is congested. Therefore, it can offer a cheaper solution to uniform the energy transmission when, for instance, there is a large amount of renewable energy supply.
- **End user/Utility consumer:** From the consumer side of the electric network, the storage technology can provide a mayor flexibility degree allowing the intra-day peak demand reduction, which leads to a decrease of the overall electricity service. Furthermore, it would increase the power quality supply and reliability protecting against on-site short-duration events.
- **Renewables integration:** The unpredictable character of renewable energies makes necessary to implement modifications of the grid operation strategies in order to deal with the changing energy power supply. The storage of bulk energy in large systems would allow the integration of renewable energies, which now is limited to the grid management. In the same way, the energy storage would avoid the loss of renewable energy potential that at that moment can not be used, due to the overcome of the actual consumption. Therefore, the most suitable technologies for that purpose are the ones which allow the store of large amounts of bulk energy, such as hydroelectric energy or compressed air energy storage.

1.2 Thermal energy storage (TES)

This project focus on the energy storage in a thermal form, therefore the different technologies based on this principle are going to be further investigated.

Heat demand accounts for the 50% of the worldwide energy consumption. In the Danish context it accounts for half of the energy consumption as well, while in the case of Germany, 85% of the household heat demand is used for space heating and sanity water heating [Al.S.Pedersen et al., 2014]. Thus heating plays a dominant role in the energy supply chain. Thermal energy storage will become a key technology for efficient generation, supplying hot or cold utilities, which do not match in time nor space [Al.S.Pedersen et al., 2014].

Thermal energy can be supplied at different range of temperature and power levels, depending on the requirements. For that exist different technologies that allow the conversion and recover of heat back to electricity. The different thermal energy storage can be classified in three main categories as function of the storage mechanism [Al.S.Pedersen et al., 2014]:

- **Sensible heat storage (SHS):** The energy is stored as sensible heat, by means of increasing the material temperature by the addition of heat. In this way, the heat stored depends on the heat capacity of the material and the storage insulation. This technology is well known from hot water tanks for district heating applications and household heating.
- **Phase change materials (PCM):** Storing heat in phase change materials implies a change of phase by the addition of heat. The phase change is associated with a heat of transformation, in which energy is absorbed or realised at constant temperature. This is known as latent heat and provide some advantages such as a higher energy density and isothermal heat transfer process.
- **Thermochemical heat storage (TCS):** The heat is stored in a reversible chemical process involving a change of enthalpy. A practical example is the use of metal hydride that dissociate the hydride when heat is required, as it constitutes an endothermic reaction.

According to the temperature range and power, three main conversion technologies exist in which the electricity can be converted into thermal energy (cooling/heating), or can be converted back into electricity by means of a thermodynamic cycle [Al.S.Pedersen et al., 2014].

- **Electricity to heat:** e.g. heat pumps (HP) and electric resistant heating
- **Electricity to cooling:** e.g. refrigeration
- **Heat to electricity:** e.g. Rankine (RK) and Organic Rankine Cycles (ORC)

As mentioned before, thermal energy is mainly applied for heating purposes, such as district heating and cooling. Nevertheless, different technologies have been developed in order to provide flexibility to different power systems as well as in order to increase the efficiency of existing technologies. Some examples of the application of Thermal Energy Storage systems for power applications are the followings:

- **Thermal storage in Concentrated Solar Power (CSP):** Thermal energy storage has been applied in CSP technology in order to extend the energy production and decouple the electrical production from the isolation hours. It is normally based in two-tank molten salt storage, with phase change material. For instance, in order to provide 50MW during approximately 8 hours it would be necessary around 30000 t of molten salts. [Schneider and Maier, 2014]
- **Application in Adiabatic Compressed Air Energy Storage (ACAES):** Compressed air energy storage is a variant of basic gas turbine technology. On the existing CAES is produced a waste heat as by-product of the compression of the air during charging. When discharging, the high-pressure stored air is released and expanded in the turbine. As previously explained in section 1.1.1, it is required the combustion of a fuel in order to increase the work of the turbine. In order to avoid the use of fossil fuels and make the system more efficient, the TES can be introduced in order to reuse the heat within the system. That leads to the concept of the actual ACAES, in which the heat released during the compression is stored and afterwards used to heat up the fluid during the expansion. [Y.Zhang et al., 2013]
- **Cryogenic Energy Storage(CES):** This technology is based on the same principle as the ACAES. During the compression and expansion of the fluid heat is realised or required for an optimal operation. In that case, a large amount of heat is exchanged with the thermal storage as this technology is based on the liquefaction of a gas. The implementation of the TES plays a key role in the increase of the system efficiency.

At the present time new technologies are under development, based on the idea of the storage of thermal energy as heat in inexpensive materials and a well-proven technology. These are two very attractive characteristics that would enable a low-cost storage system with high reliability and durability. In that field, new conceptual systems are developed as the High-Temperature Thermal Energy Storage by Henrik Stiesdal.

1.2.1 High Temperature Energy Storage (HT-TES)

The present work focuses on the analysis and development of the technologies for the storage of bulk energy for electricity supply services. From the analysed energy storage technologies, at the present time, only PHS and CAES are currently available. There are different technologies under development in order to reduce the system cost and to provide an higher performance.

One new developed system is the High-Temperature Thermal Energy Storage, based on Henrik Stiesdal patents: [Stiesdal, 2015a], [Stiesdal, 2013a]. The objective of the invention is to be able to store the excess of electricity produced by a renewable source such as wind or solar in the form of heat, which can be stored for weeks and afterwards converted back to electricity. This process converts the electrical energy into heat, increasing the temperature of a low-cost storage material, which is insulated form the environment. When there is a high electrical demand and a low renewable energy production, the stored heat can be converted back into electricity by a thermodynamic cycle. The economic profitability of the system would come from the price difference between the electricity consumed to charge the system (heat up the storage) and the electricity delivered back to the grid during the system discharging. [Stiesdal, 2015a] claims that the projected prototype would be able to

store up to 250 GWh in a 2000000 m^3 rock bed storage and a claimed overall round-trip efficiency of 80%.

The HT-TES is composed by three main components, a charging systems, a high-temperature thermal energy storage and a discharging system, steam cycle, as shown in 1.3:

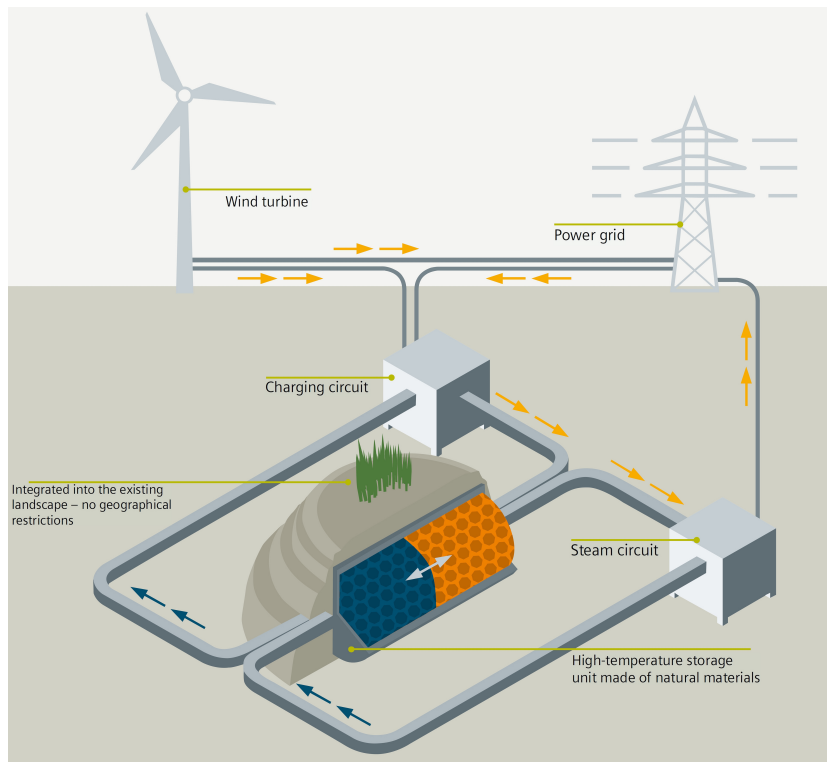


Figure 1.3. HT-TES system presented by Siemens [Siemens AG, 2016]

As proof of the viability of this system, Siemens is currently developing a pilot plant of the thermal energy storage in Hamburg alongside with the Technical University Hamburg Harburg and urban utility company Hamburg Energie. The prototype is based on the simplicity of the thermal principle, that promises an extremely low-cost set-up. The projected pilot plant is based on a tried and trusted technology that heats up the thermal storage up to 600°C, a fan that uses an electrically-heated air flow to heat the stones. During the discharging cycle, the stored energy heats up a boiler that is responsible to drive a steam turbine. The designed prototype is able to store 36 MWh in a container of around 2000 m^3 of rock, with an output up to 1.5 MW providing electricity up to 24 hours a day. The researchers expect an efficiency around 25%, being able to achieve up to 50% in future developments [Siemens AG, 2016].

This technology has already shown a great potential to play a key role in the future energy scenarios. The main advantages of this system is the maturity of its technology despite of being in an early development stage. Furthermore, It is able to store large amounts of energy deploying it at high power rates³ with moderate efficiencies. And last but not least, it does not depend on specific geographical requirements as the PHS and CAES.

It is shown in Table 1.1 the comparison of the HT-TES system with other already existing energy storage technologies.

Table 1.1. HT-TES compared with known storage technologies [H.Stiesdal, 2016]

Topic	Li-ion	Pump H2O	CAES	Hydrogen	HT-TES
Tech. readiness charge-discharge	Mature	Mature	Mature	Development stage	Mature
Tech. readiness storage unit	Mature	Mature	Mature	Mature	Development stage
Round-trip efficiency	90%	85%	40-60%	30-50%	35-50+%
Round-trip energy cost	High	Low	Low	Medium	Low
Energy density	High	Low	Low	High	High
Footprint	Small	Large	Small	Small	Small
Scalability, power	0.01-25 MW	50-1.000 MW	1-100 MWh	1-1.000 MW	1-1.000 MW
Scalability, energy	0.01-25 MWh	100-10.000 MWh	10- 1.000 MWh	1-100.000 MWh	1-100.000 MWh
Local requirements	None	Special topography	Special topography	Special topography	None
Raw material use	High	None	None	Moderate (electrolizer)	None

1.3 Problem Statement

The unpredictable availability of renewable energy sources leads to an intermittent energy production depending on the environmental conditions. The miss match between production and consumption leads to the necessity of new technological developments and strategies for the energy storage.

Thermal energy represents a low-cost reliable technology based on a proven technology, able to reach large capacities and to provide energy for long periods. Furthermore, this system is not limited by any geographical constrain. Nevertheless, the thermodynamic process involved in the energy conversion narrows the storage efficiency.

In this thesis it is carried out a technical study on thermal energy storage consisting of a packed bed of rocks. The feasibility and performance of the system is investigated in order to asses the viability of the technology.

In order to evaluate the different components of the system, the charging and discharging units are modelled in order to study the effect of the key parameters affecting the performance of both processes. In order to link both parts of the system, a heat transfer model of the packed-bed is developed for the assessment of the system behaviour.

Due to the important role that plays the thermal storage unit in the system, the cycling operation is evaluated in order to emulate the continuous operation. Furthermore, different geometrical strategies such as segmentation of the packed bed are investigated in order to improve the TES performance.

Finally, a range of possible configurations with different peculiarities are proposed and discussed.

1.4 Methodology

In order to achieve the goals presented above, the different possible system configurations are analysed based on the available technologies.

In order to assess the performance of the system, two models are developed. First the charging and discharging systems are modelled, based on the basic thermodynamic equations for the analysis of the cycles performance. In order to link both units, a dynamic one-dimension two-phase heat transfer model with variable properties for the solid and the fluid phases is developed for the rock packed-bed. Both models are performed in MATLAB 2016b.

The developed models need to be validated in order to assess its consistency. Regarding to the charging and discharging units, as no literature is available for its validation, a parametric study is carried out in order to analyse the correct system behaviour. The packed-bed model is validated based on literature results.

After that, an analysis of the charging and discharging processes of the system are carried out. Complementary, the cycling and segmentation of the storage unit are studied.

1.5 Limitations

The project is based on the investigation of a concept for which real data are not available. Therefore, the different boundaries for the analysis have been decided based on the available time-frame.

- Rankine cycle simulated as a quasi-steady state model
- The dynamic effect has not been taken into account within the thermal storage inlet/outlet
- The maximum particle size diameter is limited by the Biot number
- The thermal energy storage is defined with a cylindrical shape
- The refrigerant circuit of the cold heat exchanger of the heat pump is not analysed
- Experimental work is not carried out in this project. The models are validated with experimental results obtained from the literature sources
- The economical analysis of the system is not carried out within this project
- The HRSG is simulated in a simplified way based on LMTD method

2 System Description

2.1 HT-TES System Description

The concept of the High-Temperature Thermal Energy Storage consists of converting electricity into heat by the use of a heat pump or a high temperature electric heater. Storing the heat in a low-cost thermal storage and then reconverting it to electricity by the use of a power cycle. The analysed technology is based on a conceptual system developed by Henrik Stiesdal and afterwards implemented by Siemens in his current pilot plant in Hamburg as mentioned in the subsection 1.2.1.

The system investigated in this study is formed by three main subsystems as shown in figure 2.1: a charging unit, which can eventually be a heat pump or an electric heater; a thermal storage, constituted by the storage material, and a discharging unit, which in this case is based on a Rankine cycle.

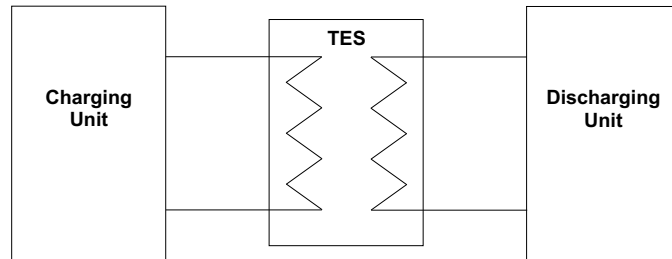


Figure 2.1. HT-TES subsystems: charging unit, thermal storage and discharging unit

2.1.1 Charging Unit

The charging system can be constituted by a heat pump, a high temperature electric heater, or with a combination of both as function of the temperature operating range. This system has the function to heat up the air flow which is going to charge the thermal energy storage.

The heat pump charging unit comprises a compressor, a gas-to-gas hot heat exchanger connected with the hot storage, a small turbine and a cold heat exchanger. It can eventually be connected with a cold storage unit, which closes the cycle and puts back the working fluid at the initial conditions.

In the compressor, the working fluid is heated up by compression in order to reach the high charging temperature. This would require at least two stages of compression due to the high compression ratio and in order to achieve a higher efficiency. Subsequently it passes through the first heat exchanger which provides the heat to the thermal storage to charge the system. Usually heat pumps use refrigerants as a working fluid, nevertheless in the current system is implied air due to its large availability, despite that the feasibility of

other fluids should be investigated. The chosen fluid should be able to reach temperatures in the order of 600°C as mentioned in [Stiesdal, 2015a].

The fluid is expanded by a turbine or a valve, bringing it back to low pressure. As consequence of this expansion, the fluid is cooled down to very low temperatures, reaching negative values. If the gas expansion is carried out by an expansion valve, it would result to be a considerably simpler system. On the other hand, the use of a turbine increases significantly the efficiency of the system and therefore is thermodynamically preferable. Finally, the temperature is raised up again until ambient condition in the cold heat exchanger, preparing the gas to start again another working cycle. This introduces some conditions on the working fluid, in order to avoid the presence of liquid in the turbine and the related issues. This problem can be solved by the use of perfectly dry air, or similar gases such Argon or Nitrogen, in a closed cycle, preventing also external moisture to get into the system. The expectation regarding this heat pump is to have a coefficient of performance (COP) greater than 1 in order to be globally more efficient than the version using electric heaters.

The charge of the storage can be performed, as mentioned above, by means of a high temperature electric heater as well. This would significantly decrease the cost and the complexity of the whole system but the performance of the charging would be drastically lower as well. The COP for the electric heater charging option is expected to be equal to 1. Figure 2.2 illustrates both possible charging configurations, based on a heat pump or a high temperature electric heater.

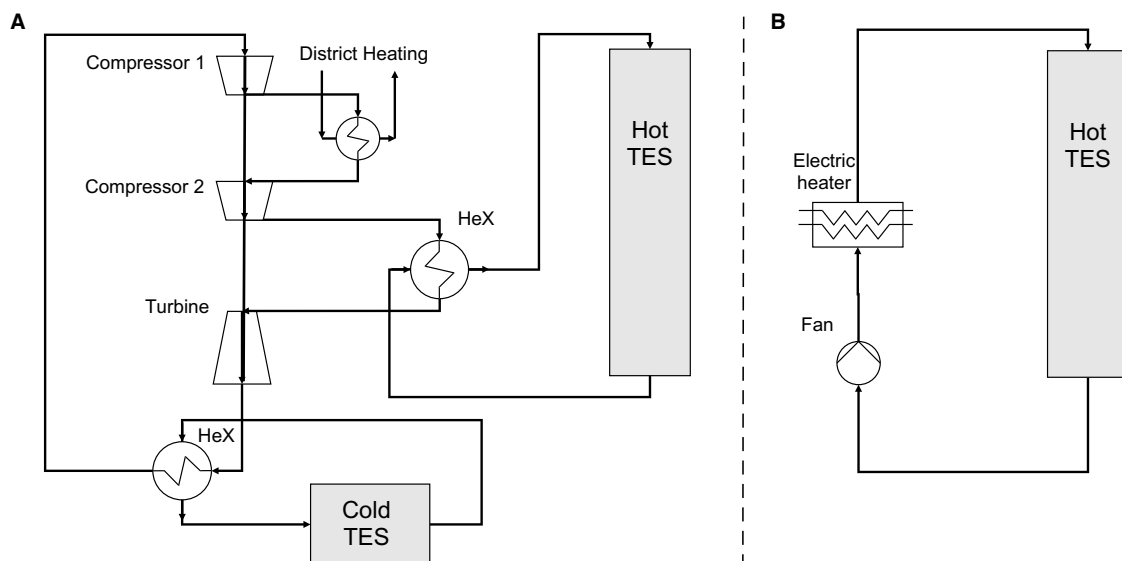


Figure 2.2. Charging unit configurations: A) Heat pump B) High temperature electric heater

Furthermore, the system can be charged by a combination of both systems in order to achieve a higher performance. In that case, a heat pump system would be used in order to rise the fluid temperature to moderate levels with an acceptable COP and complementary an electric heater to boost the temperature until the desired value, which in that case would maintain an efficiency equal to 1. In figure 2.3 is shown the configuration of the combined heat pump with the high temperature electric heater.

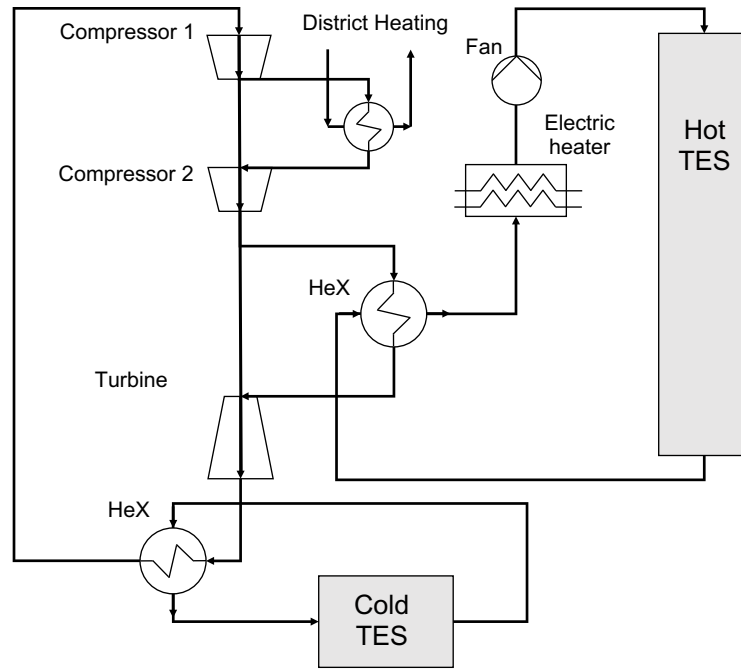


Figure 2.3. Combination of a heat pump and a electric heater as charging unit

2.1.2 Discharging Unit

The system makes use of a conventional Rankine Cycle to discharge the storage unit. Rankine cycle has the considerable advantage to be a well known, reliable and safe technology. The upper limit is determined by the thermal storage temperature which in the case of study is around 600°C [Stiesdal, 2015a]. The upper limit in conventional power plants is around $550\text{-}600^{\circ}\text{C}$ in Rankine cycles Kehlhofer [2009], due to the cost of the materials required for reaching higher temperatures in the last section of the boiler and at the turbine inlet. The lower temperature is limited by the minimum technical pressure that is achievable in the condenser of the system. Therefore, the maximum temperature spread between the hot and cold source is desirable as the maximum efficiency is limited by the well know Carnot cycle. Figure 2.4 presents the basic discharging configuration of the system.

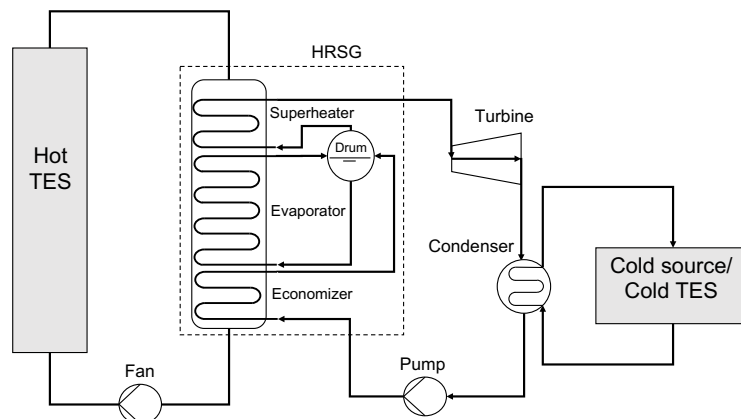


Figure 2.4. Discharging unit configuration

The level of the efficiency for complete discharge is given by the efficiency of the cycle, which is attested around 30-40%. It seems to be possible to improve the performance of this cycle by using two pressure-levels and/or regeneration within the cycle.

Using this type of cycles to discharge the system would introduce the possibility to turn standard coal-fired steam power plants into thermal energy storage units. The packed bed may be placed in the former coal yard, with no further space requirements and actually turning the plant to be a 100% green energy storage unit [H.Stiesdal, 2016].

Another chance eventually made available by the use of this technology consists of substituting the topping Brayton cycle in Combined-Cycle Gas Turbines (CCGT) with the storage unit, using therefore the existing bottoming Rankine cycle as a discharge for the system. This would also allow to save the cost of the Heat Recovery Steam Generator (HRSG), since the CCGT already makes use of it, even if it poses some challenges especially for the coupling of the old bottoming cycle with the new storage unit.

2.1.3 Thermal Energy Storage Unit

The heat storage system is constituted by a large U-shape packed-bed filled up with a solid storage material, such as crushed basalt rocks or coal ash [Stiesdal, 2015a] [Stiesdal, 2013a]. The use of a packed bed solid material without phase change is a low-cost alternative compared to other storage technologies such as PCMs. The storage system proposed by Stiesdal is constituted by a large system with a volume in the range of $2 * 10^6 m^3$ for the storage of 250 GWh [Stiesdal, 2015a]. Due to the dimensions on the packed-bed it is not viable to build a completely airtight system, therefore it is necessary to operate it close to atmospheric pressure. That leads to the necessity of a large heat exchanger when it is used a heat pump as charging system due to the pressure differences. Furthermore, it is required to be properly insulated from the environment in order to reduce heat losses. The material used for the actual system should fulfil some characteristics such as high specific capacity, high density, low cost and good mechanical behaviour in order to withstand repeated number of thermal cycles without cracking, melting or eroding.

The basic concept of a packed bed with solid storage material has been modified in order to improve the efficiency of the storage.

The first modification consists of taking advantage of the principle of counter-current heat exchange, in order to achieve a higher efficiency due to the smaller temperature differences. The idea is to reverse the flow direction of air in the storage when switching from charging to discharging mode and therefore to have the hot side of the storage at the inlet during charging and at the outlet during the discharging. Figure 2.5 shows how the temperature profile displaces back and forth along the charging/discharging cycles due to the switching direction of the flow. By placing both connections of the storage at the same side it is possible to further reduce losses since shorter pipes are required. Therefore it is recommended to design the thermal storage with a U-shape in order to reduce the cost of installation [Stiesdal, 2015a].

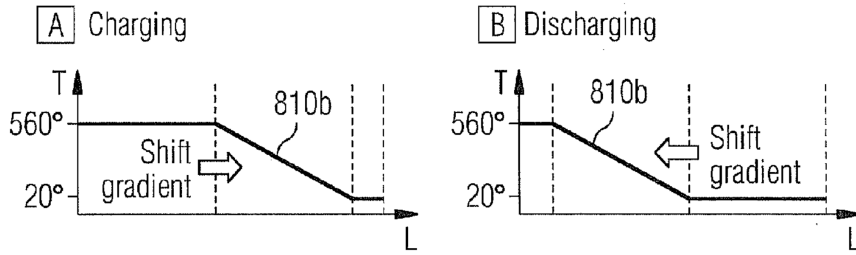


Figure 2.5. Thermocline profile change with increasing charging cycles [Stiesdal, 2015a]

The main advantages of this storage technology consist of being very cheap, easy to handle and also that pressurization is not required. As consequence of the simplicity of the system, also the maintenance costs are very low and even the whole substitution of the storage material itself does not represent a problem, due to the very low cost of the material.

Nevertheless there are some relevant disadvantages for the use of solid storage materials. The first is that the storage temperature changes with time and therefore the heat transfer is affected by this phenomenon. In fact, the heat transfer decreases during both the charging and the discharging [Hanchen et al., 2011]. The reason of this decrease is that during the load of the storage device, an increasing part of the storage unit is heated up to a temperature closer to the one of the fluid. Thus, the mean temperature difference decreases between the storage material and the air, and therefore the heat transferred between them as well. This observable fact is occurring as well during the discharge of the system.

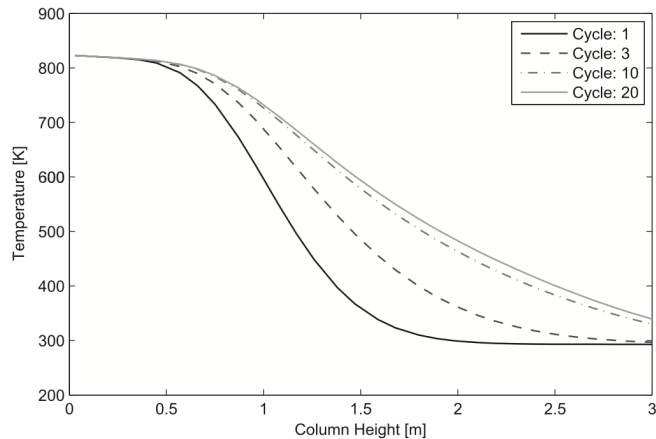


Figure 2.6. Thermocline profile change with increasing charging cycles [Hanchen et al., 2011]

Another challenge is constituted by the progressive flattening of the temperature gradient after a certain amount of incomplete charge-discharge loop. In this kind of storage unit the temperature gradient is defined as thermocline. The inlet and outlet temperatures are affected by the thermocline when it reaches the inlet or the outlet of the thermal storage. This means that the quality of heat released by the storage decreases together with the discharging efficiency. The effect of outlet temperature drop will be affected in a major grade as the thermocline becomes flatter [Hanchen et al., 2011]. It can be observed in

figure 2.6 that with an increasing number cycles the thermocline within the storage gets more horizontal. The cycling effect on the system will be further discussed in subsection 6.3.

The temperature gradient also affects the system. When the storage is neither charged nor discharged, it causes conduction through the rock-bed and convection in the fluid still present around it. This can create mixing losses and can eventually also decrease the outlet fluid temperature depending on the temperature level in the storage. Generally, the operational zone of the unit decrease because of this aspects. Stiesdal's concept consists on developing the design of the storage unit in order to limit as much as possible these inconvenient phenomenons.

Segmented packed bed: Sliding Flow Method

In order to increase the storage efficiency, it is proposed in Stiesdal's patent the development of a segmented storage. That means that the heat medium is divided into insulated segments each of them independent from each other but connected by ducts. Therefore, the different regions of the storage can be charged and discharged by the operation of the valves that connect the different sections, as shown in figure 2.8. Therefore, it can be avoided the thermal dispersion within the different regions and achieving a higher temperature independence [Stiesdal, 2015a], [Stiesdal, 2013a], [Stiesdal, 2013b] and [E.Simioni, 2016]. The internal insulation opens also several prospectives for efficient operation. This allows to adapt the size of the storage to the actual working conditions. For instance, if it is wanted to charge or discharge the storage with a smaller amount of energy only the sections closer to the hot and cold end will be used. Moreover, the different insulated sections make possible to handle the local temperature gradient as mentioned in [Stiesdal, 2013b]. The effects of segmentation in a packed bed thermal storage have been investigated in detail by [H.Bindra et al., 2014], which makes use of the sliding flow method (SFM) for the TES design. The SFM allows to reduce significantly the exergetic losses of the process compared to the conventional charging-discharging method. The traditional method of storing energy in packed beds typically has one end for the inlet and one for the outlet of the flow. In this configuration the shorter the bed, the larger is the fractional thermal energy destruction, but on the contrary a long unit would cause an higher pressure drop within the storage, which is therefore a key limiting factor to the size of the storage itself. The effects of the pressure drop on the dimensioning of the system are further analysed in section 5.1.

The SFM consists of changing the inlet/outlet ports during storage operation as the temperature front moves in the bed. In fact, in this method the bed is divided into several segments, each one of them with the same length. The flow inlet and outlet are connected to each segment. During the storage operation, i.e. in charging mode, the hot fluid is introduced into the first segment and transfers the heat to the first two segments, after that leaves the unit through the second segment outlet. Once that the first segment is fully charged and the fluid exiting from it has reached its top temperature, a switch is made to introduce the fluid at the entrance of the second segment, "partially charged" because of the heat exchange already occurred, and is extracted at the outlet of the third segment. This process is repeated until all the segments are fully saturated. With this

arrangement, the pressure drop through each segment is only a fraction of the pressure drop which would incur in the conventional method. Figure 2.7 illustrates the comparison between the SFM method just presented and the traditional method.

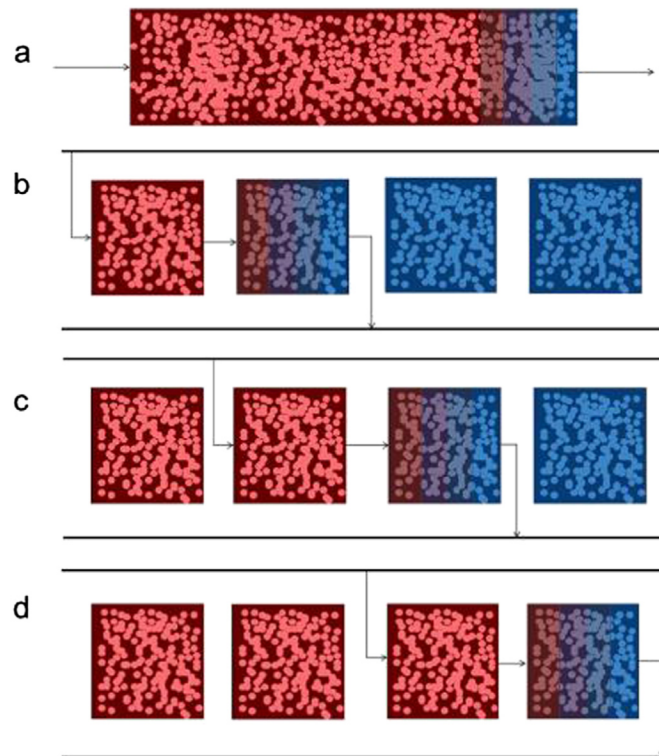


Figure 2.7. Schematic traditional packed bed thermal storage (a) and sideling flow method (b,c,d). [H.Bindra et al., 2014]

In this example the storage unit is divided into four segments of equal length with flow entering one segment and leaving from the following one.

The storage unit can be equipped also with secondary feed-in pipes that allow to blow a fluid at the desired temperature along the length of the storage instead of from the inlet section. Consequently the temperature profile can be modified and brought back to the initial shape. [Stiesdal, 2015a] [Stiesdal, 2013a] [Stiesdal, 2013b][E.Simioni, 2016] An idea of this feature is given by figure 2.8.

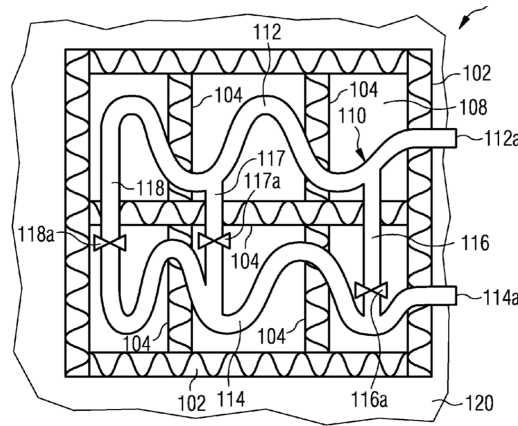


Figure 2.8. Sectioned storage presented by Stiesdal [Stiesdal, 2015a]

With the objective to keep the hot end and cold end temperatures of the storage constant at every load, it is suggested in [Stiesdal, 2013a] to build the device longitudinally, aiming to remain far enough from the thermocline region. Hence, the temperature profile moves along the storage but without reaching the boundaries. The length of the temperature profile depends on the flow characteristics, in particular from its speed and on the thermal properties of the storage, but not on the physical length of the unit. Figure 2.9 shows the hypothetical temperature profile along the thermal storage. It is recommended in [Stiesdal, 2015a] a thermal interaction region between the fluid and the heat storage medium up to 1000m.

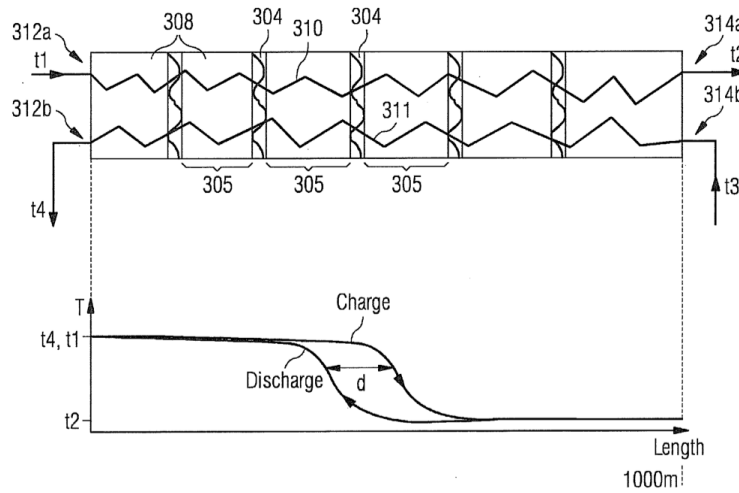


Figure 2.9. Temperature profile along the storage [Stiesdal, 2015a]

Consequently, assuming to keep approximately constant the temperature among the inlet and outlet section, the longer the unit is, the lower the thermocline flattening effect will be, and thus the operative region at maximum efficiency will be larger.

2.2 System Configurations

Once the different system units has been analysed, different plant configurations are designed based on the purpose of the system.

The main aim and philosophy of the system is to store the excess from renewable energy production in order to be converted back when needed. Therefore, it is necessary at the same time a high round-trip efficiency, allowing to generate back to the grid as much energy as possible which would lead to higher revenues.

The requirements for this study are to provide a nominal power of 45 MW for a minimum period of 24 hours. These plant specifications are justified by figure 1.2 in which the desired target area is defined as Bulk Power Management, to be ideally a competitor with PHPS and CAES. A significant advantage that should be noticed is that this system would does not depend on any geographical constrain.

Based on the two main system constrains, three configurations have been designed in order to cover the different possibilities: a balanced system with a medium efficiency, a low-cost and simple system and a combination of the two previous one with an increased complexity and higher performance. Figure 2.10 illustrates the configuration of HP-TES system.

2.2.1 Configuration 1: HP-TES

Configuration 1 (Heat-Pump Thermal Energy System) is constituted by a large heat pump as a charging unit and a steam Rankine cycle as discharging unit in order to reintroduce the electricity back to the grid. In order to store the energy, the system is combined with a high temperature TES system and a cold thermal storage in order to extract the cold produced by the cold heat exchanger of the heat pump.

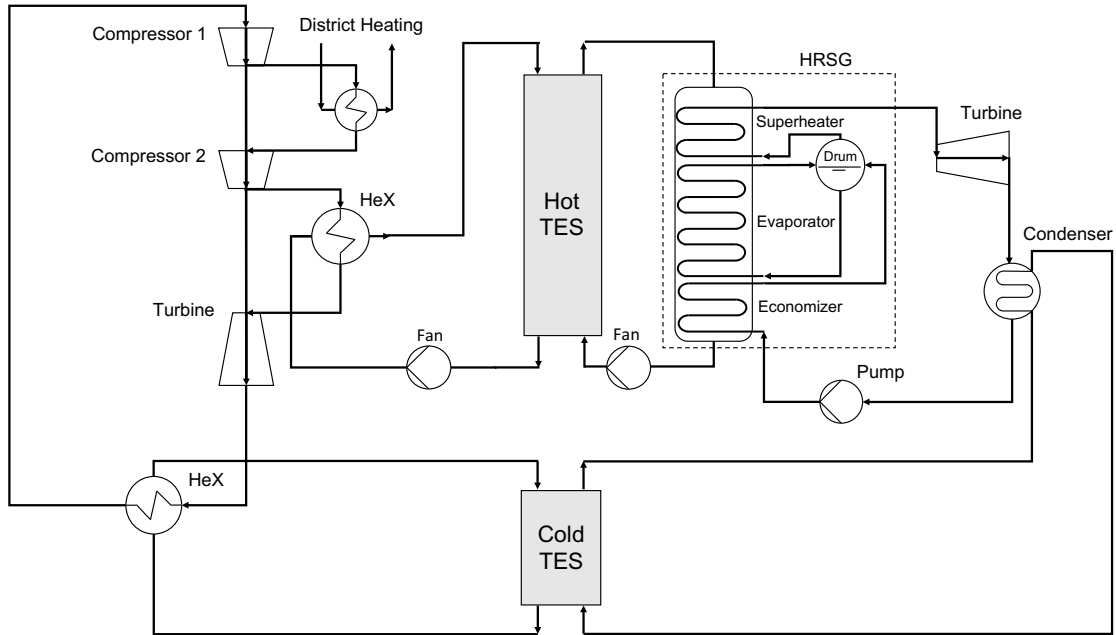


Figure 2.10. HT-TES with a heat pump as charging unit and Rankine cycle as discharging unit

The main system advantage is the higher efficiency that enables the use of a heat pump as a charging system. It is expected to reach COP close to 1.2, depending on the operation temperature of the system. Due to the dimensions of the expected plant, the heat pump system would constitute a large and complex system, which would probably need to be oversized in order to reduce the time response. It has to be noticed, that instead of an expansion valve it has been implemented a turbine instead in order to recover part of the energy during the gas expansion. To further increase the heat pump performance, a multi-staged compression would be preferable. This would allow also to implement an inter-cooler between the compressor stages in order to provide district heating (DH), which would lead to a higher system efficiency. Another advantage of using a heat pump is the low temperatures that are achieved in the cold heat exchanger. That cold source could be used to supply the energy required by the Rankine cycle condenser or in order to supply district cooling.

Nevertheless, this system has some drawbacks regarding the viability of the mentioned configuration. In first place, the system complexity and the number of components is higher compared to other possible configurations, which would lead to higher investment cost and maintenance due to the large number of moving parts. The maximum temperature system operation is limited by the feasibility of such a large heat pump, which should be further studied, since this technology clearly has not been designed for the mentioned application. Moreover, due to the fact that the high temperature TES is not able to operate at high pressures, it is required a large heat exchanger in order to separate the fluid circulating through the heat pump and the air from the storage, which would represent an important increase in the system cost. As mentioned before, in order to make use of the low temperatures achieved in the heat pump condenser, a heat exchanger and a cold thermal storage would be required, further increasing the initial investment of the plant.

2.2.2 Configuration 2: EH-TES

The second configuration (Electric-Heater Thermal Energy Storage) is constituted by a high temperature electric heater as a charging unit, and as in the configuration 1, a Rankine cycle as discharging unit. The idea behind this system is to reduce the initial plant investment and complexity, despite the lower performance of the system. The electricity-to-thermal efficiency can be considered close to 1, which is lower than in configuration 1. Figure 2.11 illustrates the EH-TES configuration for the system.

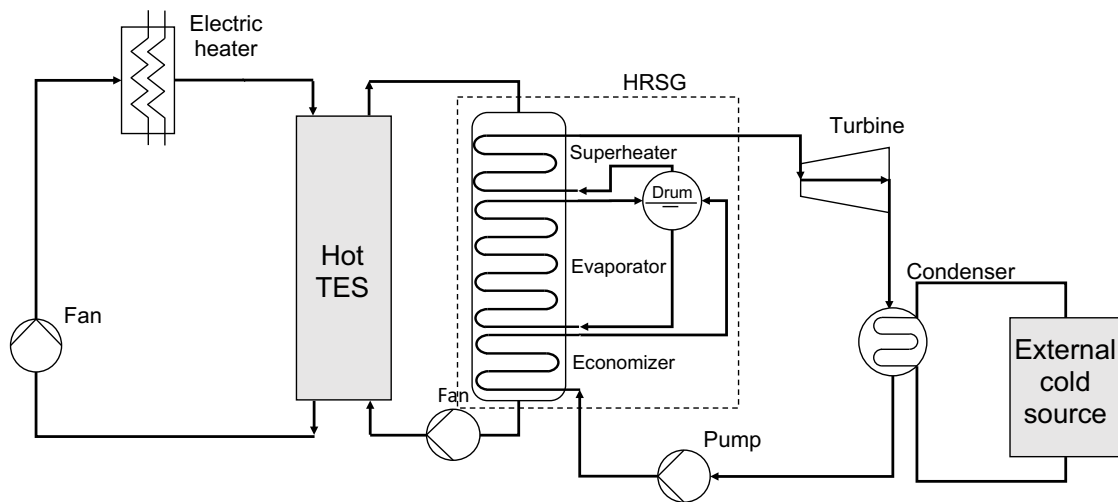


Figure 2.11. HT-TES with a high temperature electric heater as charging unit and simple Rankine as discharging unit

The main advantage of this configuration is the reduction of the complexity of the system due to the need of less components. Furthermore, as the electric heaters are not composed by any moving part, the maintenance cost of the charging unit is considerably reduced. Regarding to the system operation, since compression is not required within this charging system, the hot air can be introduced directly to the thermal storage. This avoids the need of a large intermediate heat exchanger which means a high decrease of the initial investment.

Due to the immediacy of the electric resistance behaviour, it would be possible to start-up the system on a shorter period of time, increasing the performance and operation. Another advantage of this technology is the possibility to achieve higher temperatures compared to the heat pump technology. For instance, it would be possible to reach 700°C in the storage, and still being in the feasible temperature range of the mechanical material limitations.

The main disadvantage of the the current configuration is the lower system efficiency compared to the one of the heat pump, that has to be evaluated in order to determine the economical feasibility as the initial investment cost would be lower. As well, it is not possible to provide district cooling since there is not cold production. Therefore, it is necessary to include an external cold source to remove heat from the condenser of the bottoming Rankine cycle.

2.2.3 Configuration 3: HPEH-TES

The main objective of the third configuration (Heat-Pump-Electric-Heater Thermal Energy Storage) is to design a system with a higher performance despite the increase of the initial investment cost and system complexity. For this purpose, the charging unit is designed as the combination of a heat pump and electric heater in order to increase the maximum temperature of the storage overcoming the upper temperature limit of the heat pump alone, and on the other hand taking advantage of its higher efficiency. In the discharging unit it is expected to achieve a higher global efficiency compared to the previous two configurations. The HPEH-TES system diagram is shown in figure 2.12.

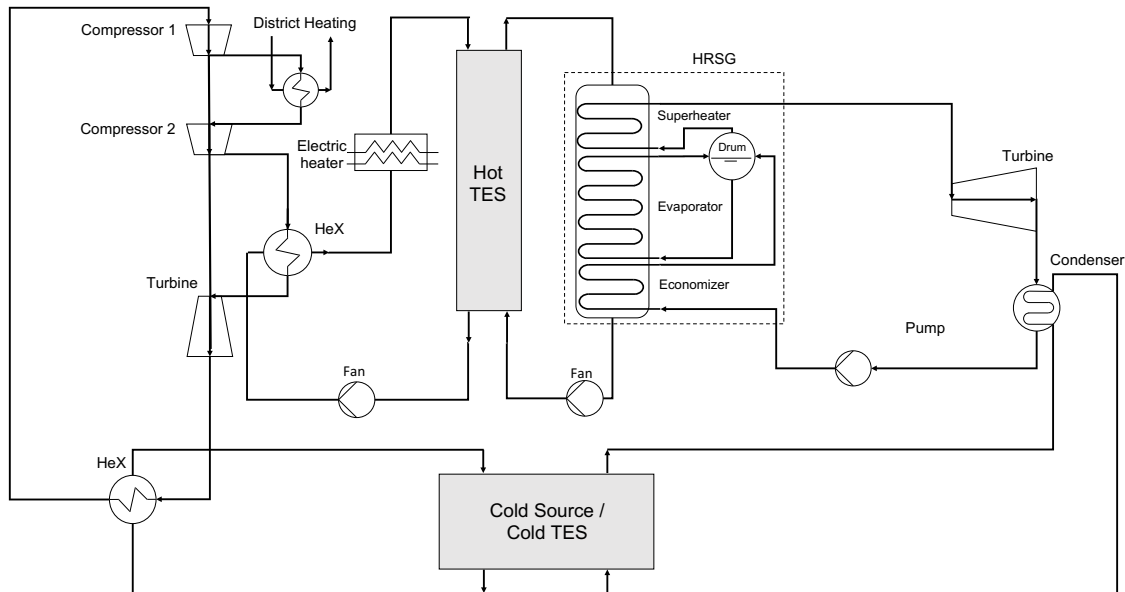


Figure 2.12. HPEH-TES with a high temperature electric heater + heat pump as charging unit

The target of combining a heat pump with an electric heater is to take advantage of the high COP of the heat pump at medium temperature range, and increasing afterwards the temperature of the fluid by means of a high temperature electric heater. This will lead to a higher efficiency of the Rankine cycle as it will work at a higher temperature range too. Another advantage is the possibility to supply district cooling and heating as the working principle of the heat pump is equivalent to the configuration 1.

This system improvements can be desirable from a technical point of view leading to a more efficient system but on the other hand, will increase the cost and the number of components of the storage system.

In order to summarise the main advantages and disadvantages of the designed system configurations, table 2.1 collects the main characteristics of the three different cases:

Table 2.1. HT-TES configurations comparison

	Cost	Complexity	Efficiency	Charging Unit		Discharging Unit		DH/DC
				HP	EH	Average η_{RK}	High η_{RK}	
I	High	Medium	Medium	✓		✓		✓
II	Low	Low	Low		✓	✓		
III	High	High	High	✓	✓		✓	✓

3 System Modelling

In order to simulate the performance of the system, a model in MATLAB R2016b has been developed. The model can be divided in two different parts. One represents the charging and discharging units and the other one simulates the operation of the TES system. The main objective of the developed model is to asses the performance and efficiency of the system, to evaluate the power and energy that is possible to store in the thermal storage, and to estimate the extend of time in which the system is able to supply electrical energy. As shown in figure 3.1, both parts of the system (charging and discharging) are linked by an independent model which simulates the heat transfer process within the thermal storage. Therefore, it is possible to analyse the complete process and performance of the plant.

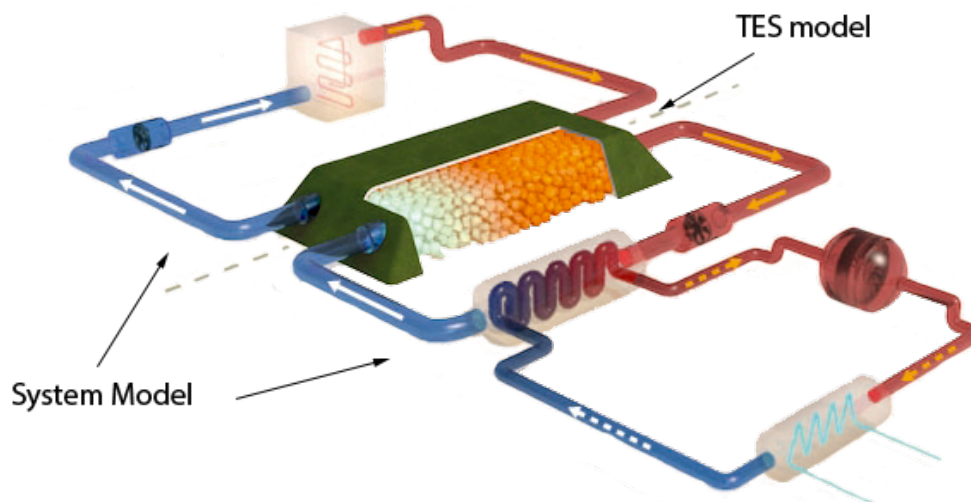


Figure 3.1. Graphic representation of the models boundaries(modified)[Siemens AG, 2016]

This chapter presents the models regarding the charge and discharge unit of the three systems described in subsection 2.2. The following chapter is structured in the way that all the relevant assumptions are first listed and discussed. After that, a system flow diagram is provided for each configuration. Then, all the governing equations as well as the methodologies used in the simulation are described. Finally, the block chart of the model functions is made available and explained at the end of the chapter.

3.1 Configuration 1: HP-TES

HP-TES configuration is based on a heat pump and a Rankine cycle as mentioned in subsection 2.2. The main equations of the modelled system are introduced in the following section.

3.1.1 General Assumptions

In order to develop the model, several assumptions are made. The assumptions done are collected in the following list:

1. Steady state model equations for the thermodynamic cycle
2. Assumed pressure loss for the different components
3. The less relevant components are modelled as a black box (input-output)
4. All the devices exchanging work are considered adiabatic
5. Heat exchangers in the charging unit are considered adiabatic

The assumed values of the system are listed in table 3.3:

Table 3.1. Input parameters of the system model HP-TES

Symbol	Value	Unit	Symbol	Value	Unit
T_{HP_1}	285	K	$W_{T,nominal}$	45	MW
P_{HP_1}	101.325	kPa	$x_{turbine}$	0.9	—
m_{HP}	120	kg/s	$U(all)$	50	W/m^2K
m_{RK}	39.25	kg/s	A_{Hex}	15000	m^2

3.1.2 Charging Unit: equations

The charging unit is constituted by a heat pump in this configuration. The calculation starts with the compressor function and followed by the high temperature TES heat exchanger. After that, the gas expansion is calculated by the turbine function and finally the cold storage heat exchanger function is executed.

Compressor and District Heating

The chosen device for this system is a two stages compressor, with inter-cooling in between the two stages. To provide the cooling, a reasonable option is to integrate the system with the district heating network, making available to exploit the heat power produced out of the first compression stage, increasing so the overall efficiency of the system. In order to obtain the work absorbed by the single compressor stage, first it is calculated the outlet pressure by equation 3.1:

$$P_2 = P_1 \cdot \frac{T_2^{\frac{\gamma m c}{\gamma - 1}}}{T_1} \quad (3.1)$$

where P_2 is the pressure at the outlet of the stage in [Pa], P_1 is the inlet pressure, T_1 and T_2 are the corresponding temperatures in [K], γ is the adimensional heat capacity ratio while η_c is the isentropic efficiency of the compressor stage. It is possible to obtain the power consumed in the stage by the expression 3.2, as an enthalpy difference:

$$\dot{W}_{stage} = \dot{m}(h_2 - h_1) \quad (3.2)$$

where h is the enthalpy at each point in [J/kg] and \dot{m} is the working fluid mass flow in [kg/s]. The isentropic efficiency of each stage is calculated by equation 3.3:

$$\eta_{is,stage} = \frac{\left(\frac{P_2}{P_1}\right)^{\frac{\gamma-1}{\gamma}} - 1}{\frac{T_2}{T_1} - 1} \quad (3.3)$$

This procedure is repeated for each stage. The total power absorbed by the compressor is given by equation 3.4:

$$\dot{W}_{c,tot} = \sum \dot{W}_{c,stage} \quad (3.4)$$

where the total power is in [W]. The district heating heat exchanger is designed according to NTU method, whose complete derivation applied to this case for the sake of brevity can be found in the appendix A.1.

Hot & Cold Storage Heat Exchangers

All the mono-phase heat exchangers analysed in this work are designed according to NTU method (appendix A.1). The output parameters of the calculation are the actual heat exchanged, the two outlet temperatures of the two fluids and the effectiveness of the heat exchanger itself. The heat capacities of the fluids are evaluated iteratively, in order to achieve a higher grade of accuracy despite a slight increase of the computational time necessary to run the simulation. Only for the cold heat exchanger after the turbine section, it is determined iteratively again the flow rate of refrigerant fluid necessary to close the cycle bringing the working fluid back to the initial conditions.

Turbine

To carry out the expansion needed from the cycle, a turbine is chosen and placed on the same shaft as the compressor, instead of a classic expansion valve. The idea is that, despite the major cost of the component, the work produced by the turbine allows the reduction of the energy consumption, since it can be used to run the compressor, increasing considerably the efficiency of the heat pump and therefore improving the performance of the whole system. To obtain the actual work of the turbine, the same approach as for the

compressor is used. First it is calculated the temperature at the outlet, defining the outlet conditions by equation 3.5:

$$T_6 = T_5 \cdot \frac{P_6^{\frac{\gamma-1}{\gamma\eta_t}}}{P_5} \quad (3.5)$$

Where η_t is the isentropic efficiency of the turbine and it is assumed constant. It is possible now to calculate the power produced by equation 3.6:

$$\dot{W}_t = \dot{m} (h_5 - h_6) \quad (3.6)$$

After that the system components are defined, it is possible to estimate the COP of the heat pump. Taken into consideration the availability for the district heating production, the COP can be evaluated with and without district heating supply, which is expressed by equations 3.7 3.8:

$$COP = \frac{\dot{Q}_{charge}}{\dot{W}_c - \dot{W}_t} \quad (3.7)$$

$$COP_{DH} = \frac{\dot{Q}_{charge} + \dot{Q}_{DH}}{\dot{W}_{c,tot} - \dot{W}_t} \quad (3.8)$$

where \dot{Q}_{charge} is the total heat power transferred to the storage after the compression in [W], and \dot{Q}_{DH} in [W] accounts for the district heating energy supply.

3.1.3 Discharge Unit: equations

The discharging unit model is composed by a steam turbine function, followed by the feed water pump and then by the HRSG. Finally the Rankine cycle is closed by the condenser.

Steam Turbine

The aim of the function is to calculate the work of the steam turbine, and therefore the discharging capacity of the system. The power of the system must be in the range of 45 MW in order to fulfill the requirement of the project, as previously exposed in section 2.2. The isentropic efficiency of the turbine is calculated by equation 3.9:

$$\eta_T = \frac{h_2 - h_3}{h_2 - h_{3,id}} \quad (3.9)$$

Where the ideal enthalpy at the outlet $h_{3,id}$ is obtained considering the whole process isentropic and calculating the point using the same entropy as in the inlet, as it is illustrated

in the figure 3.2. To estimate the turbine work it is applied the enthalpy difference relation shown in equation 3.10:

$$w_t = (h_2 - h_3) \quad (3.10)$$

where w_t is the specific real work of the steam turbine in $[J/kg]$.

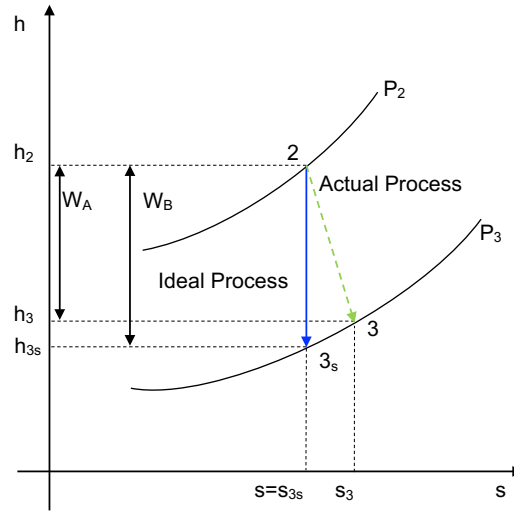


Figure 3.2. h-s diagram for the steam turbine

Feed water pump

To determine the power consumed by the feed water pump it is adopted the same strategy as for the turbine section. First it is calculated the efficiency with equation 3.9, but since in that case it is a pump, inverting numerator and denominator. Subsequently it is obtained the power absorbed from the pump by equation 3.2 by placing the correct enthalpy difference.

HRSG

The HRSG between the discharging cycle and the TES is modelled applying the LMTD (Logarithmic Mean Temperature Difference) method. The thermal efficiency of the boiler is assumed to be constant, thus it is possible to calculate the heat entering the Rankine cycle from the heat of discharge, which is expressed by equation 3.11:

$$\dot{Q}_{HRSG} = \eta_{th} \cdot \dot{Q}_{discharge} \quad (3.11)$$

where \dot{Q}_{HRSG} is the heat power in $[W]$ and η_{th} is the thermal efficiency of the HRSG, assumed constant. Once that the heat transferred is known, it is possible to obtain the

conditions of the steam leaving the HRSG by calculating the enthalpy at the outlet by equation 3.12:

$$h_{2,rk} = h_{1,rk} + \frac{\dot{Q}_{HRSG}}{\dot{m}_{rk}} \quad (3.12)$$

where \dot{m}_{rk} is the mass flow of the steam in $[kg/s]$. To estimate the heating surface of the HRSG it is possible to make use of the LMTD heat transfer equation 3.13, rearranged in order to get the required area in $[m^2]$:

$$A_{HRSG} = \frac{\dot{Q}_{HRSG}}{U \cdot LMTD} = \frac{\dot{Q}_{HRSG}}{U \cdot \frac{\Delta T_{in} - \Delta T_{out}}{\ln\left(\frac{\Delta T_{in}}{\Delta T_{out}}\right)}} \quad (3.13)$$

Where U is the heat transfer coefficient in $[W/m^2K]$ assumed constant for simplicity, and ΔT_{in} and ΔT_{out} are the temperature differences at hot and cold sides of the heat exchanger.

Condenser

The condenser section closes the discharging cycle. The heat power necessary to condense the wet steam from the turbine is calculated by equation 3.14:

$$\dot{Q}_{cond} = \dot{m}_{rk} (h_3 - h_4) \quad (3.14)$$

Efficiencies

Finally the model calculates the efficiency for the discharging circuit alone and the global efficiencies for the system. The Rankine cycle efficiency is calculated by the formula 3.15:

$$\eta_{RK} = \frac{\dot{W}_t - \dot{W}_p}{\dot{Q}_{HRSG}} \quad (3.15)$$

Where \dot{W}_t is the power output from the steam turbine and \dot{W}_p is the power absorbed by the pump in $[W]$. The Carnot efficiency gives the measure of the theoretically maximum efficiency available between the minimum and maximum temperature in the cycle. It is used as a simple reference and it is obtained by the formula 3.16:

$$\eta_{carnot} = 1 - \frac{T_3}{T_2} \quad (3.16)$$

where T_3 and T_2 are respectively the minimum and the maximum temperatures within the Rankine cycle. After the evaluation of the quality of the Rankine cycle, the model

calculates the efficiencies for the complete system. The electricity-to-electricity efficiency ratio determines how much electrical energy is introduced back to the grid based on the electrical energy consumed to charge the system. It is calculated by equation 3.17, where the COP of the heat pump is considered without the district heating:

$$\eta_{el,el} = COP \cdot \eta_{RK} \quad (3.17)$$

The round-trip efficiency takes into account the district heating energy supplied, and therefore it is given by equation 3.18:

$$\eta_{roundtrip} = COP_{DH} \cdot \eta_{RK} \quad (3.18)$$

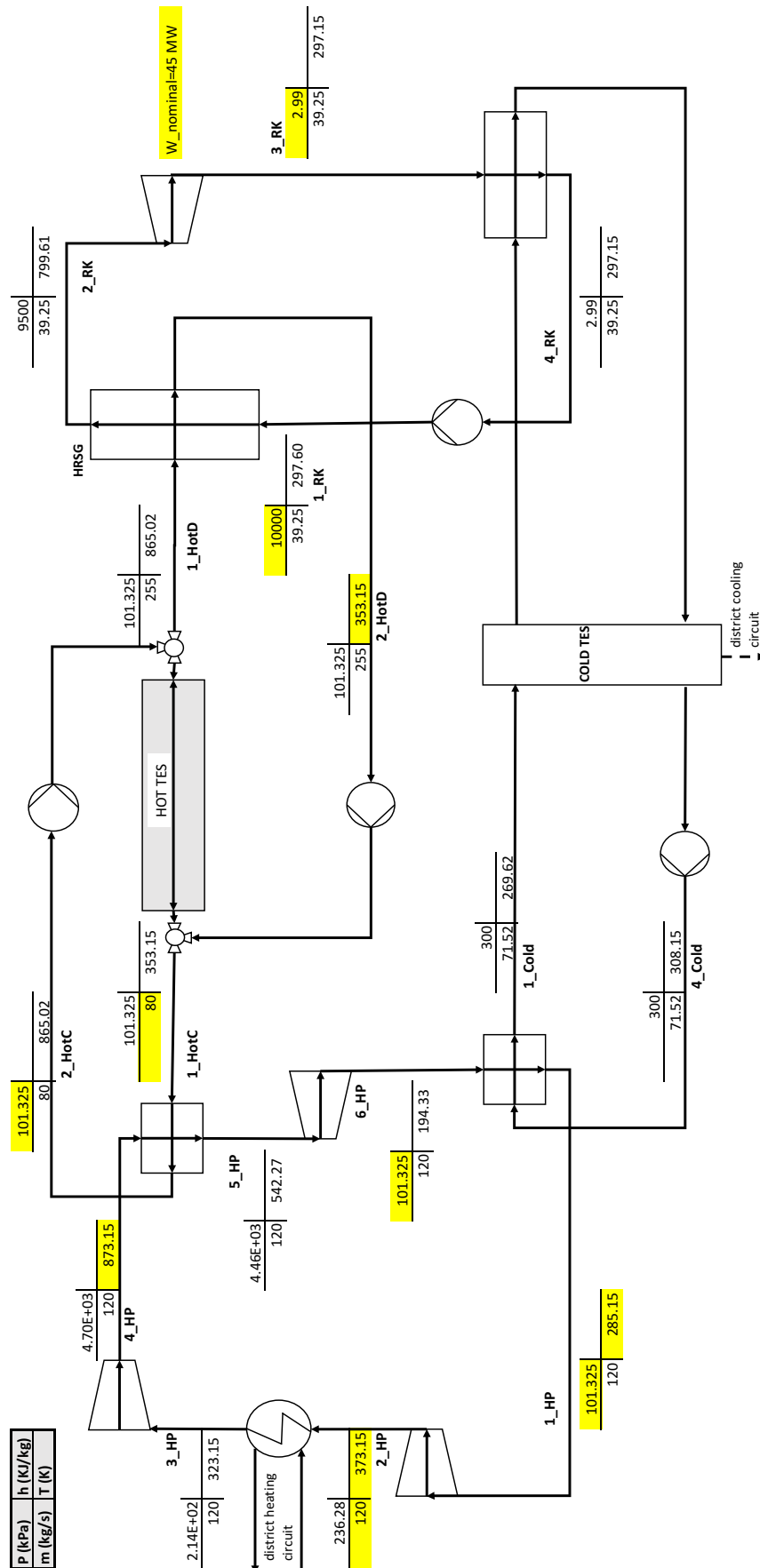


Figure 3.3. Diagram of the HP-TES configuration

3.2 Configuration 2: EH-TES

This configuration differs from the previous one since in this case the system is heated up by a high-temperature electric heater. The other components of the system remain the same as previously exposed. The discharge is still performed by means of a Rankine cycle, therefore, the model remains unvaried for the simulation of the discharge section. In order to avoid repetition, in this section are only included the expressions used for the modelling of the charging system.

3.2.1 Specific Assumptions

1. The general assumptions regarding the model are the same as in configuration 1: HP-TES (General assumptions 3.1.1)
2. The COP for the electric heater is considered unitary

Table 3.2. Input parameters of the system model EH-TES

Symbol	Value	Unit	Symbol	Value	Unit
T_{EH_1}	353.15	K	$W_{T,nominal}$	45	MW
P_{EH_1}	101.325	kPa	$x_{turbine}$	0.9	—
m_{EH}	120	kg	$U(all)$	50	W/m^2K
m_{RK}	36	kg	A_{Hex}	15000	m^2

3.2.2 Charging Unit equations

The EH-TES configuration differs from the previous one in the charging unit system. In that case, the system is heated up by a high-temperature electric heater, reducing therefore the complexity of the model. The simulation of the charging unit is performed as follows.

Electric heater

Since the COP for this device is assumed to be 1, it means that the power necessary to heat up the working fluid is exactly the same as the heat required from the fluid to reach the desired temperature. Then, rearranging formula 3.7 can be obtained expression 3.19:

$$\dot{W}_{EH} = \frac{\dot{Q}_{charge}}{COP} \quad (3.19)$$

Where \dot{Q}_{charge} is just obtained from the difference of enthalpy between the inlet and the outlet, multiplied by the mass flow of air circulating within the system.

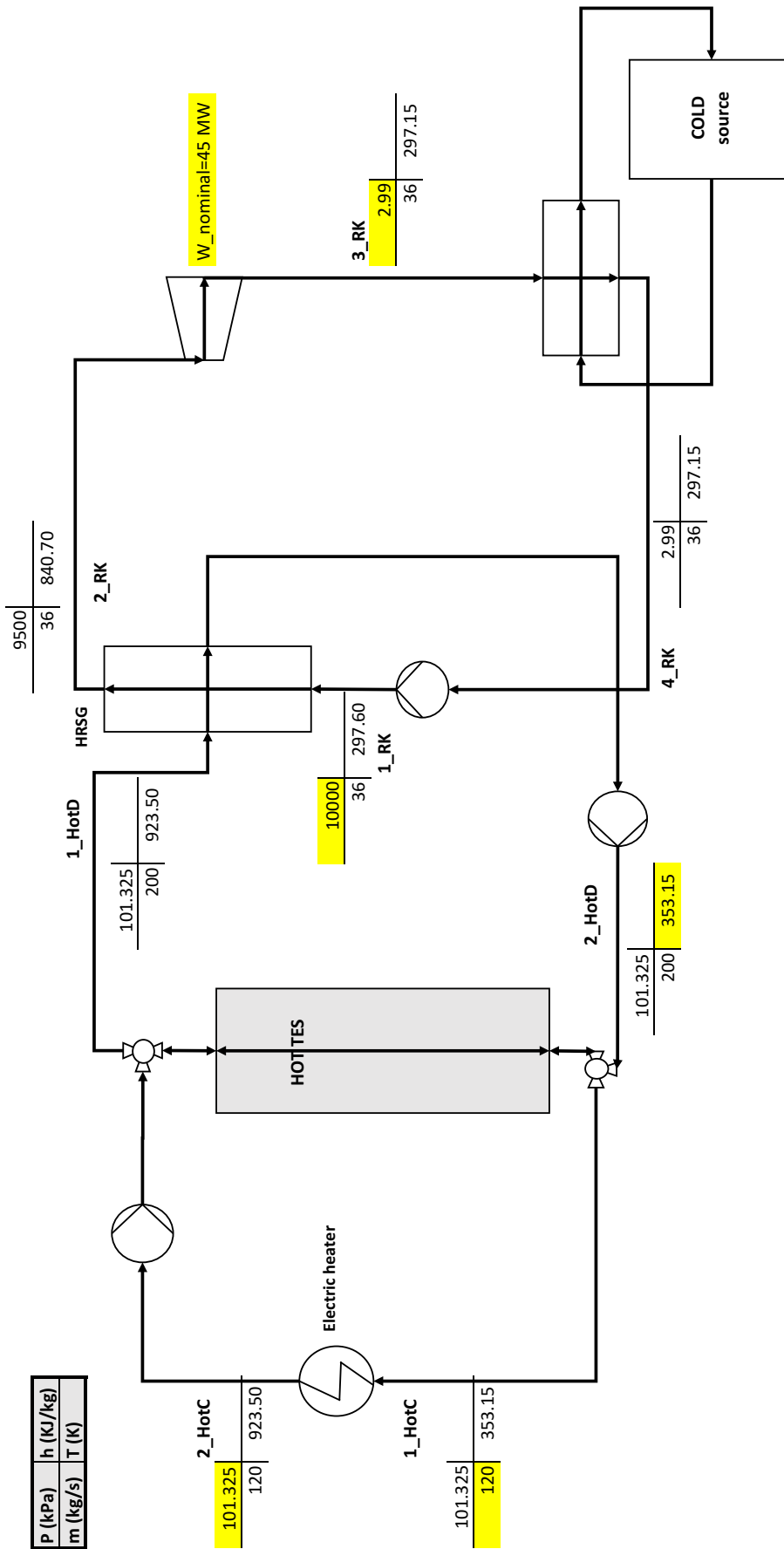


Figure 3.4. Diagram of the EH-TES configuration

3.3 Configuration 3: HPEH-TES

The idea of the HPEH-TES configuration is to merge the higher COP of the heat pump of the HP-TES with the higher maximum temperature achievable by the mean of the electric heater. The charging unit is a combination of the previous two, with the electric heater placed within the storage circuit.

3.3.1 Specific Assumptions

1. The general assumptions regarding the model are the same as in configuration 1:HP-TES (General assumptions 3.1.1)

Table 3.3. Input parameters of the system model HP-TES

Symbol	Value	Unit	Symbol	Value	Unit
$T_{HP,in}$	285	K	$W_{T,nominal}$	45	MW
$P_{HP,in}$	101.325	kPa	$quality_{turbine}$	0.9	–
m_{HP}	120	kg/s	$U(all)$	50	W/m^2K
m_{RK}	36	kg/s	A_{Hex}	15000	m^2
m_{EH}	80	kg/s			

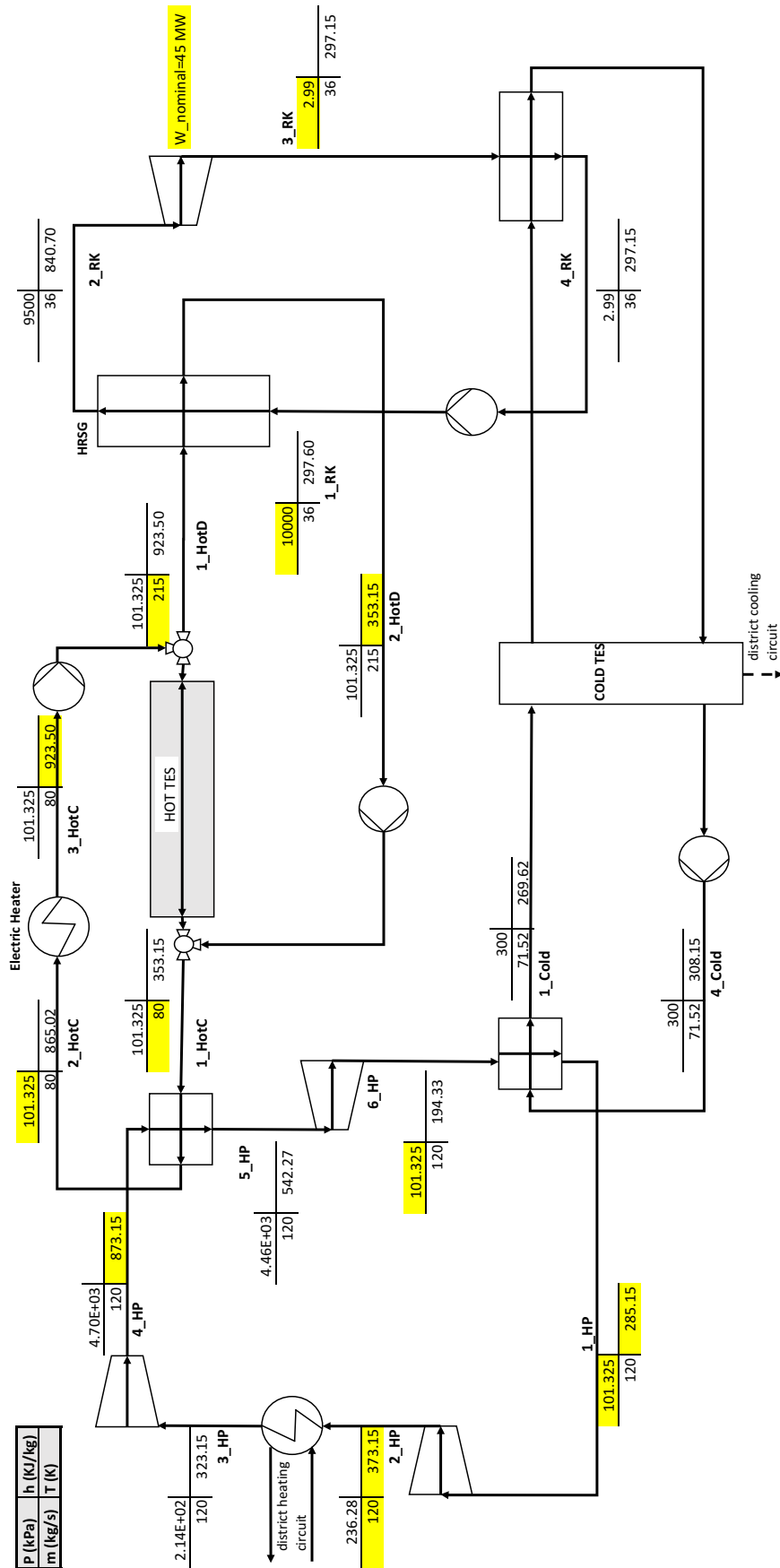


Figure 3.5. Diagram of the HPEH-TES configuration

3.4 System model: Block Diagram

Diagram 3.6 illustrates the structure for the model relative to the charge and discharge units of the system. Each block represents a function constituting the system and shows the key energy output for each component. The direction of the arrow representing the output parameter tells whether the energy needs to be added to the system or in the contrary, if it is produced by the system.

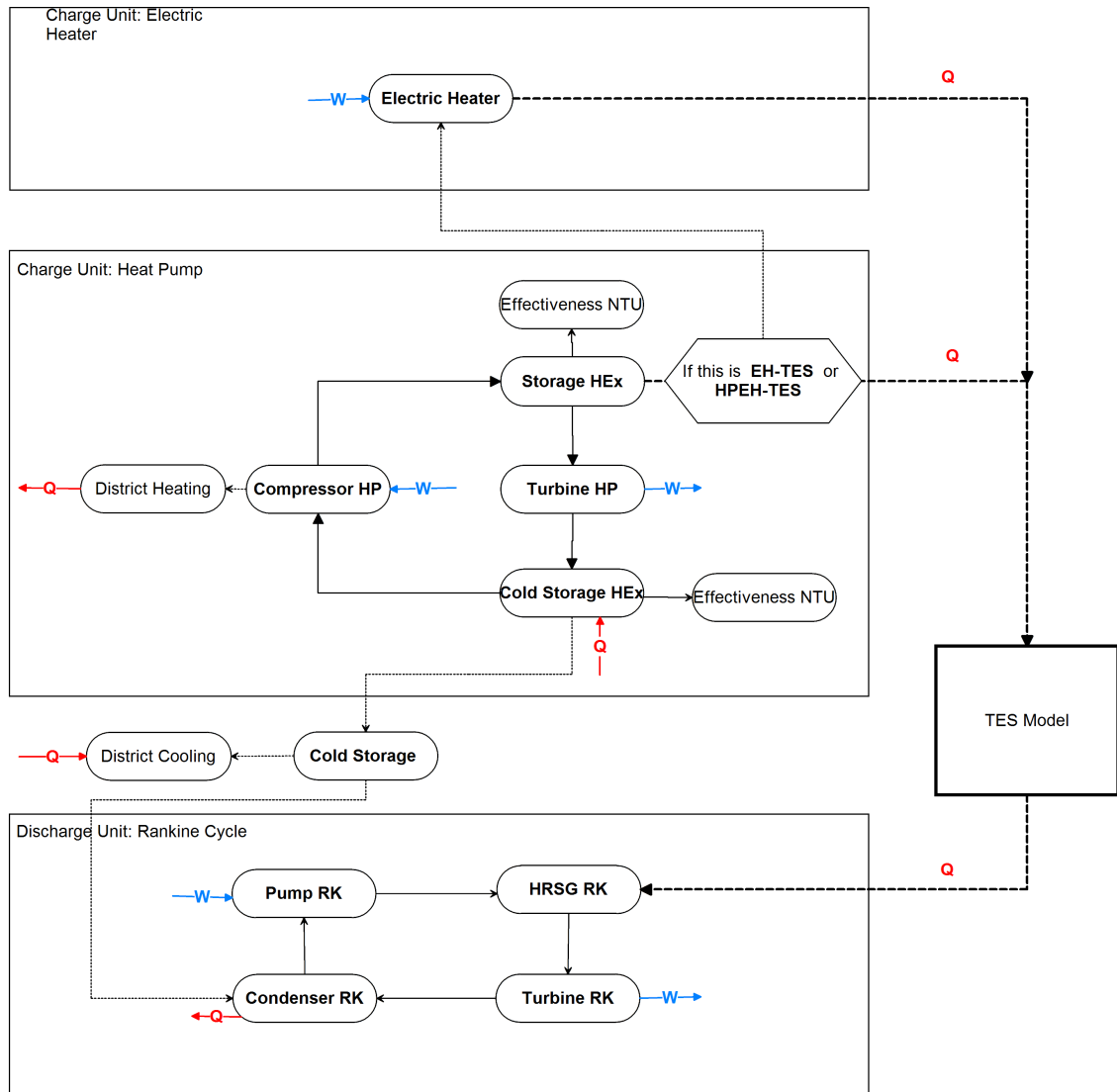


Figure 3.6. Schematic representation of the charging/discharging model

The calculation begins with the compressor, which requires power in order to elevate the pressure of the working fluid and to increase its temperature. The diagram shows the heat that is eventually leaving the system due to the district heating heat exchanger. After that, the calculation continues through the hot storage heat exchanger, which evaluates the heat that is sent to the TES model. The remaining part of the charge unit is formed by the turbine function, which produces work that is added to the compressor in order to save energy. Afterwards, the cold storage heat exchanger absorbs heat from an external source in order to heat up the working fluid to the initial conditions. This close cold

circuit can be exploited to supply district cooling for different purposes, or in particular it can be set to be the cold source for the condenser in the Rankine cycle, which would require anyway a cold source to condense the steam coming out from the turbine. In the case where the charging unit is constituted by an electric heater, the model evaluates the energy consumed by this component in order to rise the temperature of the working fluid to the desired temperature. Therefore, the heat pump functions would be bypassed for this configurations.

The calculations relative to the discharge cycle starts with the feed pump function, which determines the temperature inlet for the steam generator and the power absorbed. After that the model runs the HRSG function, whose tasks are to calculate the required heat in order to run the Rankine cycle and to couple the circuit with the outputs from the TES model, checking the results by means of an energy balance. Then the steam turbine function determines the necessary work in order to fulfil the nominal power requirement for the global system. Finally, the condenser calculates the heat of condensation and checks that the Rankine cycle is well designed by doing a global balance of all the powers involved in the system.

4 Thermal Storage Model

4.1 Literature Review

In the following section, a review of published literature within the topic of high temperature packed bed thermal energy storage system is discussed. A wide range of publications have investigated the numerical modelling of packed bed TES systems. They are all based on the work originally made by [Schumann, 1929], which describes the analytical solution for the heat transfer between a flow and a mass of crushed material through a porous prism.

[Ismail and Stuginski, 1991] compares the results of a numerical investigation of six possible models to simulate the thermal behaviour of fixed bed storage units. This comparison includes the original analytical solution by [Schumann, 1929], two unique phase models, two models taking into account the two different phases present within the storage unit (continuous and solid), and finally a concentric dispersion model. For the unique phase models it is necessary to assume the instantaneous temperature to be equal in the fluid and in the solid phase. The continuous solid phase models consider instead the two phases separately, increasing the accuracy of the solution compared to the previous one. The concentric dispersion models allow also to analyse the effects of the temperature gradient within the solid particles keeping the one-dimensional formulation.

The scientific paper [Zanganeh et al., 2012] concerns the packed bed TES for CSP applications. A TES consisting of a packed bed filled with rocks as storage material and air at ambient pressure as heat transfer fluid is taken into analysis. A 6.5 MWh pilot-scale thermal storage unit is built to support the analysis of thermoclines, and a dynamic numerical model in the range of 293-923K is made and validated for the different solid and fluid phase with variable thermo-physical properties. The model is further applied to design and simulate an industrial-scale TES unit, with 7.2 GWh of capacity during charging cycles of 8 h and discharging cycles of 16 h, with an overall thermal efficiency of 95 %. The numerical model is based on the analytical solution proposed by [Schumann, 1929], and includes 1D and 2D heat transfer model with the two different phases.

[Agalit et al., 2015] concerns a numerical investigation of high temperature packed bed TES systems for hybrid solar tower power plants. The developed model in this work is a dynamic one dimensional two phase heat transfer model, which considers variable properties for both fluid and solid phases. The model is validated with previous simulation and experimental studies. Of particular interest for this work is the second TES system described in this article, which is designed to store energy at 923K and at atmospheric pressure. Despite the low cost of a unit using rocks as storage material heated up by hot air, this technology presents some risks related to the thermal expansion of rock size during cyclic operation, which can eventually bring to mechanical breaks on the container. This phenomena has been analysed by [Dreißigacker et al., 2010] with a thermomechanical

model of the packed bed. [Agalit et al., 2015] bases its numerical model on the previous work developed by [Zanganeh et al., 2012], extending the coverage to high temperatures (up to $1273K$), and evaluating the impact on the system of the use of different materials in the storage, such as ACW ceramics, and utilizing the empirical correlation proposed by [Coutier and Farber, 1982] to calculate the volumetric heat transfer coefficient, which is based on a more in-depth experimental studies.

Another solution with similar assumptions for the high temperature TES packed bed is modelled by [Hanchen et al., 2011], which validates the simulation with an experimental setup consisting of crushed steatite at $764K$. To evaluate the charging/discharging characteristics, cyclic operations, capacity ratio and thermal efficiency, this publication describes a parameter study of packed bed dimensions, fluid flow rate and particle diameter.

4.2 Model assumptions

The developed model is based on the mathematical equations that are going to be introduced below. The main physical assumptions of the system considered are collected as follows:

1. Quasi-one-dimensional model with cylindrical geometry and axial flow direction.
2. Convection, conduction and radiation heat transfer are considered.
3. The system is divided into a two-phase model, with a solid and fluid phase.
4. The flow is considered 1D Newtonian plug flow, with variable thermo-dependent properties.
5. Uniformly packed bed with variable heat capacity and thermal conductivity but constant density for the solid phase.
6. Quartzite rock is implied as filling material for the storage
7. Temperature gradient in radial direction is neglected.
8. No heat loss through the lid and bottom
9. Temperature inside the particles is considered uniform, as long as $Bi \ll 1$
10. No internal heat generation
11. No mass transfer

4.3 Mathematical equations

The thermal energy storage model is developed based on the previous studies mentioned before. Most the modelling strategies are based on the analytical solution provided by [Schumann, 1929], in which the temperature profile of the solid and fluid phase are solved separately. The current model is especially based on the work developed by [Hanchen et al., 2011], [Agalit et al., 2015] and [Zanganeh et al., 2012].

4.3.1 Heat transfer model and boundary conditions

The developed simulation is based on a quasi-one-dimensional two-phase heat transfer process. The model investigates the heat transfer between the crushed stones which constitutes the packed-bed storage and the air flowing through the system. This analysis takes into account the unsteady-state energy equation of the convective heat transfer

between the fluid and the solid phase as well as the radiation heat transfer mechanism within the particles due to the high temperature operating range. Regarding to the axial dispersion, it is considered the conduction and radiation through the solid phase [Zanganeh et al., 2012].

Within the single particles, it is assumed a uniform temperature, therefore there is not a temperature gradient inside the stones. It is justified by a $Bi \ll 1$, which means that that the heat transfer by convection of particle has a mayor effect than the conduction inside the solid material, as shown in equation 4.1. This condition is fulfilled for all the analysed operating conditions of the system, reaching a maximum $Bi = 0.25$ in the worse case scenario. In the case of increasing the particle size diameter, it would be necessary to modify the approach analysis in order to take into account the temperature gradient within the particles.

$$Bi = \frac{h_p d}{k_s} \quad (4.1)$$

where h_p is the particle heat transfer coefficient expressed in $[W/m^2K]$ and k_s is the solid thermal conductivity in $[W/mK]$. The fluid flow within the system is considered plug flow, which simplifies the analysis as the velocity profile is assumed to be constant at any cross-section along the longitudinal axis of the storage. Therefore, the viscous and pressure terms are neglected in the model [Zanganeh et al., 2012].

Regarding to the materials properties, it is considered a temperature-dependent property change of the solid and fluid phase in the temperature range of 293-923K.

The domain consists of a cylindrical tank which is divided into a solid medium, the packed-bed filling material, and the fluid going through the void areas left between the particles. The heat transfer analysis is built based on the energy balance, which has to be fulfilled for each phase.

For the fluid phase, the net flux, \dot{Q} , in and out of the of the fluid phase is defined the energy conservation expression, [Panton, 2005], by equation 4.2:

$$\dot{Q} = \frac{\partial(\varepsilon A \rho_f h_f \delta_x)}{\delta t} + \dot{m} \frac{\partial(h_f \delta_t)}{\delta t} \quad (4.2)$$

where ε is the void fraction, A is the cross sectional area in $[m^2]$, ρ_f is the density of the fluid in $[kg/m^3]$. The first and second term on the right-hand side define the change of specific enthalpy of the fluid over time and space respectively. Where the mass flow rate is given by $\dot{m} = v \varepsilon A \rho_f$. The net flux rate has to be equal to the heat transferred to the solid phase and the losses through the wall as expressed by equation 4.3:

$$\dot{Q} = Ah_v \delta_x (T_s - T_a) + U_{wall} D \delta_x (T_\infty - T_a) \quad (4.3)$$

The first term accounts for the convective heat transfer between the fluid and the filling material of the storage, while the second term represents the heat transferred to the environment by the lateral walls. It has not been taken into consideration the energy loss by conduction throughout the lid and bottom of the storage.

Regarding to the solid phase, the energy conservation equation is presented in equation 4.4:

$$\frac{\partial((1-\varepsilon)A\rho_s u_s \delta_x)}{\partial t} = Ah_v \delta_x (T_a - T_s) + \frac{\partial}{\partial x} (k_{eff} A \frac{\partial T_s}{\partial t}) \delta x \quad (4.4)$$

where u_s is the specific internal energy in $[J/kg]$, h_v is the volumetric convective heat transfer coefficient in $[W/m^3K]$ and k_{eff} is effective thermal conductivity in $[W/mK]$. The left-hand side determines the change of internal energy with time. On the right-hand side of the expression, the first term accounts for the heat transferred by convection with the air, which is the coupling term between the solid and fluid phases. The second term describes the axial dispersion by conduction and radiation.

Figure 4.1 depicts each component of the heat transfer phenomena occurring within the thermal storage system and how the system is discretized in the x-axis.

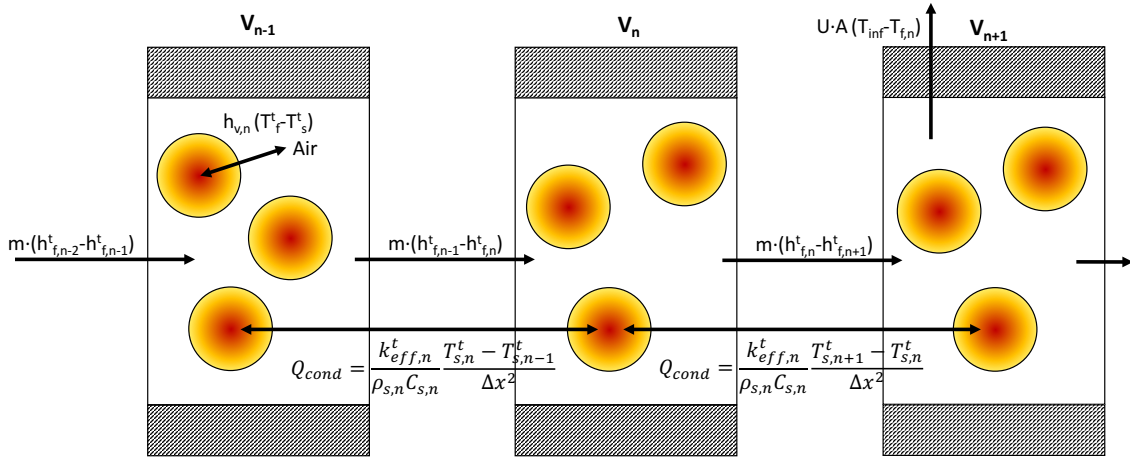


Figure 4.1. Storage finite volume method representation

In order to solve the set of equations, the boundary conditions of the system have to be set. The left-hand side boundary is constituted by the airflow inlet which charges the storage. The air is flowing to the right-hand side of the x axis. It is assumed that the temperature at the inlet of the storage is specified, corresponding to the charging temperature. With respect to the right-side boundary, the outlet of the system, it is set that there is not heat flux as shown in equations 4.5:

$$T_a(x=0) = T_{in} \quad \frac{\partial T_a(x=L)}{\partial x} = 0 \quad (4.5)$$

Regarding to the solid phase, there is no heat flux neither in the inlet or the outlet of the system, therefore the system is bounded by equal conditions at both ends as described by equations 4.6:

$$\frac{\partial T_s(x=0)}{\partial x} = \frac{\partial T_s(x=L)}{\partial x} = 0 \quad (4.6)$$

Additionally, it is necessary to establish the initial conditions of the system. Thus, the initial solid and fluid temperature distribution of the packed bed are set, nevertheless they have not to be necessarily uniform.

4.3.2 Numerical resolution

In order to solve the set of equations for T_f and T_s at the next time step, $t+\Delta t$, the finite difference method (FDM) is applied to the system in space and time obtaining equations 4.7 and 4.8 for the fluid and solid phase, derived from the equations previously shown 4.2, 4.3 and 4.4. In order to discretize the system, the storage has been divided into a number of n layers in order to calculate the thermophysical properties and temperatures at each point as shown in figure 4.2.

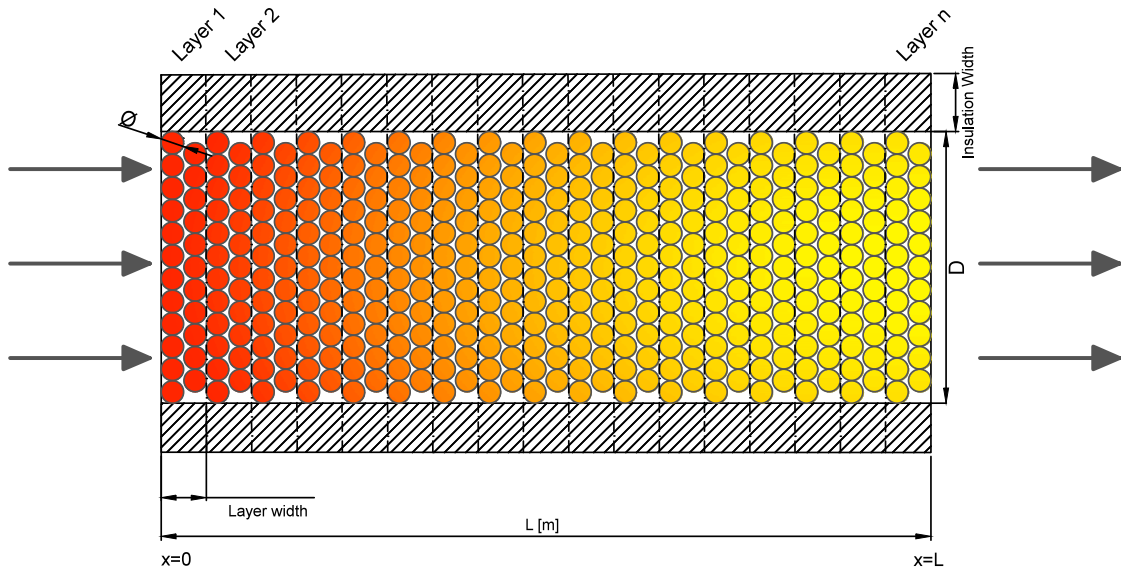


Figure 4.2. Storage discretization

For the fluid phase time derivative, it has been taken out from the derivative the void fraction and the cross-section area as they are independent of time. It is applied a first-order forward difference in time, and first-order backward difference in space for the first derivatives [Zanganeh et al., 2012], [Agalit et al., 2015]. Equation 4.2 and 4.3 become:

$$\varepsilon_n A_n \rho_{f,n}^t \frac{h_{f,n}^{t+1} - h_{f,n}^t}{\Delta t} + \dot{m}^t \frac{h_{f,n}^t - h_{f,n-1}^t}{\Delta x} = A_n h_{v,n}^t (T_{s,n}^t - T_{f,n}^t) + U_{wall,n}^t D (T_\infty - T_{f,n}^t) \quad (4.7)$$

The subscript n and t denote the spatial and temporal position respectively. Regarding the solid phase expression, the rocks density is not varying with time [Somerton, 1992], but the effective thermal conductivity does indeed. A first-order forward difference in time for the first derivative and second order central difference in space for the second derivative is applied [Zanganeh et al., 2012], equation 4.4 becomes:

$$(1-\varepsilon)\rho_s \frac{u_{s,n}^{t+1} - u_{s,n}^t}{\Delta t} = h_{v,n}^t (T_{f,n}^t - T_{s,n}^t) + \left(\frac{k_{eff,n}^t (T_{s,n+1}^t - T_{s,n}^t) - k_{eff,n-1}^t (T_{s,n}^t - T_{s,n-1}^t)}{\Delta x^2} \right) \quad (4.8)$$

The specific enthalpy of the fluid phase and the internal energy of the solid are determined by equations 4.9 and 4.10 [Zanganeh et al., 2012]:

$$h_f = \int_{T_{ref}}^T c_{p,f} dT \quad (4.9)$$

$$u_s = \int_{T_{ref}}^T c_s dT \quad (4.10)$$

The temperature dependent parameters for the fluid phase are obtained from the software REFPROP and by its implementation in MATLAB.

For the solid phase, C_s is calculated according to [Kelley, 1960] correlation to extrapolate the results experimentally obtained by [Zanganeh et al., 2012]. The heat capacity, k_s variation is extrapolated from experimental data by means of Tikhomirov's correlation [Somerton, 1992]. The mentioned correlations will be further introduced in the following section.

Equations 4.7 and 4.8 now can be solved explicitly for $h_{f,n}^{t+1}$ and $u_{s,n}^{t+1}$, for each time-step and every layer of the storage. In order to calculate the temperature at each instant and position, the known correlations of $c_{p,f}$ and c_s has to be evaluated. One possible option is to use a numerical method such as Newton-Raphson in order to obtain the temperature profile. Due to the fact of the high computational requirements to execute the mentioned procedure at every time-step, it has been decided to implement a polynomial fitting to obtain the inverse function [Agalit et al., 2015]. Therefore, the simulation time is reduced twenty-two times compared to the Newton-Raphson method with a deviation of 0.05°C and 0.1°C for the solid and fluid temperature profile respectively, as stated by [Agalit et al., 2015]. The specific enthalpy of the fluid and specific internal energy of the solid are approximated by the polynomials expressed by equations 4.11 and 4.12 [Agalit et al., 2015]:

$$T_f(K) = 1.732e^{-17}h_f^3 - 1.088e^{-10}h_f^2 + 1.016e^{-3}h_f + 271.814 \quad (4.11)$$

$$T_s(K) = 2.139e^{-28}u_s^5 - 5.408e^{-22}u_s^4 + 6.908e^{-16}u_s^3 - 7.406e^{-10}u_s^2 + 0.00137u_s + 278.541 \quad (4.12)$$

Figure 4.3 shows the variation of the specific enthalpy of the fluid and specific internal energy of the solid as function of the temperature:

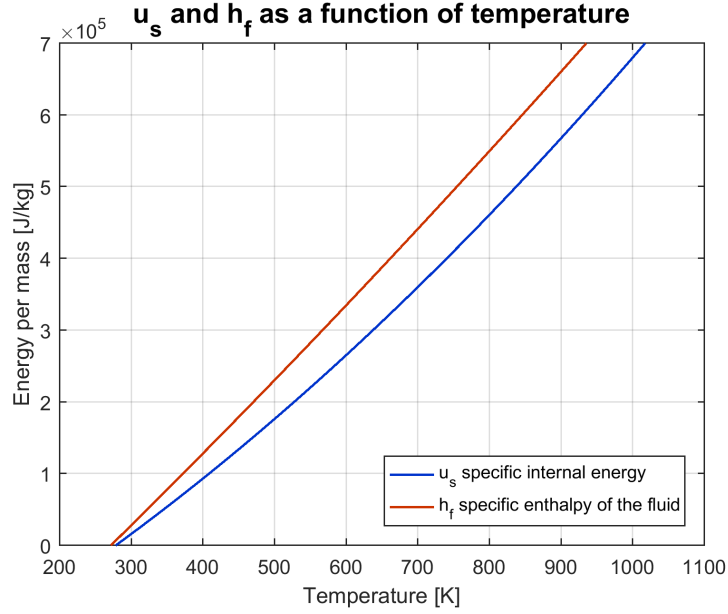


Figure 4.3. Specific enthalpy of the fluid and specific internal energy of the solid as function of the temperature

Due to the large variation of the thermophysical properties of the solid and fluid phase, the temperature dependent coefficients are updated every time-step for every layer at the new conditions.

In order to ensure the numerical stability of the calculations, the more restrictive Courant-Friedrichs-Lewy condition [Courant et al., 1928] for the fluid and solid phases are applied. As reported by Von Neumann stability analysis [J.D.J.Anderson, 1995] on the equations 4.7 and 4.8 neglecting the source term, the criteria are shown in equations 4.41 and 4.40:

For the fluid phase:

$$CFL = \frac{v\Delta t}{\Delta x} < 1 \quad (4.13)$$

For the solid phase:

$$\Delta t < \frac{1}{2}\Delta x^2 \frac{(1-\varepsilon)\rho_s C_s}{k_{eff}} \quad (4.14)$$

4.3.3 Thermophysical properties

Due to the large range of temperature operation of the thermal storage, it is necessary to take into account the variation of the temperature dependent parameters for both the solid and the fluid phase.

Fluid phase

The selected working fluid for the system is air, since the storage works at ambient pressure. Due to its size a complete airtight system would not be feasible. During the charging and discharging process, the temperature inside the TES ranges between 293-923K, leading to considerable properties change that cannot be neglected. Hence, four main temperature dependent working fluid properties are calculated: density, ρ_f , heat capacity, C_f , thermal conductivity, k_f and dynamic viscosity, μ_f .

It can be seen in figures 4.4 and 4.5 how the density becomes almost one third of the original value with an increase of 630 degrees. The dynamic viscosity as well doubles its initial value at 293K with the same temperature increase.

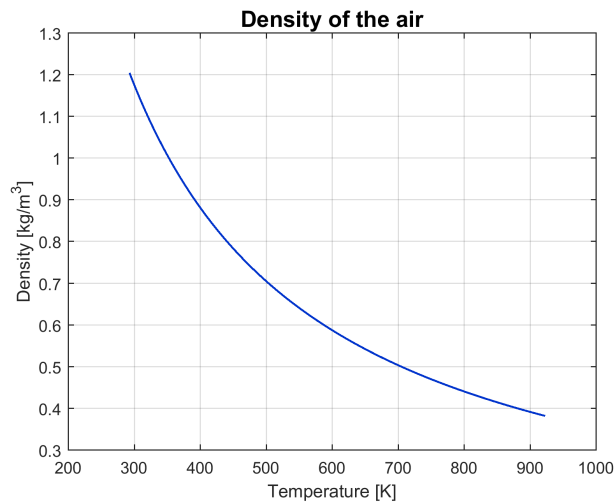


Figure 4.4. Density of the air

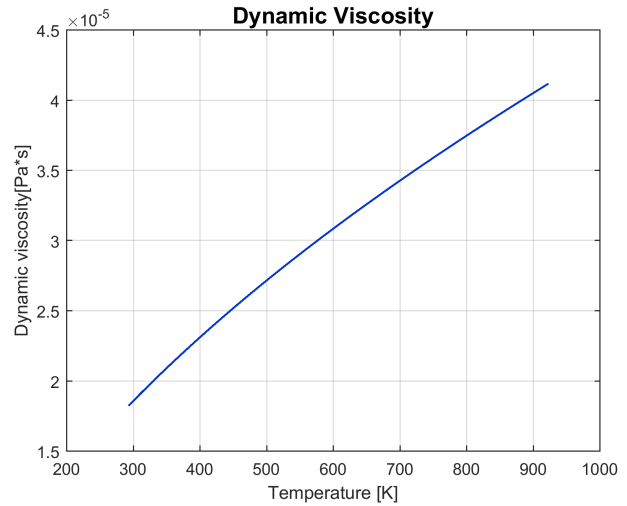


Figure 4.5. Dynamic viscosity of the air

Regarding to the C_f and k_f , both of them follow the same increasing trend with a rising temperature as shown in figure 4.6:

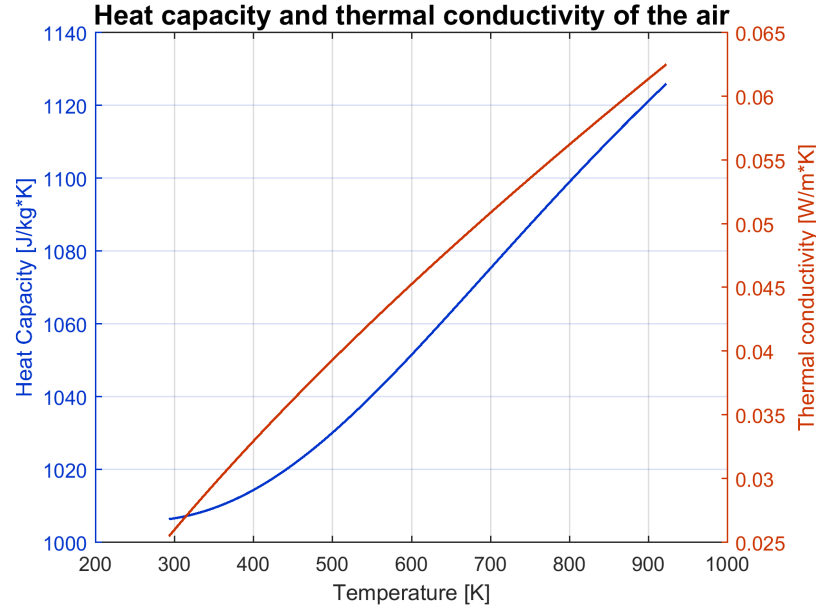


Figure 4.6. Heat capacity and thermal conductivity of the air

Solid phase

The thermal properties of the Quartzite rocks have been obtained experimentally and extrapolated for the temperature operating range of 293-923K by [Zanganeh et al., 2012]. The thermal conductivity of the solid material has been determined by means of the Tikhomirov's correlation [Somerton, 1992] and extrapolated to 923K, as shown in equation 4.15:

$$k(T) = k_{20} - 1.10e^{-3}(T - 293)(k_{20} - 1.38) \left[k_{20}(1.70e^{-3}T)^{-0.25k_{20}} + 1.28 \right] k_{20}^{-0.65} \quad (4.15)$$

Where k_{20} is the thermal conductivity at ambient temperature, and T in K. It can be seen in figure 4.7 the reduction of the thermal conductivity with and increasing temperature.

The heat capacity of the filling material has been experimentally analysed by [Zanganeh et al., 2012] and the results are extrapolated up to 923K by means of [Kelley, 1960] correlation, as shown in equation 4.16:

$$C_s(T) = 705 \left(1 + 6.14e^{-4}T + \frac{1.93e^4}{T^2} \right) \quad (4.16)$$

In that case, the heat capacity behaviour is opposite to the thermal conductivity. It increases with temperature by nearly 60% increase with a temperature rise from 293 to 923K.

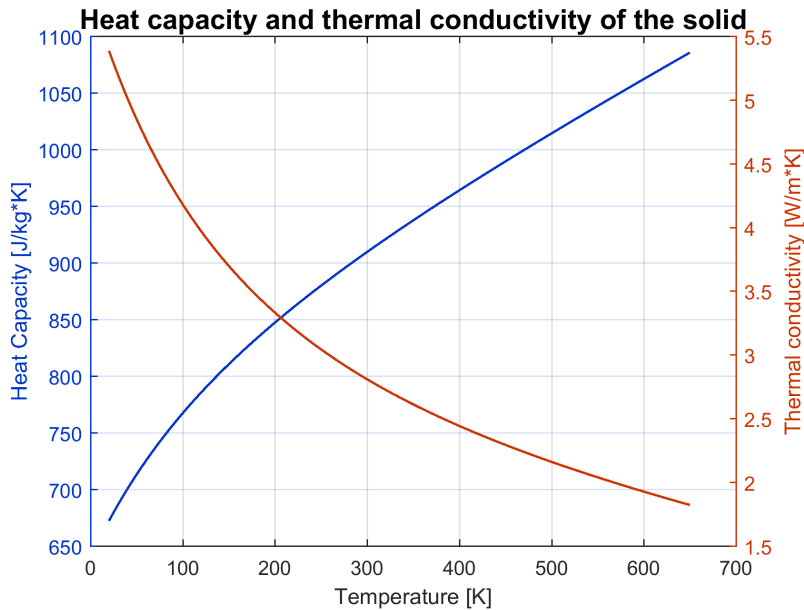


Figure 4.7. Heat capacity and thermal conductivity of the solid

4.3.4 Physical correlations

Volumetric heat transfer coefficient

The convective heat transfer mechanism has been extensively studied, and many correlations have been developed, such as [Coutier and Farber, 1982] and [R.Pfeffer, 1964]. Two different approaches are investigated in this work, based on the reported analysis developed by [Agalit et al., 2015] and [Zanganeh et al., 2012]:

[Agalit et al., 2015] considered a constant volumetric heat transfer coefficient within the packed bed. This approach accounts for the heat transfer between the solid phase and the fluid based on the correlation developed by [Coutier and Farber, 1982] which accounts for the convective heat transfer. This correlation has been previously used in similar numerical investigations, and provides a good match between experimental and theoretical results [Hanchen et al., 2011].

$$h_v = 700 \left(\frac{G}{d} \right)^{0.76} \quad (4.17)$$

The second chosen approach has been studied by [Zanganeh et al., 2012], it considers the convective heat transfer mechanism and the effective thermal conductivity on the packed bed which also includes the effect of heat transfer by radiation. The correlation shown in equation 4.18 was developed by [R.Pfeffer, 1964], which applies for small Reynolds number and $Pe \gg 1$.

$$h_p = 1.26 \left[\frac{1 - (1.\varepsilon)^{\frac{5}{3}}}{W} \right]^{\frac{1}{3}} (C_p G)^{\frac{1}{3}} \left(\frac{k}{d} \right)^{\frac{2}{3}} \quad (4.18)$$

Where $W = 2 - 3\gamma + 3\gamma^5 - 2\gamma^6$ with $\gamma = (1 - \varepsilon)^{\frac{1}{3}}$. Furthermore, the particle and the volumetric convective heat transfer coefficients are related by equation 4.19:

$$h_v = h_p \frac{6(1 - \varepsilon)}{d} \quad (4.19)$$

Effective thermal conductivity

Regarding to the effective thermal conductivity in the packed bed, it is considered the effect of the heat transfer by radiation, since the system operates at temperatures in the order of 873 K. Therefore, this effect has to be considered within the charging and discharging process. Consequently, the Kunii and Smith correlation is implemented, as it considers the thermal conductivity of the solid and fluid phases, as well as the radiative heat transfer [Kunii and Smith, 1960] and [Yagi and D.Kunii, 1957], as shown in equations from 4.20 to 4.24:

$$k_{eff} = k_f \left[\varepsilon \left(1 - \beta \frac{h_{rv}d}{k_f} \right) + \frac{\beta(1 - \varepsilon)}{\frac{1}{\phi} + \frac{h_{rs}d}{k_f} + \gamma \left(\frac{k_f}{k_s} \right)} \right] \quad (4.20)$$

The void to void radiative heat transfer coefficient, h_{rv} , is expressed by equation 4.21:

$$h_{rv} = \left[\frac{0.1952}{\left(1 + \frac{\varepsilon}{2(1-\varepsilon)} \frac{1-\varepsilon_s}{\varepsilon_s} \right)} \right] \left(\frac{T_f}{100} \right)^3 \quad (4.21)$$

The solid surface to solid surface radiative heat transfer coefficient, h_{rs} , is determined by equation 4.22:

$$h_{rs} = 0.1952 \left(\frac{\varepsilon_s}{2 - \varepsilon_s} \right) \left(\frac{T_s}{100} \right)^3 \quad (4.22)$$

Where ε_s is the emissivity of the rocks and β is defined as the ratio of the average length between the distance of the centre between two neighbour solid particles and the mean diameter of the particles. These values indicate how tight or loose is the packing within the rock-bed. The parameter γ relates the ratio of the length of the solid which is affected by the thermal conductivity with the mean particle diameter. The factor ϕ is defined in order to account for the effective thickness of the fluid adjacent to the contact surface of two solid particles, which is expressed by equation 4.23:

$$\phi = \phi_2 + (\phi_1 - \phi_2) \frac{\varepsilon - \varepsilon_2}{\varepsilon_1 - \varepsilon_2} \quad (4.23)$$

Where ε_1 and ε_2 represent the two extreme cases of void fraction. These parameters are calculated by equation 4.24:

$$\phi_i = \frac{1}{2} \frac{\left(\frac{\kappa-1}{\kappa}\right) \sin^2 \theta_i}{\ln(\kappa - (\kappa - 1)) - \frac{\kappa-1}{\kappa} (1 - \cos \theta_i)} - \frac{2}{3} \frac{1}{\kappa} \quad (4.24)$$

With $\kappa = k_s/k_f$ and $\sin^2 \theta_i = 1/n_i$. n accounts for the number of contact points on a semispherical surface between the solid particles of the storage.

Radiation plays a relevant role in the heat transfer process at high temperatures, increasing the heat exchanged within the particles. Figure 4.8 depicts the effective heat transfer coefficient as function of temperature, as well as the contribution of the conduction and radiation to the effective thermal conductivity. It can be seen that radiation reaches a higher contribution at temperatures higher than 473K, while conduction reduces its contribution.

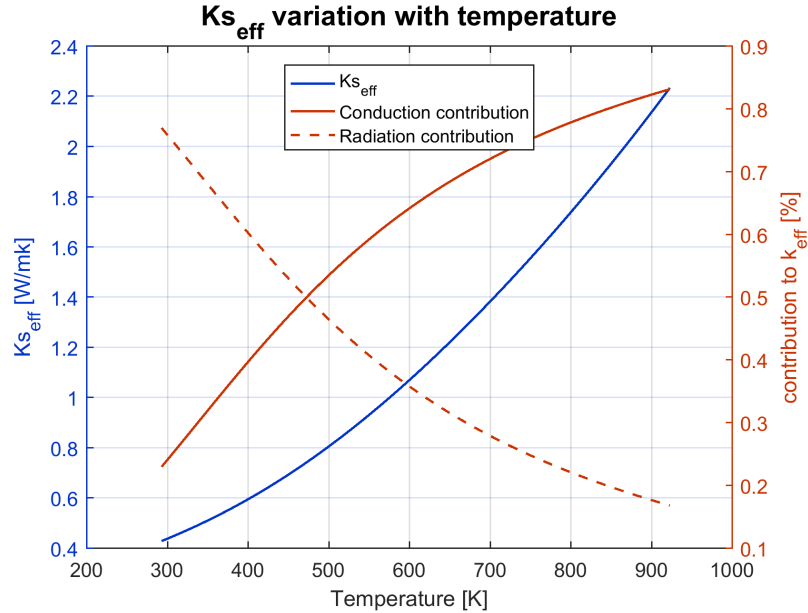


Figure 4.8. Effective thermal conductivity coefficient and

Thermal wall losses

Regarding to the heat loss to the environment, the heat transfer through the lateral walls is analysed. It has to be mentioned that the energy losses through the lid and bottom of the storage are not considered. The overall heat loss coefficient is given by equation 4.25 [T.L Bergman, 2011]:

$$\frac{1}{U_{wall}} = \frac{1}{\alpha_{inside}} + r_{inside} \sum_{j=1}^n \frac{1}{k_{j+1}} \ln \frac{r_{j+1}}{r_j} + \frac{1}{\alpha_{outside}} \quad (4.25)$$

With n the number of layers of insulation. The first term on the right-hand side corresponds to the convective heat transfer in the inner side of the wall, the second one to the conductive heat transfer within the insulation and the last one to the convective heat transfer to the environment. The Nusselt number related to the convective heat transfer at the inner side corresponds to equation 4.26 [Beek, 1962]:

$$Nu = 3.22Re^{\frac{1}{3}}Pr^{\frac{1}{3}} + 0.117Re^{0.8}Pr^{0.4} \quad (4.26)$$

In order to account for the heat transferred to a particle and to a wall, the previous expression is multiplied by a factor of 0.8 [Beek, 1962], therefore equation 4.26 constituting the convective heat transfer coefficient inside the storage becomes 4.27:

$$\alpha_{inside} = \left(\frac{k_f}{d}\right) 2.58Re^{\frac{1}{3}}Pr^{\frac{1}{3}} + 0.094Re^{0.8}Pr^{0.4} \quad (4.27)$$

The convective heat transfer on the outside of the tank is given by equation 4.28 [Serth and Lestina, 2014] for $Re < 5 \cdot 10^5$:

$$\alpha_{outside} = \left(\frac{k_a}{D}\right) (0.664Re^{\frac{1}{2}}Pr^{\frac{1}{3}}) \quad (4.28)$$

Where the mean outside velocity is considered equal to $5m/s$ with constant thermophysical properties. The Reynolds number Re_{∞} is given by equation 4.29:

$$Re_{\infty} = \frac{Dv_{\infty}\rho_a}{\mu_a} \quad (4.29)$$

where μ_a is the dynamic viscosity of the fluid, expressed in $[Pas]$

Pressure drop

The pressure loss along the storage initially has been calculated from the equation developed by [Ergun, 1952], as shown in equation 4.30:

$$\Delta p = \frac{LG^2}{\rho d} \left(150 \frac{(1-\varepsilon)^2}{\varepsilon^3} \frac{\mu}{Gd} + 1.75 \frac{1-\varepsilon}{\varepsilon^3} \right) \quad (4.30)$$

Where the first and second term in the brackets accounts for the viscous and kinetic energy losses respectively and G is the specific mass flow rate per unit of surface (cross-section) in $[kg/(m^2s)]$. The pressure loss is calculated at every time-step for each layer since it is dependent on the dynamic viscosity which depends on temperature.

Equation 4.30 has been modified by several authors, mainly in order to better estimate the numerical coefficients 150 and 1.75, which are not taking into account the variation of porosity. [Wu et al., 2008] expresses the coefficients in function of the tortuosity τ and β , both depending on the porosity. These parameters are defined as follows, in equations 4.31 and 4.32:

$$\tau = \frac{1}{2} \cdot \left[1 + \frac{1}{2} \cdot \sqrt{1-\varepsilon} + \sqrt{1-\varepsilon} \cdot \frac{\sqrt{\left(\frac{1}{\sqrt{1-\varepsilon}} - 1\right)^2 + \frac{1}{4}}}{1 - \sqrt{1-\varepsilon}} \right] \quad (4.31)$$

$$\beta = \frac{1}{1 - \sqrt{1-\varepsilon}} \quad (4.32)$$

As it is possible to see from the equations, both parameters are function of the void fraction ε . [Ergun, 1952] equation including the influence of this parameters becomes equation Ergun-Wu 4.33:

$$\frac{\Delta p}{L} = 72\tau \frac{(1-\varepsilon)^2}{\varepsilon^3} \frac{\mu U}{d^2} + 0.75\tau \frac{\rho(1-\varepsilon)}{\varepsilon^3} \cdot \frac{U^2}{d} \cdot \left(\frac{3}{2} + \frac{1}{\beta^4} - \frac{5}{2\beta^2} \right) \quad (4.33)$$

A comparison of the result achieved by the two different approaches is described in section 5.1.

Process efficiency

Along the operational cycles of the thermal storage, the system efficiency during the charging and discharging process must be evaluated.

The charging efficiency corresponds to the fraction stored in the rock-bed (and the air in between the rocks) at the end of the process compared to the net thermal energy introduced to the system, as shown in equation 4.34 [Zanganeh et al., 2012]:

$$\eta_{charging} = \frac{E_{stored}}{E_{Net.input} + E_{fan.charging}} \quad (4.34)$$

Where the energy consumed by the fan is described by equation 4.35:

$$E_{fan.charging} = \sum_{i=0}^{T_{charging}} \frac{\Delta p_i \dot{m} \Delta t}{\rho_f \eta_{fan} \eta_{Rankine}} \quad (4.35)$$

Where the input energy is $E_{Net.input} = E_{input} - E_{output}$. The energy consumed by the fan considers the required thermal energy for the Rankine cycle to produce the electrical energy consumed [Zanganeh et al., 2012].

Equivalently, the discharging efficiency is defined as the percentage of recovered energy to the stored plus the pumping energy:

$$\eta_{discharging} = \frac{E_{recovered}}{E_{stored} + E_{fan.charging}} \quad (4.36)$$

Loss fraction and capacity ratio

The energy losses of the system are constituted by the thermal losses through the lateral walls. The fraction of losses are defined by equations 4.37 and 4.38 for the wall and fan respectively:

$$f_{WallLoss} = \frac{E_{WallLoss,cycle}}{E_{NetInput}} \quad (4.37)$$

$$f_{fan} = \frac{E_{fan}}{E_{NetInput}} \quad (4.38)$$

The capacity ratio indicates to which percentage the storage has been charged, compared to the theoretical maximum energy that can be stored, defined by equation 4.39:

$$\sigma = \frac{E_{stored}}{E_{stored,max}} \quad (4.39)$$

4.4 Numeric assumptions

For the development of the thermal storage, some of the system parameters have been set based on previous studies and physical properties of the materials. The values are collected in table 4.1:

Table 4.1. Numeric assumptions [Zanganeh et al., 2012]

Symbol	Value	Unit	Symbol	Value	Unit
d	0.03	m	ϵ_s	0.85	(-)
p	101.325	kPa	β	0.9	(-)
T_{amb}	285	K	k_{20}	5.39	$\frac{W}{mK}$
ρ_s	2618	$\frac{kg}{m^3}$	γ	$\frac{2}{3}$	(-)
ε	0.342	(-)	n_1	1.5	(-)
ε_1	0.476	(-)	n_2	$4\sqrt{3}$	(-)
ε_2	0.26	(-)			

4.5 TES model: Block Diagram

The diagram shown in figure 4.9 depicts the simulation strategy followed to obtain the temperature profile of the system along the charging and discharging process, as well as the stored energy and pressure drop.

The model is initialized by specifying the initial temperature of the solid and fluid phases. Complementary, it has to be defined the simulation parameters which determines the number of spatial divisions for the discretization, the duration of the simulation and the time-step length. It has to be noticed that the numerical stability has to be fulfilled as mentioned in subsection 4.3.2. The inlet conditions of the flow that are introduced to the system have to be determined by means of the temperature and entering mass flow.

Should be noticed that the pressure inside the storage is considered constant, therefore the properties of the solid and fluid phases only depend on the temperature at each point.

Once that the different parameters have been initialized (at $t = 0$), the charging process takes place. As mentioned in subsection 4.3.2, $h_f = \int_{T_{ref}}^T c_{p,f} dT$ and $u_s = \int_{T_{ref}}^T c_s dT$ are calculated by a polynomial approximation function which is initialize for the temperature range at which the system operates. At this point, the time loop starts with the calculation of the enthalpy of the fluid at each layer for the first time-step. Then, the internal energy of the solid phase is evaluated as well for each layer.

Once that the new h_f and u_s are known at each layer for the current time-step, the temperatures of the solid a fluid phase are calculated by means of the polynomial approximation. It must be noticed that the entering mass flow is flowing to the positive direction of the x axis, increasing first the temperature of the left-hand side of the storage.

At this point of the simulation, the temperature profiles are obtained. The next step of the process is to update the properties within the system. Regarding to the fluid phase the air properties (ρ_a, C_a, K_a, μ_a) are updated at the given temperature at each point. With respect to the solid phase, the temperature dependant properties (C_s, K_s) are calculated. It is updated as well the effective thermal conductivity coefficient, $k_{s,eff}$, since it depends on the temperature as well as the solid and fluid properties. Furthermore, at each time-step the pressure drop is calculated based on the properties of the fluid phase, and the energy stored in the rock-bed is evaluated.

After that the temperatures of both phases are determined, the time step is increased and the calculation process starts again. The simulation keeps calculating until the simulation is completed. Figure 4.9 illustrates the calculation procedure for the heat transfer simulation of the thermal energy storage system.

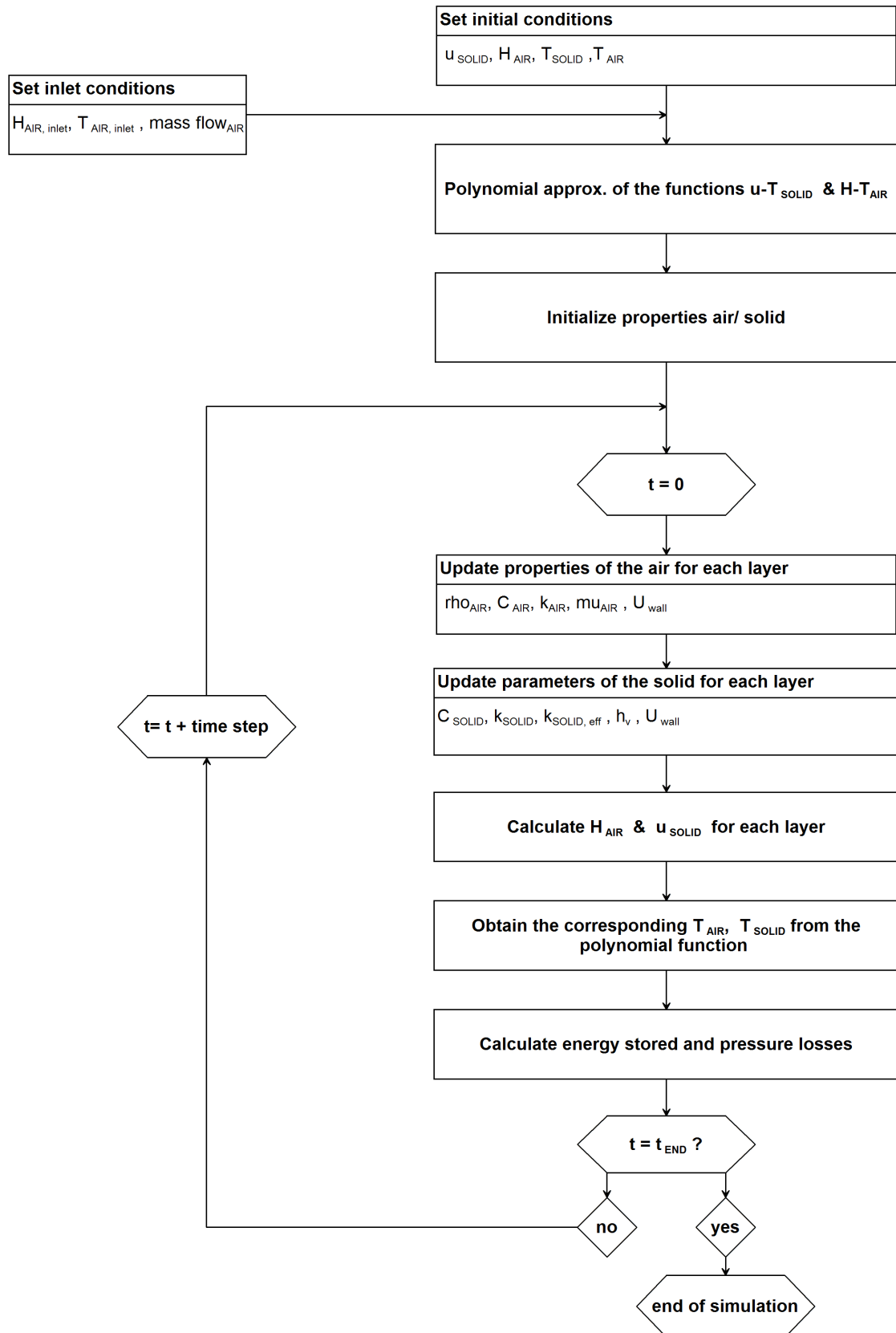


Figure 4.9. Schematic representation of the TES model

4.6 TES model validation

The current simulation tool has been developed in MATLAB R2016b combined with REFPROP in order to obtain the thermodynamic properties of the working fluid. The model enables the prediction of the thermodynamic behaviour of the packed-bed storage and the system performance for different charging and discharging cycles.

The simulation tool requires a number of input parameters in order to obtain the desired results, as shown in figure 4.10. The inputs are constituted by the geometry, the operational conditions, the temporal and space subdivision, the boundary conditions and the thermo-physical correlations for the fluid and solid phases. The outputs of the simulation tool are the temperature profiles, stored and input energy, losses, efficiencies, required fan energy and capacity ratio.

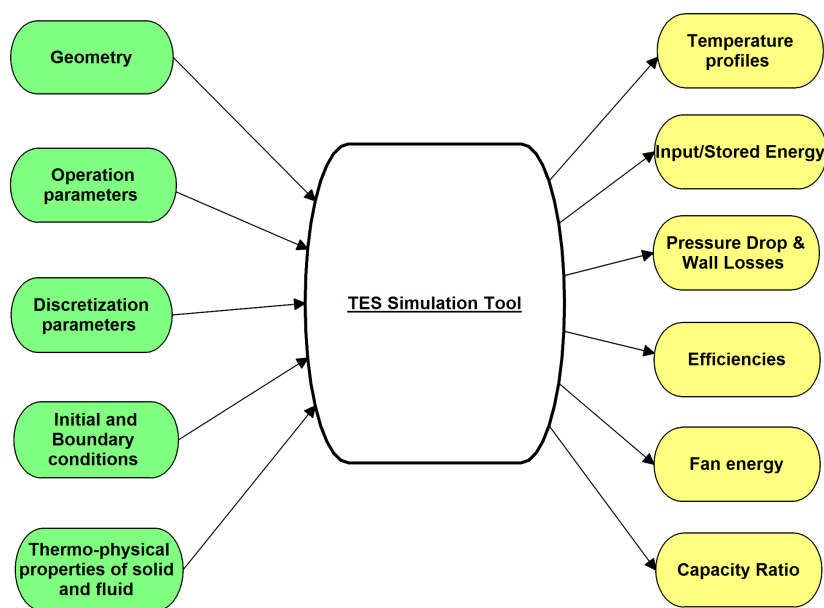


Figure 4.10. Inputs and outputs of the simulation tool

Several models for the heat transfer phenomena have been developed, but most of them assume temperature-invariant properties for the fluid and solid phases [Hanchen et al., 2011], [Meier et al., 1991]. This assumption could lead to important deviations with a large temperature operational range. Currently the only model which takes into consideration the variability of the thermo-physical properties is the one developed by [Zanganeh et al., 2012] and [Agalit et al., 2015]. This second one is actually built on the mathematical expressions stated by the first. It should be mentioned that [Zanganeh et al., 2012] has been validated with own experimental data in order to assess the accuracy of the developed model. Regarding to [Agalit et al., 2015], the model has been validated based on experimental data acquired by [Meier et al., 1991] and with [Zanganeh et al., 2012] results.

As previously mentioned, [Agalit et al., 2015] is based on the previous work developed by [Zanganeh et al., 2012], which obtains slightly different results. This deviation could be motivated by the different considerations made in the analysis which are collected in table 4.2.

Table 4.2. Validation parameters comparison

<i>Parameter</i>	[Zanganeh et al., 2012]	[Agalit et al., 2015]	Own calculations
<i>Filling material</i>	Not specified	Quartzite rock	Quartzite rock
<i>Fluid properties</i>	Polynomial	Polynomial	REFPROP
<i>h_f and u_s calculation</i>	Newton-Raphson	Polynomial	Polynomial
<i>Lid and bottom heat losses</i>	Considered	Not considered	Not considered
<i>Insulation prop/geom</i>	Not specified	Not specified	Specified
<i>Charging time</i>	8 hours	8 hours	8 hours
<i>h_v</i>	Variable	Constant	Constant/Variable

One of the assumptions with a higher influence is that different expressions are selected for the calculation of the volumetric heat transfer coefficient h_v . [Zanganeh et al., 2012] chooses [R.Pfeffer, 1964] correlation, which is dependent on the heat capacity of the air that changes over time. Regarding to [Agalit et al., 2015] instead, this parameter is evaluated following the [Hanchen et al., 2011] approach, which considers the volumetric heat transfer coefficient as temperature-independent. Figure 4.11 compares the results obtained by [Zanganeh et al., 2012] and [Agalit et al., 2015] with the calculations done in the current work.

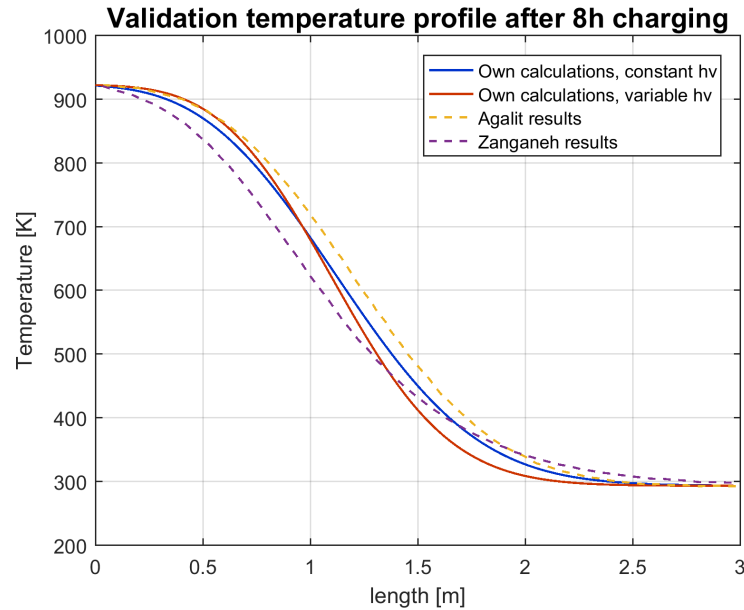


Figure 4.11. TES model validation

It should be noticed that it is simulated the heat transfer process with the two mentioned correlations for the volumetric heat transfer coefficient as mentioned in section 4.3.4. The results obtained with a constant h_v are closer to the reference data, therefore it has been decided to set a constant h_v for now on in the TES simulations. The corresponding simulation settings has been set in accordance to the reference, as shown in table 4.3.

Table 4.3. Dimensions and operating parameters of the TES system [Zanganeh et al., 2012],[Agalit et al., 2015]

<i>Geometry</i>		<i>Operating parameters</i>	
L	3 m	T_{ch}	923K
D	3m	T_{amb}	293K
d	0.03m	t_{ch}	8h
V	$21m^3$	m_{ch}	0.4 kg/s
ε	0.342	Pressure	101.325 kPa

Figure 4.11 shows a slight deviation from [Agalit et al., 2015], whose settings are similar to the current calculations. This can be motivated by the following reasons: i) The thermodynamic properties of the fluid have been determined by means of the software REFPROP; ii) The thermodynamic properties are updated every $0.1K$; iii) The insulation properties and geometrical characteristics are not specified in the sources. Considering the mentioned points, and due to the reduced deviation from the reference values, the simulation tool is validated for the temperature dependent thermo-physical properties with a constant h_v . In order to fully validate the developed simulation tool, experimental analysis at higher scale and with closer operating conditions should be performed, to be able to contrast the obtained results.

4.6.1 Grid independence

In order to justify the number or layer in which the storage is divided, four simulations are carried out with different discretion parameters. The charging process is simulated with the geometry configuration from table 4.3 for 25.5 *hours* with 50, 100, 200 and 300 grid points. From the obtained results the fluid temperature is compared for the different four cases. It can be observed in figure 4.12 the convergence of the temperature profiles with an increasing number of grid points.

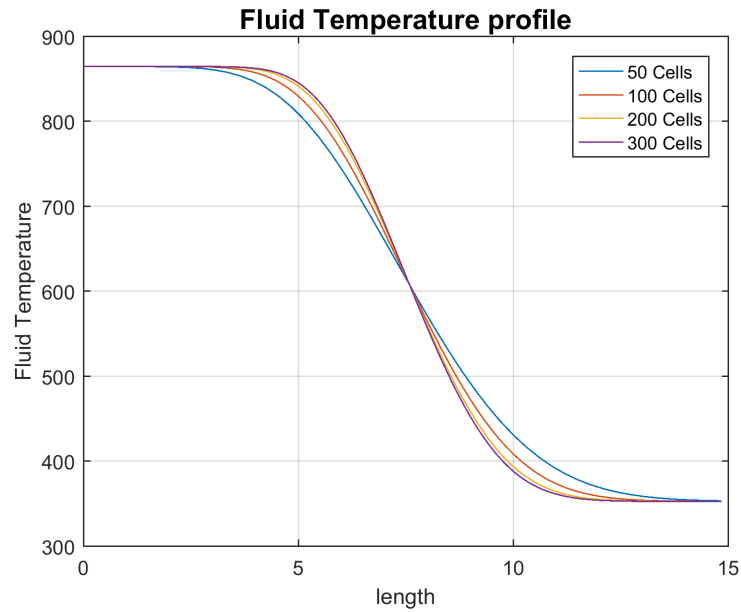


Figure 4.12. Comparison of the temperature profiles with different number of grid points

It has to be noticed the reduction of the deviation with the increasing number of grid points, achieving accurate results with 200 and 300 divisions. In order to evaluate this deviation, the average root mean square is performed with respect to the most refined grid. In all cases has been used a uniform time-step of $0.02s$, with a maximum CFL=0.35 in the case of 300 grid points. The normalised results are shown in figure 4.13, where it can be noted the convergence of the results with an increasing number of grid points. Due to the rise of the computational time with the refinement of the grid, the selection of the number of layers is a trade-off between accuracy and computational time. 200 grid points have been therefore chosen for the analysis of the system.

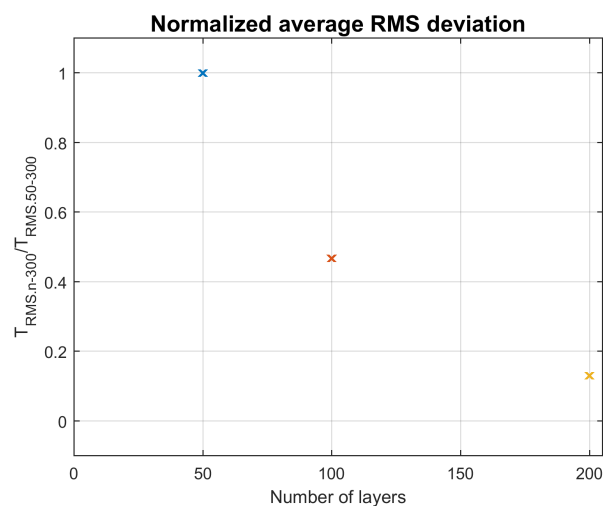


Figure 4.13. Normalised average RMS deviation

4.6.2 Time resolution

The *Von Neuman Stability Method* is used to ensure the stability of the difference scheme applied to the solid phase, which is frequently used to study the stability properties of linear partial differential equations. This method determines the maximum allowed Δt for a given Δx , satisfying equation 4.40 as mentioned in subsection 4.3.2:

$$\Delta t < \frac{1}{2} \Delta x^2 \frac{(1 - \varepsilon) \rho_s C_s}{k_{eff}} \quad (4.40)$$

As long as the condition is fulfilled, the error will not grow for the subsequent steps in t , and the numerical solution will proceed in a stable manner. Otherwise, if the condition is not satisfied, the error will progressively increase until the solution will "blow up" [J.D.J.Anderson, 1995].

Regarding to the stability condition for the fluid phase, the condition which has to be fulfilled in order to achieve a solution with a stable proceed manner, is the the more restrictive Courant-Friedrichs-Lewy(CFL) condition [Courant et al., 1928], as previously mentioned in subsection 4.3.2. It represents the ratio between the time and the residence time in a finite volume. Therefore, from that relation can be determined the minimum time-step required, as shown in equation:

$$CFL = \frac{v \Delta t}{\Delta x} < 1 \quad (4.41)$$

In the case of study, the most restrictive condition which determines the maximum time-step for the set grid is the fluid phase stability condition. That corresponds to a $CFL = 0.235$ with $\Delta t = 0.02s$, 200 cells and $\Delta x = 0.0717m$

4.6.3 Energy balance

The simulation is developed on a explicit scheme. This method is based on a backward differencing and its Taylor series truncation error accuracy is first-order with respect to time [Versteeg and Malalasekera, 2007]. This low level of accuracy could lead eventually to deviations during the simulations. In order to ensure the correct value of the calculations, it is evaluated the energy unbalance of the simulations. Therefore, regarding to the charging process, it is detected an imbalance of 0.0025% of the total energy introduced to the system. That miss-match could be caused by three different reasons: i) the inaccuracy of the mathematical procedure due to the explicit scheme, ii) a rounding effect as MATLAB works with a limited accuracy, or iii) the properties of the solid and fluid phase are evaluated at every 0.1K temperature change.

Another reason for the mentioned imbalance is the fact that the temperature of the solid and the fluid are approximated to the corresponding temperature by a polynomial correlation, which could lead to inaccuracies in the energy balance. Due to the reduced miss-match it is assumed the validity of the results. Despite that fact, it is recommended the improvement of the enthalpy calculation by means of a numerical method in order to

obtain more precise results. Complementary, it is reasonable to calculate the solid and fluid properties at each time-step if the calculation time is not a limiting factor.

4.6.4 Optimization of the computational time

As mentioned in subsection 4.3.2, the specific enthalpy of the fluid h_f and the specific internal energy of the solid phase are calculated by an approximation of the inverse polynomial function of equations 4.9 and 4.10 based on [Agalit et al., 2015]. This approximation is calculated in the temperature range between 285-923K. Within this temperature range, the temperature is then divided into small intervals and then the images of the obtained points are calculated using equations 4.9 and 4.10. The obtained functions can be treated as quasi-linear and bijective, consequently each point of the divided interval has a unique image.

By this approximation, it is avoided the use of a numerical method such as Newton-Raphson for each time-step, which would lead instead to an increase of the computational requirements. Therefore, the simulation time is reduced twenty-two times compared to the mentioned method with a deviation of 0.05K and 0.1K for the solid and fluid temperature profile respectively, as stated by [Agalit et al., 2015].

In order to further reduce the computational requirements, the code is implemented in the way that for each time-step the temperature-dependent parameters are updated only for the layers in which is detected a temperature increase of more than a set value (for the developed model, 0.1K). In this way it is considerably reduced the number of calculations for each time-step.

5 Analysis and optimisation

The developed simulation tool enables the study of the different system parameters and operating conditions. The thermal energy storage and the charging and discharging units are designed based on the limiting factors which determine the performance. A parametric study is carried out in order to analyse the sensitivity of different parameters of the system.

5.1 Geometry of the TES

The TES constitutes the core component of the thermal storage plant. Its function is to store the electrical energy as heat within the storage filling material. It is necessary to ensure an efficient storage system with a reduced pressure drop and an optimized system performance.

5.1.1 TES limitations

The storage unit design is determined by the amount of energy to store, the filling material properties, the range of operating temperatures and the maximum pressure drop.

Natural rocks are a potential candidate for the thermal storage, due to the low cost and the high availability in nature. The chosen filling material for the current storage system is Quartzite rocks, due to its suitability for sensible storage application with an ambient temperature up to $923K$ [Allen et al., 2015]. In order to reduce the storage volume, other materials could be considered such as encapsulated phase change materials, with a significant increase of the cost.

The maximum energy which is possible to store is limited by the maximum and minimum operating temperatures. These are determined by the highest temperature achievable by the charging unit and the minimum temperature of the air returning from the HRSG. Therefore, if that temperature span is higher, the required volume of the TES would be reduced. Hence, as mentioned in section 2.2, it is possible to achieve a higher temperature when the electric heater is used as charging unit (EH-TES and HPEH-TES configurations) as shown in table 5.1. This would lead to higher TES energy capacity, regardless that the minimum temperature remains constant.

The main objective of the TES is to provide the highest temperature for the longest period to the HRSG in order to produce electricity at the highest Rankine efficiency. Consequently, it is preferable that the storage unit is designed with a longitudinal shape, increasing the useful area before the fluid temperature outlet starts to decrease. Hence, a smaller cross section in order to increase the length is preferable but, at the same time, this parameter is determined by the maximum admissible pressure drop.

Another limitation to the system operation is constituted by the thermal cracking of the filling material when a numerous charging and discharging cycles are performed. In

accordance to [Hall and Andre, 2001], quartzite and taconite are less susceptible to thermal shock failure than basalt. This characteristic makes that material suitable for the purpose of thermal storage with a low degradation.

TES dimensioning

The TES volume depends on the power output of the bottoming cycle and the number of working hours of the system. The thermal power in [W] required by the HRSG is determined by expression 5.1:

$$\dot{Q}_{HRSG} = \frac{\dot{W}_{rk}}{\eta_{rk}} \quad (5.1)$$

The mass flows for the charging and discharging process are determined by the enthalpy change and the required/provided power from the charging and discharging unit 5.4:

$$\dot{m}_{ch} = \frac{\dot{Q}_{Charging.Unit}}{h_{a.Tmax} - h_{a.Tmin}} \quad \dot{m}_{disch} = \frac{\dot{Q}_{HRSG}}{h_{a.Tmax} - h_{a.Tmin}} \quad (5.2)$$

where $h_{a.T}$ are the maximum and minimum enthalpies of the air in the storage, expressed in [J/kg]. The required energy to store can be calculated by equation 5.3:

$$Q_{storage} = \frac{\dot{W}_{T,rk}}{\eta_{rk} t_{discharging}} \quad (5.3)$$

where $\dot{W}_{T,rk}$ is the power output from the steam turbine, η_{rk} is the Rankine cycle efficiency and $t_{discharging}$ is the time of discharge (24 hours) expressed in [s]. From the required energy to store, it can be calculated the required charging time in [s] by expression 5.4:

$$t_{ch} = \frac{Q_{storage}}{\dot{m}_{ch}(h_{a.Tmax} - h_{a.Tmin})} \quad (5.4)$$

Consequently, the storage volume can be calculated from the change of internal energy of the solid and enthalpy of the fluid as shown in equation 5.5. This is determined by the charging and discharging temperature of the TES at each configuration as shown in table 5.1. The calculated volume corresponds to the maximum energy that can be stored from a complete charge and a complete discharge. In the real process that would probably not be achieved as the last period of charging and discharging requires longer time. Therefore, complete cycle will not be feasible, leading to the necessity of an oversizing of the TES for the storage of the same energy amount.

$$V_{storage} = \frac{Q_{storage}}{(\rho_s(1 - \varepsilon)(u_{s.Tmax} - u_{s.Tmin})) + (\rho_a \varepsilon (h_{a.Tmax} - h_{a.Tmin}))} \quad (5.5)$$

Once that the minimum required volume of the TES has been determined, the cross section and length of the system are determined by the pressure drop. According to the expression defined by equations 4.30 [Ergun, 1952] and 4.33 [Wu et al., 2008], the pressure drop is calculated evaluating it at the mean temperature. The results are shown in figure 5.1:

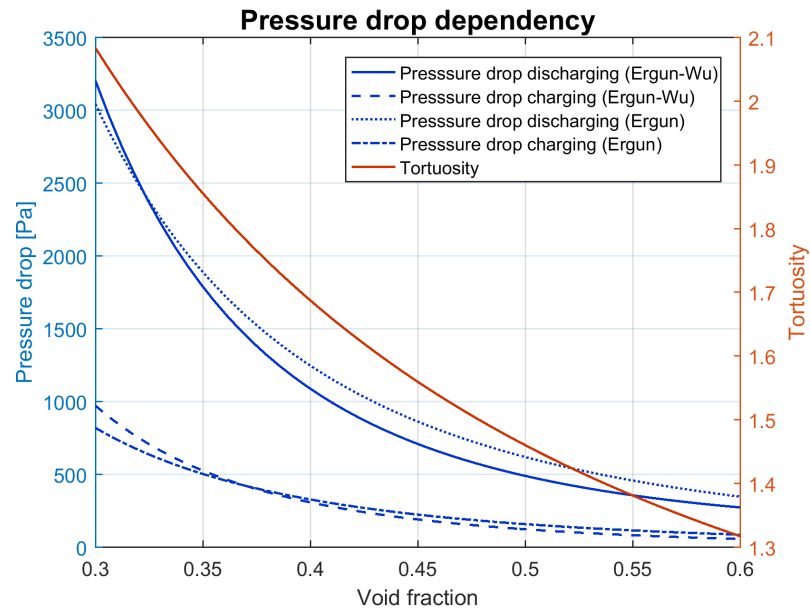


Figure 5.1. Pressure drop over time evaluated with [Ergun, 1952] and [Wu et al., 2008]

Because of the more accurate assumptions, the pressure drop evaluated by [Wu et al., 2008] has been chosen to define the geometry of the storage unit. The obtained pressure drop corresponds to an approximation of the expected results obtained in the simulations as it is evaluated at the mean temperature.

5.1.2 Particle size effect

The particle size affects the temperature profile shape of the TES. The smaller the particle diameter, the steeper is the thermocline [Hanchen et al., 2011]. This leads to a smaller temperature difference between the solid and the fluid phase, which is a proof of a higher heat transfer by convection between the solid and the fluid. On the other hand, the smaller the particle size, the higher pressure drop is produced. Figure 5.2 shows the pressure drop corresponding to the mass-flows for the charging and the discharging for particle diameters ranging between 1 to 40mm.

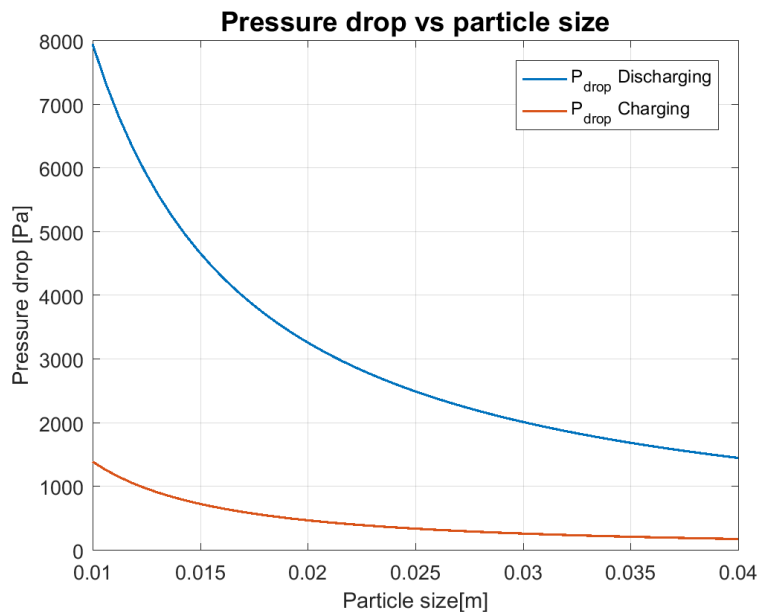


Figure 5.2. Pressure drop as function of the particle size

In order to obtain a reduced pressure drop, it has been decided to select a particle size of 30mm for the design of the TES.

5.1.3 Void fraction effect

The criteria established for the maximum admissible pressure drop in the TES is that the equivalent thermal energy consumed by this component should be less than the 2% of the stored energy. In order to reduce the height of the TES, it has been decided to divide the storage into 2 parallel units. Having a configuration in parallel of both units, it is possible to reduce the cross section per unit with the pressure drop. Hence, the mass flow is divided between the two TES units as well. It can be evaluated the pressure drop as function of the void fraction and radius of the TES as shown in figure 5.3.

It is represented the feasible combinations of radius of the TES and the void fractions to obtain a pressure drop lower than the maximum value set. Based on the fact that the selected particle diameter is 0.03m, the corresponding void fraction is $\varepsilon = 0.342$ as stated by [Zanganeh et al., 2012] from experimental results.

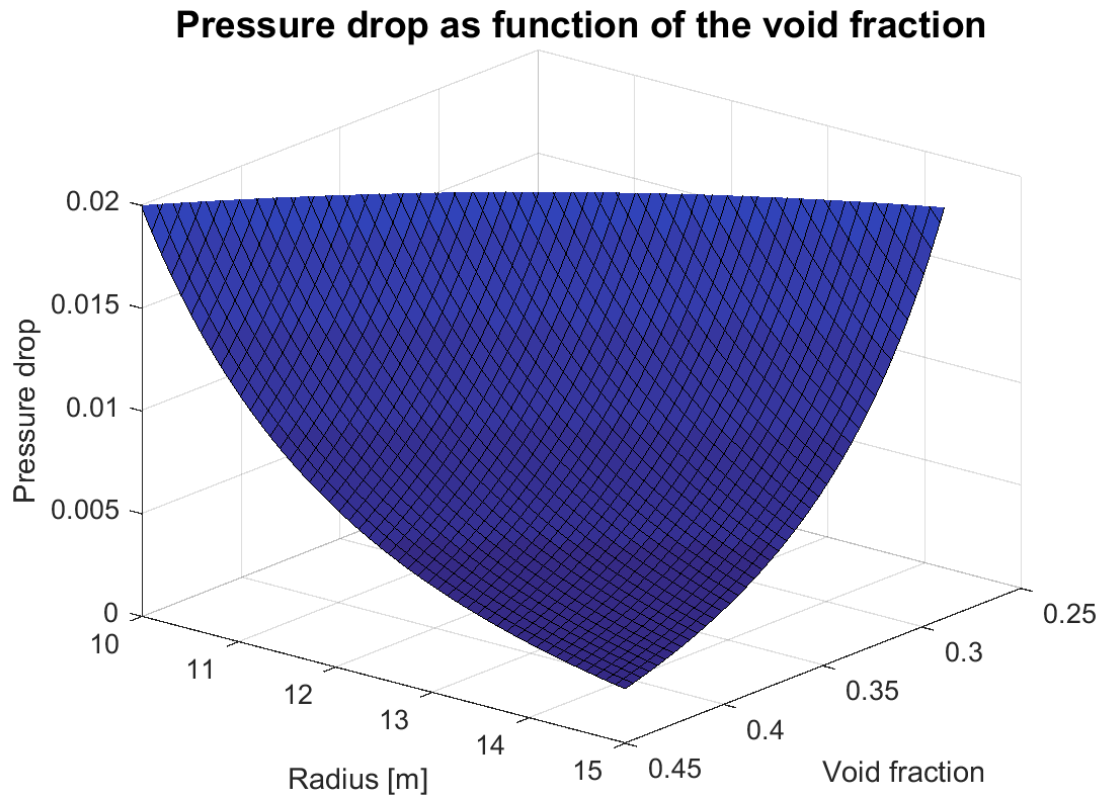


Figure 5.3. Pressure drop as function of the TES radius and the void fraction

5.1.4 TES cross section effect

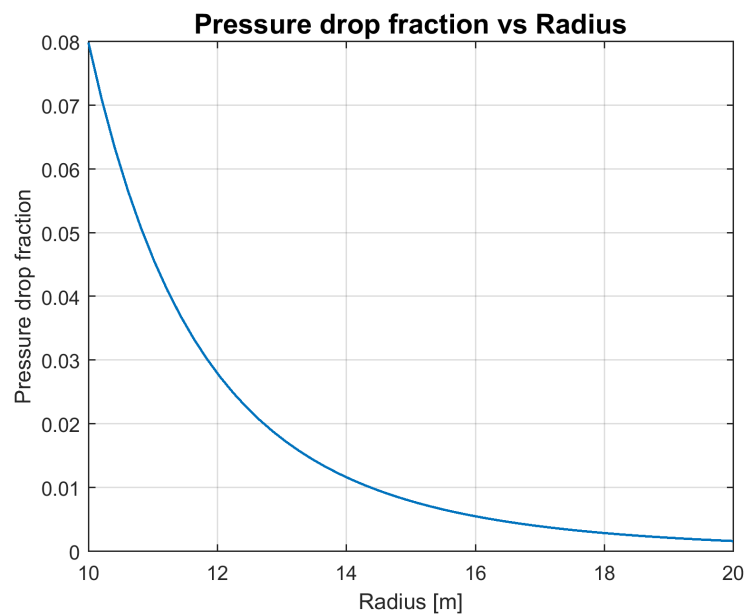


Figure 5.4. Pressure drop as function of the TES radius with $\varepsilon = 0.342$

In figure 5.4 the pressure drop with $\varepsilon = 0.342$ as function of the radius is represented. From the obtained values, it has been concluded that the minimum required radius of the

TES is $12.73m$. In order to be able to store the required calculated energy, the length of the system is $14.34m$. That lead to a total TES volume of $7300 m^3$.

The obtained geometrical and operational parameters for the three different configurations are collected in table 5.1. It should be mentioned that the obtained values are calculated for a mean temperature.

Table 5.1. Operating parameters of the different configurations

	Conf I	Conf II	Conf III	Units
T_{charging}	865.02	923.5	923.5	K
$T_{\text{discharging}}$	353.15	353.15	353.15	K
T_{ambient}	285.15	285.15	285.15	K
t_{charging}	76.50	51.65	77.47	h
$t_{\text{discharging}}$	24	24	24	h
m_{charging}	80/2	120/2	80/2	kg/s
$m_{\text{discharging}}$	255/2	215/2	215/2	kg/s
$P_{\text{loss ch(mean T)}}$	<0.5%	<0.5%	<0.5%	[-]
$P_{\text{loss disch(mean T)}}$	<2%	<2%	<2%	[-]
N° units	2	2	2	[-]
Length	14.34	14.34	14.34	m
Radius	12.73	12.73	12.73	m
Volume	7300	7300	7300	m^3
ε	0.342	0.342	0.342	[-]
ρ_{solid}	2618	2618	2618	kg/m^3
Insulation thickness	1	1	1	m
$E_{\text{stored.max total}}$	3.31	3.75	3.75	GWh

5.2 System: Parametric Analysis

The charging and discharging units define the performance of the system enabling the conversion of electric energy into heat and vice-versa. It is of great importance to be able to achieve the optimum thermodynamic conditions in order to be able to store and extract the energy from the TES in the most efficient way. Therefore, in the following subsections, the main parameters that affect the system performance are analysed.

5.2.1 Charging unit maximum temperature

This section investigates the effects on the system of the highest temperature of the charging unit cycle.

In the heat pump configuration, the fluid temperature at the last stage outlet of compression, named as $T_{HP,4}$ in chapter 3.1.1, corresponds to the maximum temperature of the charging unit. Regarding to the electric heater configuration, this temperature corresponds to the temperature out of the electric heater itself. In order to provide an immediate picture of the behaviour of the system on the temperature variation, the efficiencies depict properly the system behaviour in order to develop the analysis.

Figure 5.5 shows the impact of the temperature at the outlet of the compressor on the COP. The blue line corresponds the COP in the simple case, while the dotted red line corresponds to the COP including the heat supplied for district heating. In fact, the intercooling required in between the stages of the compressor provides the the energy supplied for the district heating network, increasing at the same time the overall heat pump efficiency.

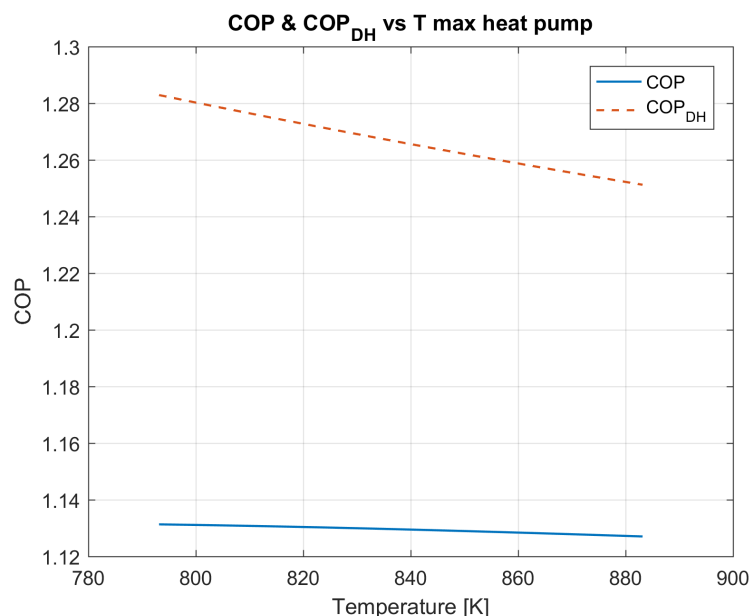


Figure 5.5. COP and COP_{dh} as function of the maximum temperature of the heat pump

The maximum temperature achievable in the heat pump is set to $873K$, due to the limitations of the heat exchangers involved in the process. The plot describes how the

efficiency of the heat pump decreases linearly together with the increase of the maximum temperature.

After the analysis of the COP behaviour, it is interesting to study the effect of the maximum temperature of heat pump compared to the electricity to electricity efficiency as well as on the round-trip efficiency. Figure 5.6 and 5.7 illustrate the performance of the system with and without district heating supply. It should be noticed that higher charging temperatures lead to higher operational temperatures in the bottoming cycle. Hence, while the heat pump efficiency decreases when it works at higher temperatures, the Rankine efficiency increases, but in a major grade. Therefore, the trend of the overall efficiency in both figures is increasing with temperature since the increase of the Rankine cycle efficiency has a major effect on the overall plant compared to the heat pump.

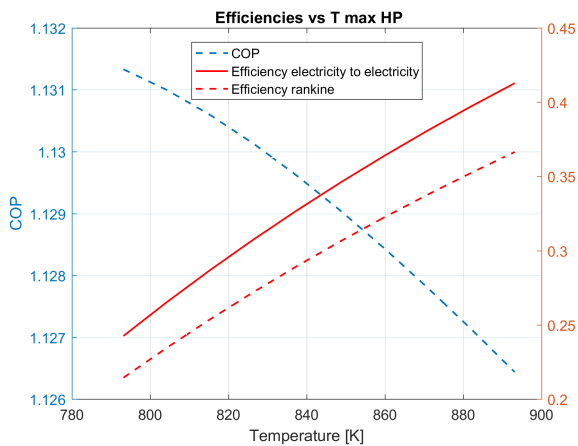


Figure 5.6. COP and Efficiencies simple case vs Temperature max heat pump

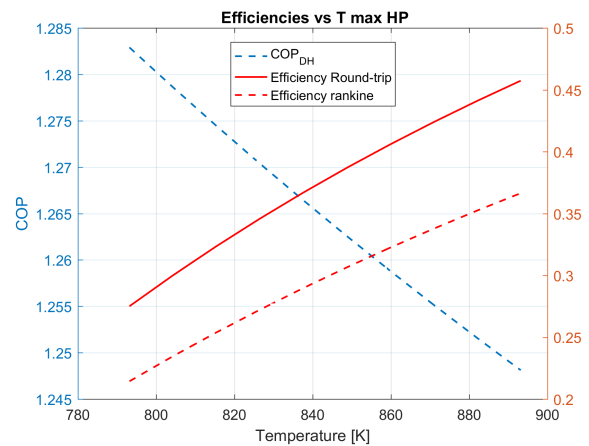


Figure 5.7. COP and Efficiencies with district heating vs Temperature max heat pump

It can be observed how the round-trip and electricity to electricity efficiencies increases despite the reduction of the COP. This can be explained by the rankine cycle efficiency. The reason of this increase is that by rising the maximum temperature of the system, both, the amount and the quality of the heat recovered in the HRSG are higher. Therefore, the efficiency of discharge is strongly affected by the maximum temperature achievable in the heat pump.

The system performance is therefore positively affected by an increase in the maximum temperature in the heat pump. Nevertheless, an increase of the temperature also results into an increase of the heat transfer surface in the heat exchanger, which must be taken into account as well. Figure 5.8 depicts the trend of the charging unit heat exchanger surface with a variation of the maximum temperature of the cycle.

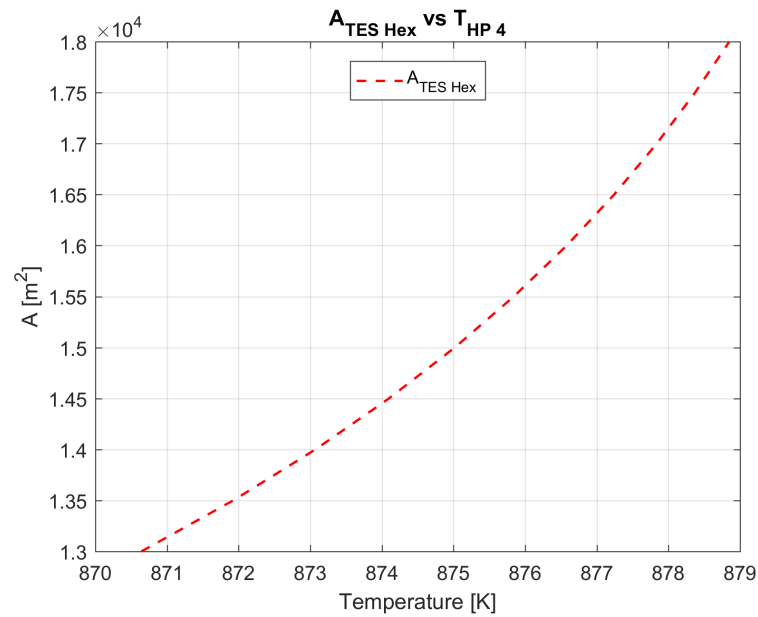


Figure 5.8. Heating surface of the heat pump hot heat exchanger vs Temperature max within the Heat pump

The heat exchanger size is strongly affecting the global cost of the system, although it allows to reach higher heat exchange efficiencies, improving the system performance. A balance should be found between cost and efficiency in order to properly design the heat exchanger. This component dimensions depends on the particular system requirements and on the application.

5.2.2 Discharging unit maximum temperature

The bottoming cycle is constituted by a Rankine cycle. Its performance is defined by the maximum and minimum temperature achievable. These corresponds to the inlet of the steam turbine, named $T_{RK,2}$, and the temperature in the condenser, named $T_{RK,4}$, as mentioned in section 3.1.1. Due to the fact that the condensing temperature is fixed by the cold source, it is not going to be further analysed. Equivalently, the system performance is assessed based on the system efficiency.

Figure 5.9 shows the dependency of the Rankine cycle and round-trip efficiency on the temperature inlet of the turbine.

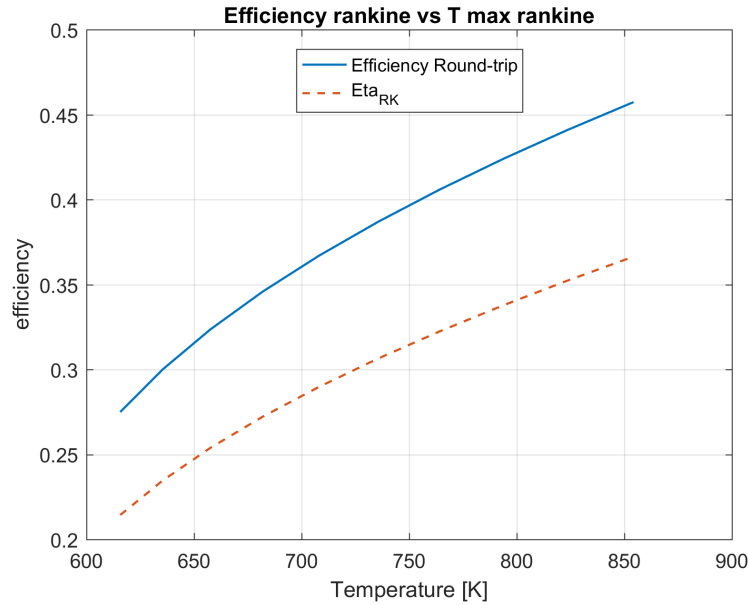


Figure 5.9. Rankine efficiency vs Temperature max rankine cycle

It is possible to notice that the system has a higher efficiency with the higher temperature. This trend is justified by the definition of the Carnot efficiency, which is only dependent on the maximum and minimum temperature in the cycle.

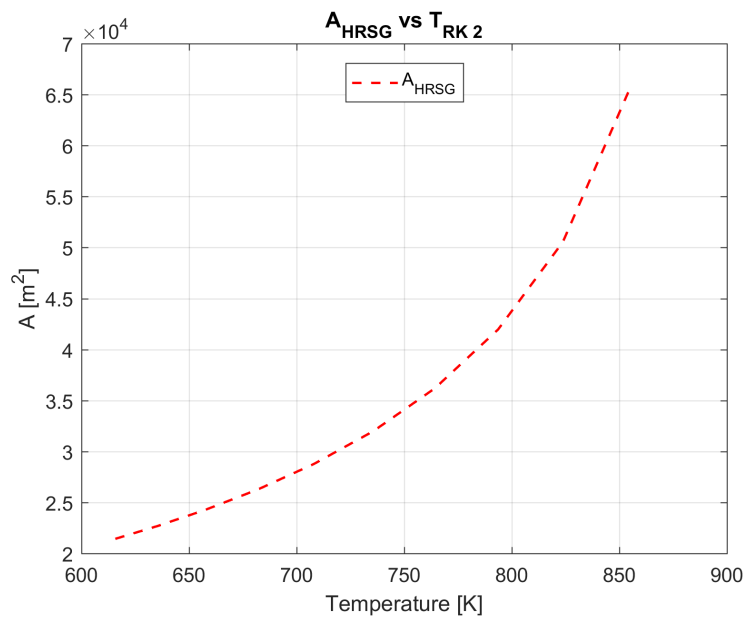


Figure 5.10. HRSG heating surface vs Temperature max Rankine cycle

According to the analysis of the heat pump heat exchanger, the higher is the temperature in the discharging unit, the larger area is required in the HRSG. Nevertheless, the performance of the system is increased as previously justified. Figure 5.10 illustrates the required exchange area as function of the maximum rankine temperature. According to the results,

the heat exchanger cost highly increases with the maximum temperature due the amount of required area.

The upper temperature limit for the inlet of the turbine is considered $853K$, which is in the operating range of the most efficient steam power stations. It is important to specify also that such a high temperature is very close to the technology limitations of the Rankine cycles, without implying special materials to avoid the mechanical breakdown due to the high temperatures.

5.2.3 Steam quality at the turbine outlet

The efficiency of the discharging unit depends also on the performance of the steam turbine. Figure 5.11 shows how the isentropic efficiency changes with the variation of the moisture content at the outlet of the last stage of the turbine.

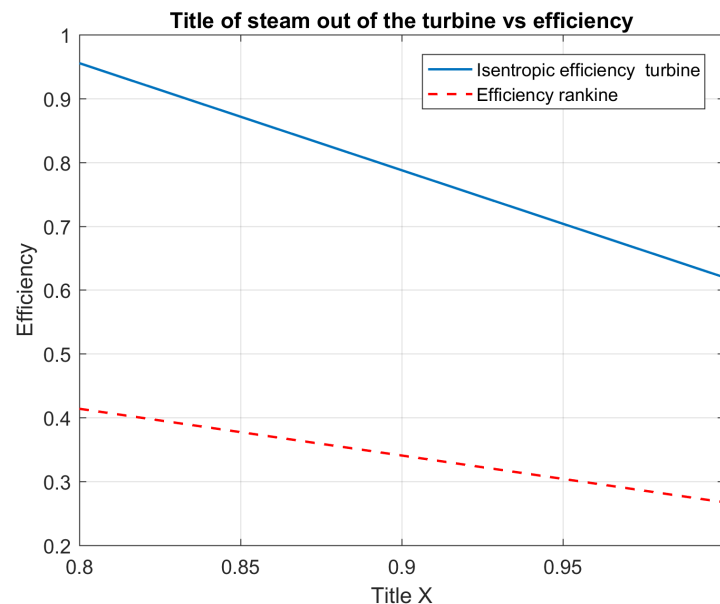


Figure 5.11. Effects on isentropic efficiency of the variation of the steam quality

The quality of the steam, defined as $x_{vap} = m_{vap}/m_{tot}$, is an important parameter for steam turbine's design. In fact, a large content of liquid water in the lasts stages of the turbine could causes considerable damages to the blades and would drastically reduce the life-time of the device. Figure 5.11 depicts the linear dependency of the Rankine efficiency on the isentropic efficiency of the turbine.

6 Results and Discussion

After having validated the simulating tool and analysed the main parameters that affect the system behaviour, the next step is to determine the system performance in the different scenarios.

It is necessary to analyse the charging and discharging process of the TES independently, in order to assess the performance of the charging/discharging based on a one-cycle simulation. Additionally, it is analysed the performance of the thermal storage after several charging and discharging cycles, as the real system would operate cyclically. It should be mentioned that the previous analysis is based on a TES constituted by two units in parallel in order to reduce the height of the storage as mentioned in section 5.1. The main parameters of the storage are collected in table 6.1.

Complementary to the basic configuration of a large traditional thermal storage, it is developed the analysis based on a segmented TES. That strategy enables the development of a high capacity thermal storage with a reduced pressure drop due to the sliding flow method. This process consists on the subsequent charging of the different segments that constitutes the storage. Therefore, with that technique is possible to construct a longitudinal TES with a reduced pressure drop as proposed by [Stiesdal, 2015b].

Table 6.1. TES simulation parameters

Symbol	Value	Unit	Parameter
R	12.73	m	Radius of the cross section
L	14.34	m	Length of the storage unit
d	0.03	m	Particle diameter
ε	0.342	[-]	Void fraction
Insulation thickness	1	m	Insulation thickness
k_{ins}	0.09	W/m K	Thermal conductivity insulation
N° Units	2	[-]	Number of units

It has to be mentioned that in this section are presented the results only from the simulations corresponding to the HP-TES configuration. In order to avoid repetitions it has been decided not to include the figures relative to EH-TES and HPEH-TES configurations. Nevertheless, it is developed a comparisons about the differences between the obtained results from the three configurations.

6.1 Charging process

The TES model simulates the charging mode, with special focus on the solid and fluid temperature profiles and the pressure drop. The system is considered to be completely discharged at the beginning of the process with an homogeneous temperature of 353.15K . The inlet temperature is set constant along the charging process with different values for each configuration, depending on the charging unit, as shown in table 6.2. The simulation time is set according the minimum required charging time in order to provide the desired amount of energy to the system, as shown previously in section 5.1. It should be noticed that the dynamic effect of the outlet temperature in the charging process are not considered. The operating conditions of the three different configurations are shown in table 6.2.

Table 6.2. Comparison of the charging conditions for the three different configurations

Configuration	T_{inlet} [K]	$T_{initial}$ Solid/ Fluid [K]	t charging [h]	\dot{m} charging [kg/s]
I	865.02	353.15	76.50	80/2
II	923.5	353.15	51.65	120/2
III	923.5	353.15	77.47	80/2

Figures 6.1 and 6.2 shows the variation of the temperature profiles of the fluid and of the solid phases over time and length of the storage.

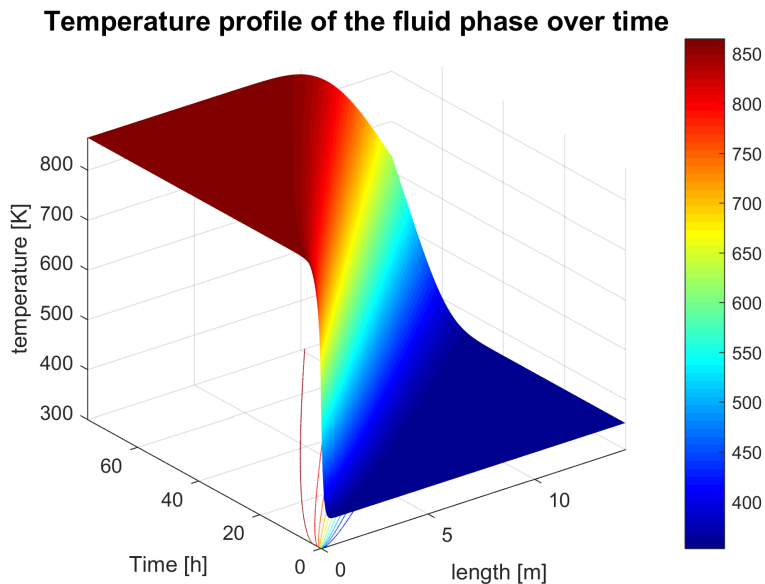


Figure 6.1. Temperature profile of the fluid phase over time for the charging process

It can be observed that there is the same trend in the temperatures profiles of both phases as expected. The thermocline displace along the storage over time heating up progressively the TES. The final temperature of the storage is not homogeneous as the system require a longer time to be fully charged.

The shown plots refer to the HP-TES configuration, which corresponds to a 51 hours charging simulation. The minimum temperature of the storage is set to $353.15K$ (blue area), which is limited due to the heating surface area of the HRSG. It is considered that it would be required a larger surface to further reduce the temperature of the air returning from the HRSG. This minimum temperature selection criteria is applied for each one of the three studied configurations. The maximum temperature (red area) is aiming to reach the inlet temperature, that in that case corresponds to to be $865.02K$. This value is related to the maximum temperature achievable for each configuration, which in this case is the heat pump with a maximum temperature set equal to $873K$.

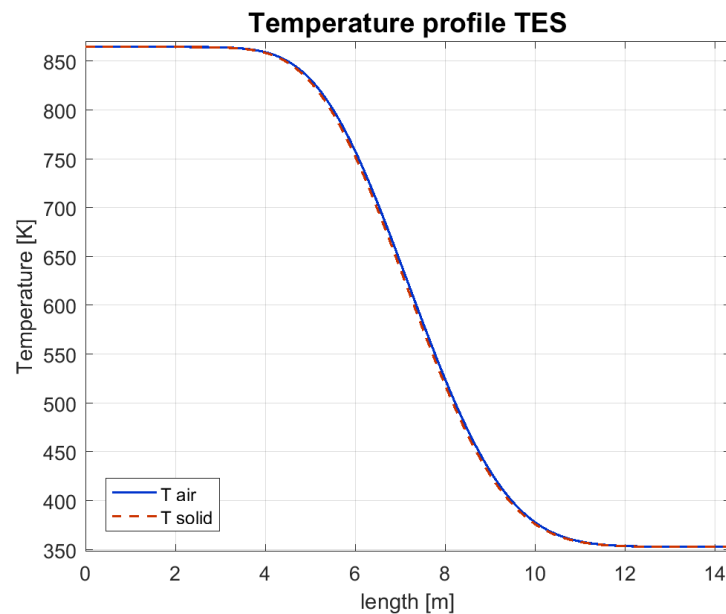


Figure 6.2. Temperature profile of the solid and fluid phases over the length

The upper limit of the storage temperature differs in the EH-TES and HPEH-TES configurations. In fact, the heat pump limitation does not constitute a problem any more for these systems, since it can be overcome by the electric heater. The maximum temperature within the storage for these two configurations is determined instead by the limitations of the Rankine cycle, which in this work is considered to have a maximum temperature of $853K$ which is not exceeded in any configuration.

Figure 6.3 depicts the evolution of energy stored in the system and the behaviour of different key temperatures over time.

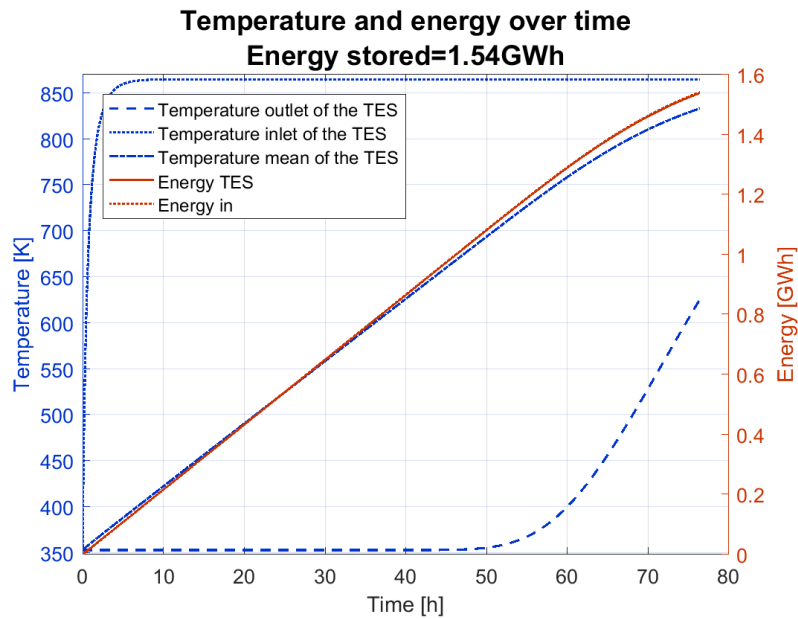


Figure 6.3. Temperature and energy over time for the charging process

The inlet and outlet temperatures refers respectively to the first and the last grid point of the filling material. The inlet raises very quickly, since it is the first section of the storage to be charged, while the outlet temperature starts to increase only after approximately 50 hours, as it corresponds to the last section of the storage.

The amount of energy stored shows a linear increase until the temperature outlet starts to increase 6.7. This is explained as the thermocline reaches the outlet boundary of the storage, and therefore it is not possible to extract all the energy content of the fluid phase. For the same reason, the mean temperature within the TES shows the same behaviour. The total energy stored from a complete discharge, rises up to 1.54GWh for each of the storage unit. The overlap of the temperature into the TES and the energy stored (red lines) should be noticed, due to the reduced losses to the environment.

Figure 6.4 illustrates the efficiencies relative to the charging process and the energy losses expressed in percentage of the total energy stored.

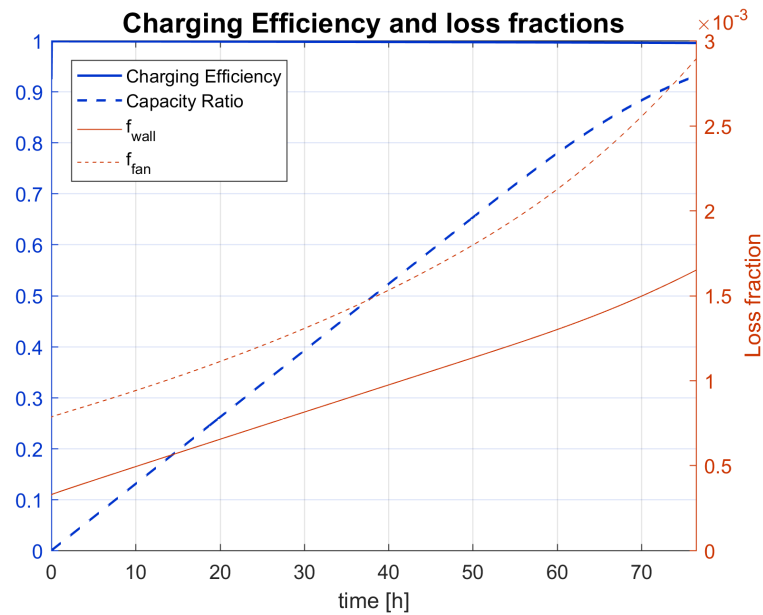


Figure 6.4. Charging efficiency and loss fraction for the charging process

The capacity ratio, defined as the ratio between the energy stored and the ideal maximum energy achievable, is increasing linearly until the outlet temperature starts to increase as already shown in the previous plot 6.3. The system after the 76.5 hours of charging is not fully charged when the temperature outlet starts to increase, hence the system is not able to exchange as much energy as at the beginning of the process. Therefore, in order to obtain a fully charged system it is necessary to operate the system for a longer period than the theoretically calculated.

The losses through the walls and the ones due to the fan operation are relatively small compared to the size of the system, therefore the charging efficiency is above 99 %. In that case the loss fraction corresponding to the fan are lower than the 0.3% of the total stored energy.

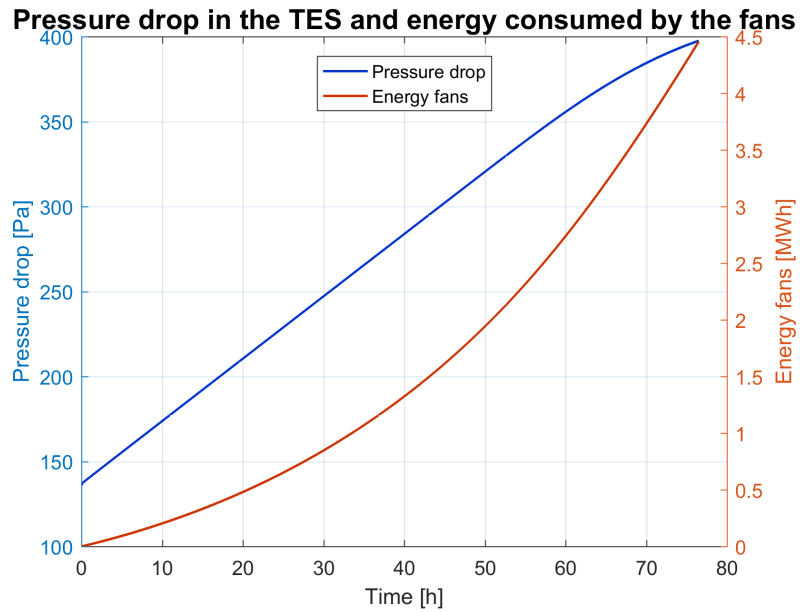


Figure 6.5. Pressure drop and accumulated fan energy consumption for the charging process

From figure 6.5 it is possible to see the trend of the energy consumed by the fan together with the pressure drop in [Pa] over the time. The pressure drop over the length increases according to the Ergun-Wu equation 4.33, which especially depends on the increase of the dynamic viscosity and the decrease of the density. Therefore, due to the decrease of the density, the fan needs progressively more power, hence it is increasing faster than the pressure drop. As a consequence of the lower mass flow compared to discharging process, the pressure loss is significantly smaller.

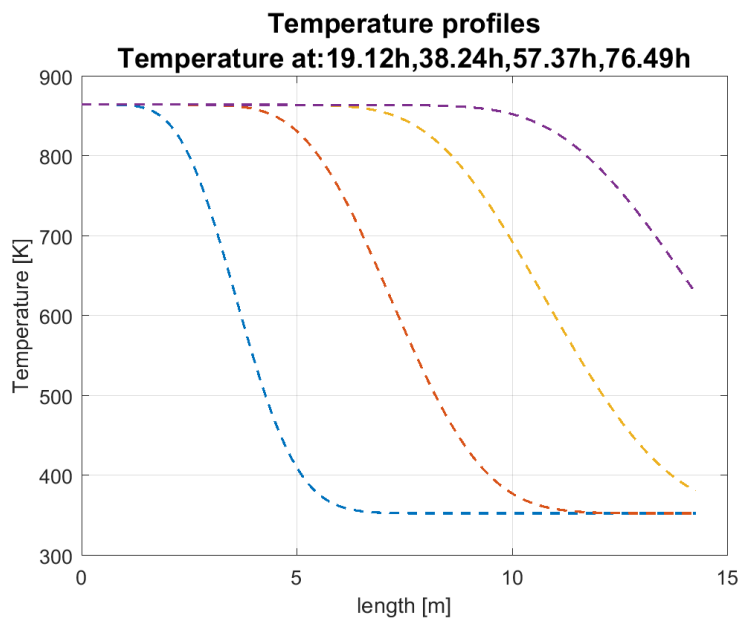


Figure 6.6. Sequential temperature profiles of the charging process

Figure 6.6 depicts the different thermoclines of the packed bed after several hours of charge. Corresponding to several "instantaneous pictures" of the temperature profile over the length, taken at every 1/4 of the charging process.

The thermocline is progressively displacing to the right while the filling material is heated up. It is clear from figure 6.6 that the temperature outlet after 50 hours begins to raise. This temperature increase reduces the useful portion of the thermocline and consequently reduces the amount of energy that is stored per time. This effect reduces the performance of the storage requiring a longer period in order to be fully charged.

Furthermore, it should be mentioned that the increase in the temperature outlet of the TES would affect the heat exchange with the charging unit, and therefore would modify the temperature inlet of the TES. Within the project limitations, it is neglected the dynamic effect of the temperature between the outlet and the inlet of the TES.

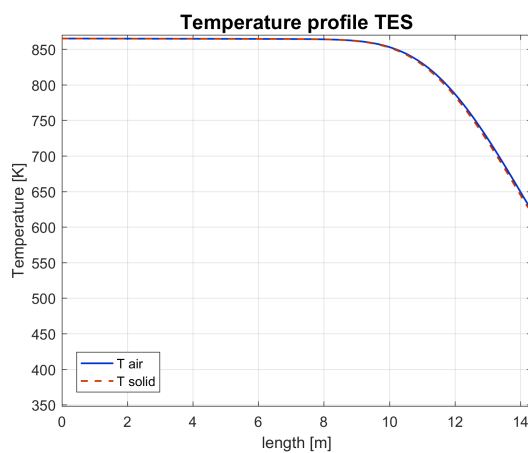


Figure 6.7. Temperature profile at the end of the 76 hours simulation

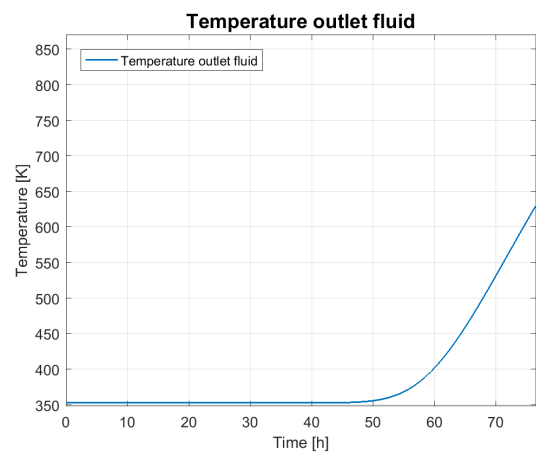


Figure 6.8. Temperature outlet of the fluid over time

Figures 6.7 and 6.8 illustrate clearly the variation of the temperature outlet over the time and length. It can be observed that after 50 hours of charging, the temperature outlet of the storage starts to rise, which would affect to the system performance as previously mentioned.

6.2 Discharging process

For the discharging process, the flow direction is reversed in order to extract the energy at the higher possible temperature. Nevertheless, in the following simulation, it is considered that the TES is fully charged, therefore it is initialized to the maximum temperature at which it can be charged at each configuration, as shown in table 6.3.

The inlet to the system is determined by the air returning from the HRSG to the TES. This parameter is set constant and equal to $353.15K$ as is determined by the heat exchange. It should be noticed that the dynamic effect of the outlet temperature of the TES going back to the inlet is not considered, thus the inlet temperature is kept constant with time.

Table 6.3. Comparison of the discharging conditions for the three different configurations

Configuration	T inlet [K]	T initial Solid/ Fluid [K]	Time charging [h]	\dot{m} charging [kg/s]
I	353.15	865.02	24	255/2
II	353.15	923.5	28.83	215/2
III	353.15	923.5	28.83	215/2

Figures 6.9 and 6.10 shows the variation of the temperature profiles of the fluid and of the solid phases over time and length of the storage.

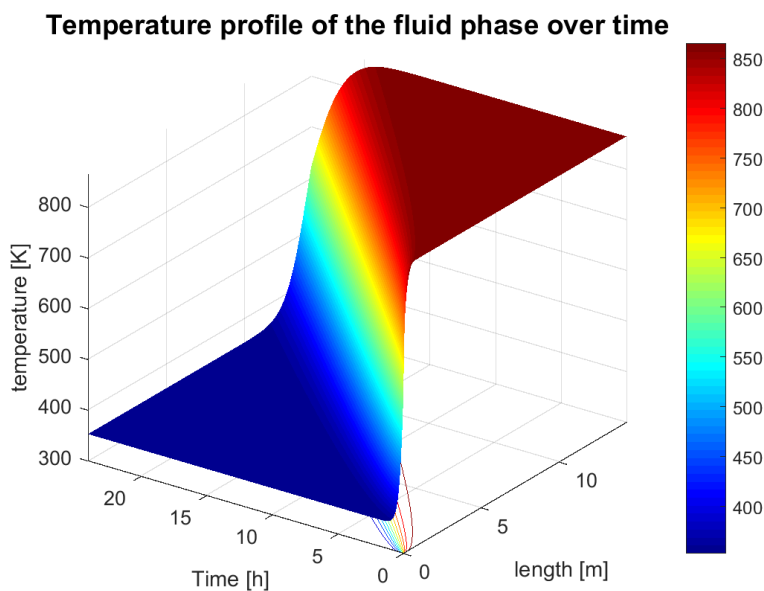


Figure 6.9. Temperature profile of the fluid phase over time for the discharging process

Analogously to the charging process, it can be seen the displacement of the thermocline along the storage over time. In that case the TES is cooled down while the energy is extracted. It can be appreciated the same trend in both, the fluid and solid phase, along the process with a small difference of temperature between them.

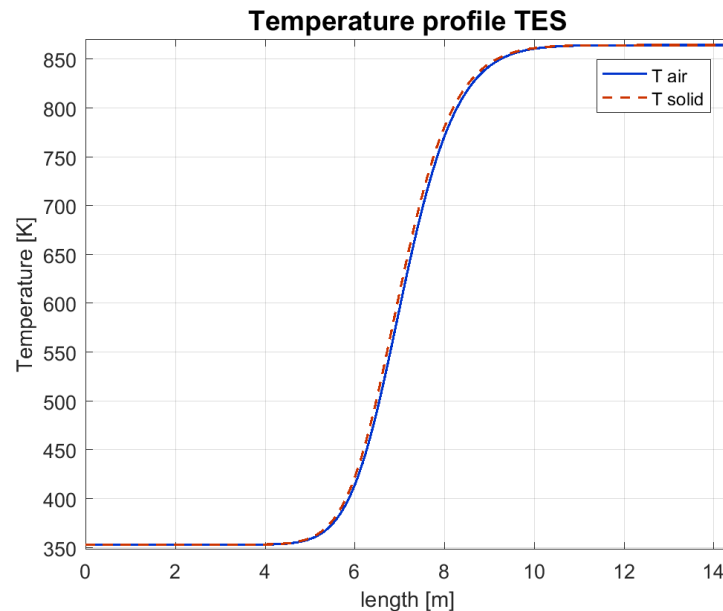


Figure 6.10. Temperature profile of the solid and fluid phases over the length

Equivalently to the charging process, the inlet temperature is determined by the minimum achievable temperature returning from the HRSG with the set parameters, corresponding to $353.15K$. As previously stated, the dynamic effect on the TES is not considered.

The discharging time is set to 24 hours, which is the aimed period for the system to supply the nominal power of $45 MW$, according to theoretical calculations. That is based on energy calculations, in which the TES is fully discharged, and without taking into account the outlet temperature decreasing.

Figure 6.11 depicts the evolution of the energy introduced in the system and the behaviour of different key temperatures over time. The total discharged energy is equal to $1.59 GWh$ for the HP-TES configuration. The inlet and outlet temperatures refer respectively to the first and the last grid point of the TES.

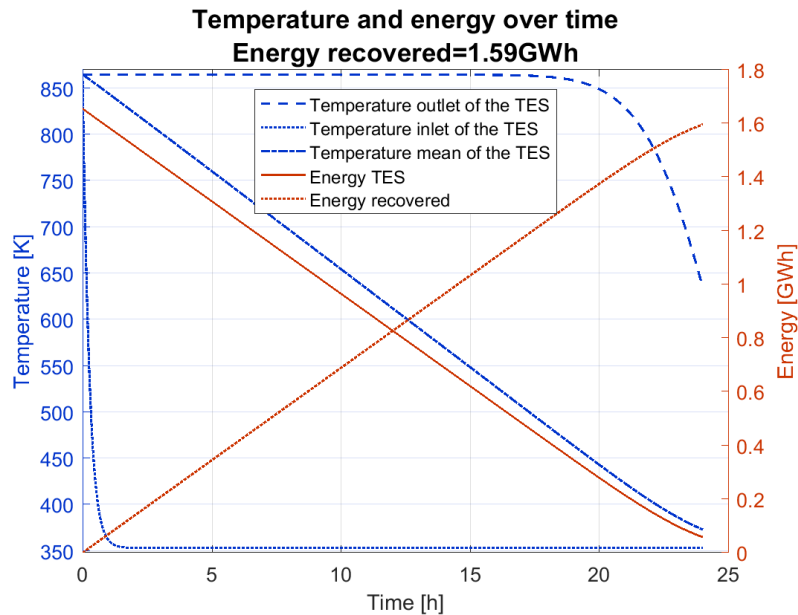


Figure 6.11. Temperature and energy over time for the discharging process

During the discharge, the inlet temperature decreases very quickly since it is the first section of the storage to be discharged. The outlet temperature starts to decrease only after approximately 17 hours, since it refers to the last section of the storage.

Regarding to the energy, while the energy is recovered to power the Rankine cycle, the remaining energy in the TES decreases proportionally with a linear behaviour until the last period. The moment in which the thermocline reaches the end of the storage, the energy extraction is reduced, and therefore the bottoming cycle is affected. That leads to the necessity of designing the TES as long as possible, in order to delay the moment in which the temperature outlet of the TES starts to decrease.

Figure 6.12 illustrates the efficiencies relative to the discharging process and the energy losses expressed in percentage of the total energy stored.

The capacity ratio is defined as the ratio between the energy discharged and the maximum energy that the TES can store. Initially it is equal to 1 as the system is considered to be fully charged at the beginning of the process. It is decreasing linearly over time until the outlet temperature starts to decrease, as already shown in figure 6.11.

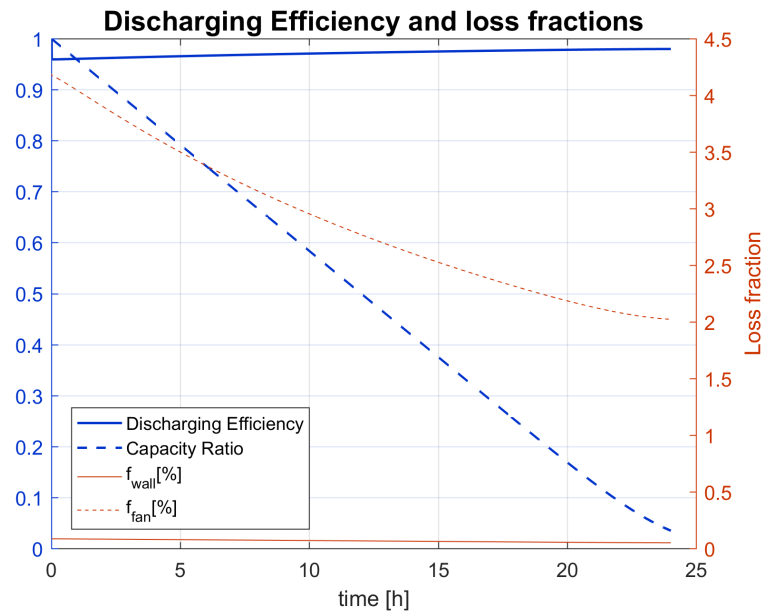


Figure 6.12. Charging efficiency and loss fraction for the discharging process

Regarding to the losses, both of them decreases over time. The losses through the wall are relatively small as in the charging process. These are reducing over time as the filling material is being cooled down and therefore, the heat transfer through the walls is reduced. The losses due to the pumping power are considerably larger compared to the charging process. This is motivated due to the larger mass flow going throughout the system, representing at the end of the cycle a 2% of the total energy extracted from the system.

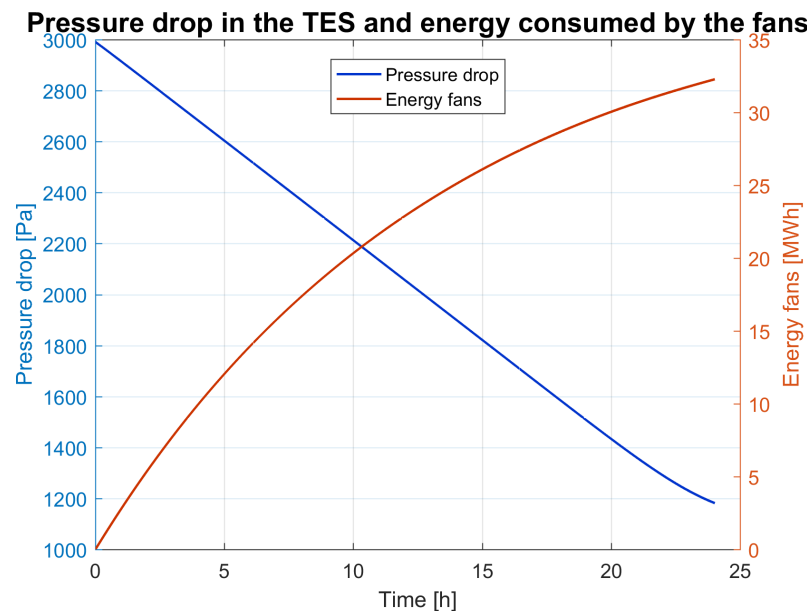


Figure 6.13. Pressure drop and fans energy consumption for the discharging process

The efficiency of the discharge process accounts for the overall losses: the wall losses and pumping energy required. Due to the cooling down of the TES, both of them are reduced over time, which motivates the increasing efficiency of the process. Nevertheless, due to the larger energy consumed by the fans, the efficiency is lower than for the charging process.

Figure 6.13 depicts the energy consumed by the fans together with the pressure drop in $[Pa]$ over the time of discharge of the TES. The pressure drop is decreasing over time, due to the decrease of the dynamic viscosity and increase of the density with the temperature. Furthermore, the energy consumed by the fans is function of the pressure drop and the mean density of the air over time. Therefore, during the discharging of the TES, the slope of the energy consumed by the fans gets flatter. It has to be noticed that the mean pressure drop in the discharging process is close to four times higher compared to the charging process, with a flow rate over two times higher.

Figure 6.14 presents the different thermoclines of the packed bed after 24 hours of discharge. It can be seen as the sum of several "instantaneous pictures" of the temperature profile over the length, taking them at every 1/4 of the discharging process.

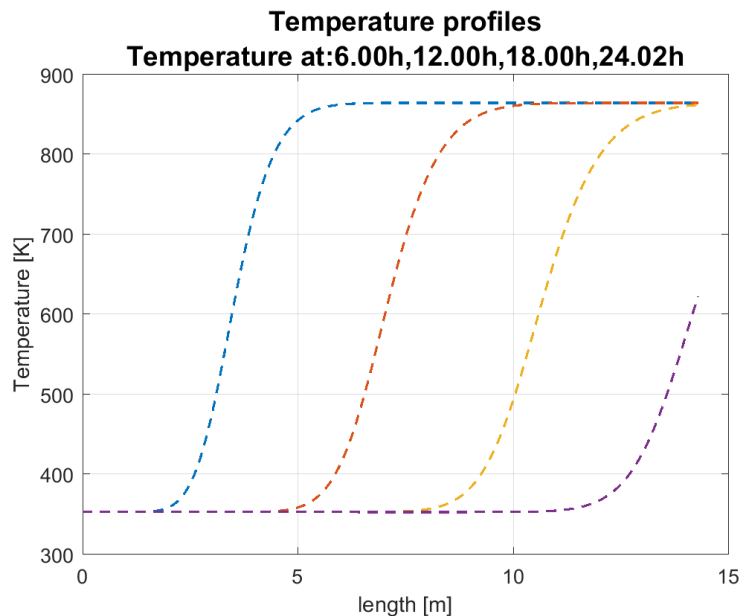


Figure 6.14. Sequential temperature profiles of the discharging process

While the TES is discharged, the thermocline moves through the length of the storage to the right. The outlet temperature remains constant for the first 17 hours but, after that moment, the temperature of the air leaving the storage starts to decrease. The outlet temperature decrease affects heavily the efficiency of the bottoming Rankine cycle, to the point of preventing its operation in extreme cases.

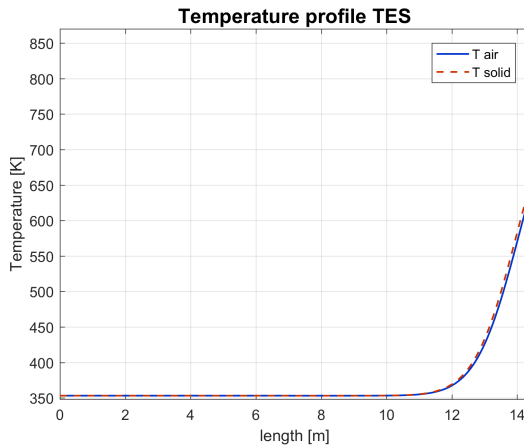


Figure 6.15. Temperature profile at the end of the 24 hours simulation

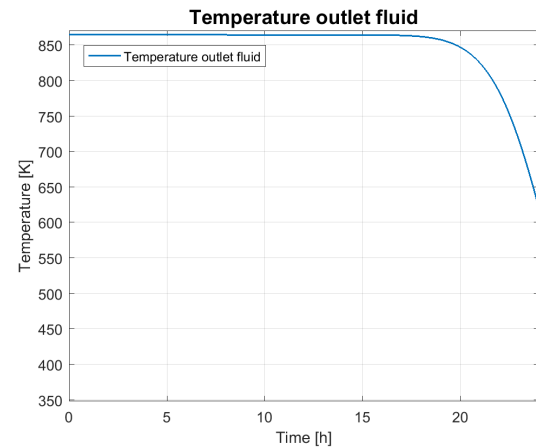


Figure 6.16. Temperature outlet of the fluid over time

Figures 6.15 and 6.16 shows clearly the variation of the temperature outlet over time and length. It can be observed that after 17 hours of discharging, the temperature outlet of the storage starts to decrease, directly affecting the bottoming cycle performance.

6.3 Cycling effect

During continuous operation, the TES is charged and discharged several times. This process could lead to a thermocline distortion and to an unpredictable behaviour. It is of vital importance to be able to assess the thermal performance of the system especially due to the dependency on the power block with the outlet temperature of the storage. Moreover, this analysis is relevant to ensure the correct performance of the charging unit due to its dynamic effect on the heat exchanger.

The thermal storage unit is simulated for a series of consecutive 12 hours charging and 12 hours discharging for 10 cycles, as shown in Figure 6.17. It can be observed the flattening of the thermocline over the number of cycles, approaching a steady state cyclic behaviour which is in accordance with [Agalit et al., 2015]. Due to the flattening the mean temperature of the storage increases as can be observed in the plot, leading to a more homogeneous temperature in the TES. The flattening of the thermocline anticipates the moment in which the temperature outlet increases during the charging (and vice-versa decreases during the discharge), therefore, the temperature outlet of the system is not constant during cyclic operation.

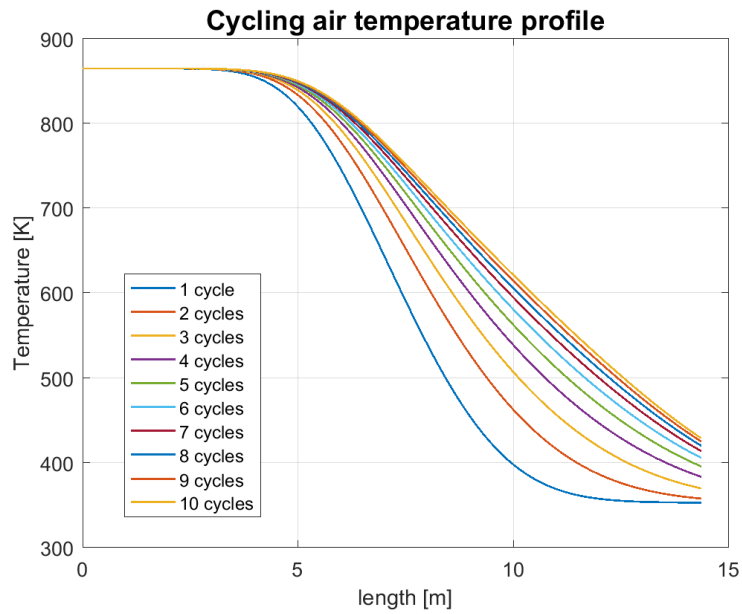


Figure 6.17. Charging temperature profile at the end of the charging for 10 cycles with 12 hours charging/discharging cycles

Along the partial charging/discharging cycles, the outlet temperature during the discharging periods rises, affecting significantly the performance of the Rankine cycle. As shown in figure 6.18, the outlet temperature at the end of the charging and discharging process increases over the number of cycles. This is due to the temperature profile modification and to the increase of the mean temperature of the TES as previously mentioned and it is shown in figure 6.18. Nevertheless, that new shape of the temperature profile leads to a premature decrease of the outlet temperature during discharge.

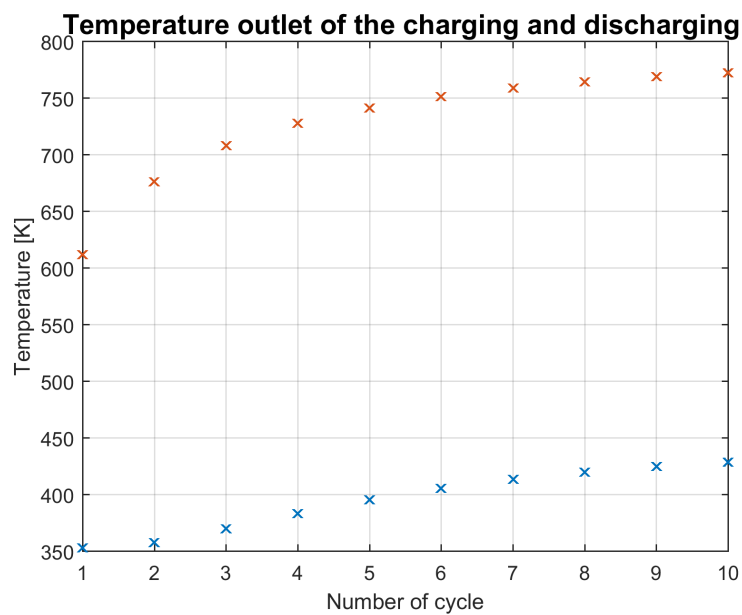


Figure 6.18. Temperature outlet after each charging and discharging process for 10 cycles

6.4 Segmentation

The maximum capacity of the TES unit is strongly determined by the pressure drop, which is function of the TES geometry and the mass flow going through the system. The thermal storage system proposed by [Stiesdal, 2015a] is constituted by a high capacity thermal storage unit with a longitudinal shape. The reason why the geometry is like that is trying to maintain the thermocline within the TES boundaries to obtain therefore a constant inlet/outlet temperature profile.

Within this work, it has been determined that the large pressure drop occurring within the standard TES does not permit the design of such a system with a long interacting region. Therefore, as determined in section 5.1, the system diameter is larger than the length of the system. This fact sets a breakpoint in the maximum capacity of the TES unless a different approach is set.

To enable the possibility of a high capacity TES with a reduced pressure drop, a segmented TES system is required making use of the Sliding Flow Method. This strategy is based on the division on the thermal storage into smaller units, which are thermally insulated and independent from each other, but interconnected by ducts. This expedient enables the sequential charging of the different segments by the operation of the valves, as previously explained in subsection 2.1.3. That procedure reduces the exergy destruction, as the pressure drop is reduced and the temperature dispersion is limited by the insulated segments. Another advantage of that technique is the possibility of restoring the temperature profile within the TES by blowing fluid at a specific temperature to a determined segment, bringing it back to the initial temperature.

Table 6.4. Comparison of the main parameters of the segmented TES

	Traditional TES	Segmented TES (segment/total)
Units	2	2
Segments	-	4
R	12.73	11.27
L	14.34	4.57/18.3
Volume	14601	14601
\dot{m} (charg./discharg.) per unit	40/127.5	40/127.5
Charging T	865.02	865.02
Max P.drop(charg./discharg.)	0.26%/2%	0.25%/2%
N° cells	200	64/256
Δx	0.0717	0.0717

In order to analyse the segmentation effect, the original TES has been divided into 4 smaller units, maintaining the same volume as the original system. In order to increase the length of the system, the cross section is reduced limited by the constrain of the

maximum pressure loss fraction. In order to be consistent with the previous analysis, it is maintained the same Δx , which in that case correspond to 64 grid points per segment. The main relevant parameters are collected in table 6.4:

The carried simulation corresponds to the charging process of the segmented TES constituted by four units. During that operation, there are always two units being charged and connected in series. When the outlet temperature of the first one reaches 860K, that subunit is disconnected, switching to the next "discharged" unit. The SFM is explained more in detail in section 2.1.3. It is shown in figure 6.19 the temperature profile of the four different segments, as well as the mean TES temperature. It can be easily recognised the instants in which the switch takes place, as the temperature of a new segment starts rapidly to increase. At the end of the process the TES storage tends to reach the inlet temperature.

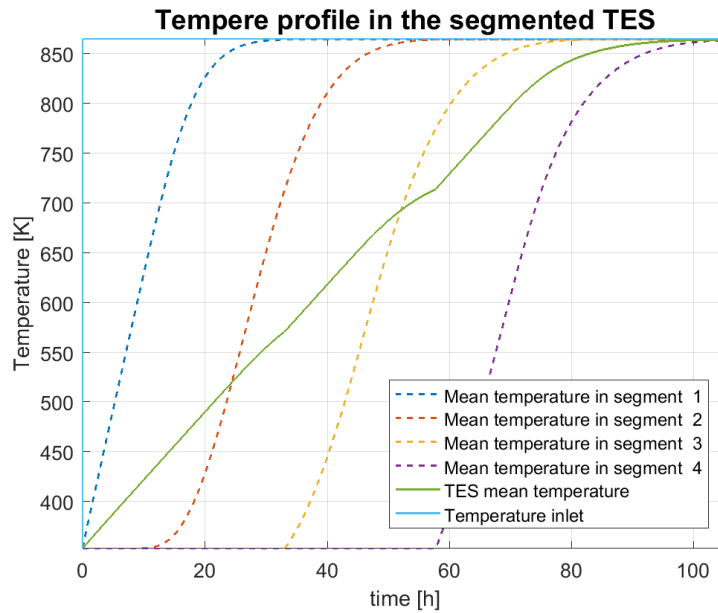


Figure 6.19. Temperature profiles of the TES segments during charging

Analogously to the temperature profiles, figure 6.20 depicts the energy content of each segment over time. Complementary, the total energy in the TES is presented. It can be detected also when a new section is connected to the charging stream. It should be noticed that at the end of the process all the different segments acquire the same energy content.

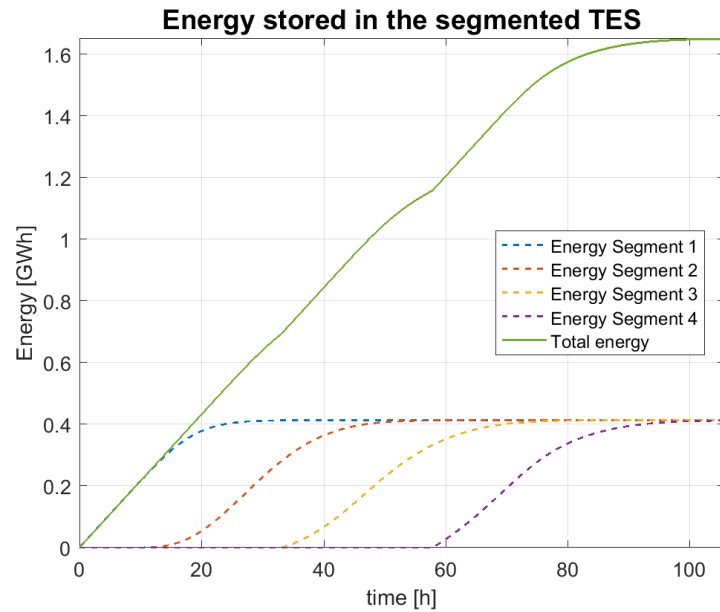


Figure 6.20. Energy stored in the TES segments during charging

One of the most relevant advantages is the reduction of the pressure drop during the charging process. The pressure drop fluctuates between two limits due to the switches. Therefore, the pressure drop is decreased at the switch because of the lower dynamic viscosity and higher density of the fluid. Figure 6.21 shows how the pressure drop is reduced due to the slide of the thermal units. It can be seen as well the accumulated total energy consumed by the fans that circulates the air within the TES.

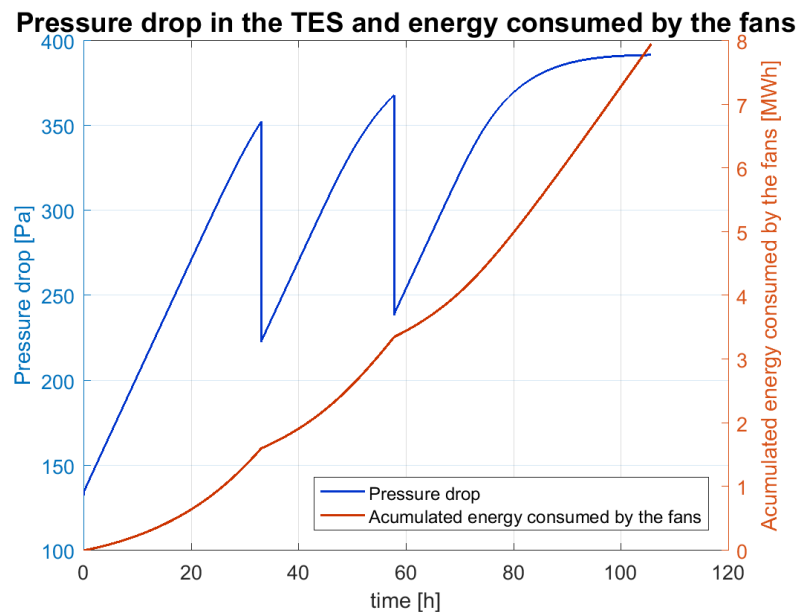


Figure 6.21. Pressure drop and energy consumed by the fans in the segmented TES

Another advantage of the segmentation of the TES is the possibility to further upgrade

the system capacity by just adding more segments to the existing system. Therefore, as the mass-flow is maintained constant, the only effect on the system would be the required period to charge and discharge the system as the capacity is increased.

One interesting possibility of the segmented unit, is the possibility to make use of the remaining residual heat that can not be used in the bottom cycle due to its relative low temperature. That heat could be used instead to provide the required heat for district heating, due to its closer temperature range.

Nevertheless, it should be taken into account the economical impact that would have this strategy. The higher number of segments would lead to a higher investment due to the increase of the number of components. Therefore, the system design should be a trade-off between the increase of the system performance and the additional cost.

6.5 Configuration results

6.5.1 Results HP-TES

Table 6.5 collects all the main results from the simulation of HP-TES configuration. This setup implies that the heat pump heats up the air until 873 K, the storage is charged/discharged until 865 K and the Rankine cycle operates with a maximum temperature of 799.6 K. Besides the results related to power production, table 6.5 shows also the amount of heat power available for district heating Q_{DH} and district cooling Q_{DC} , together with their COPs. A_{HRSG} and A_{Hex} are respectively the heating surface of the HRSG and of the heat exchanger between the heat pump and the storage. W_{comp} is the total power absorbed by the compressor in order to run the system.

Table 6.5. Main results for HP-TES simulation

Symbol	Value	Unit	Symbol	Value	Unit
A_{HRSG}	43404	m^2	$\eta_{is,comp,stage}$	0.832/0.780	-
A_{Hex}	15000	m^2	$\eta_{is,st,turb}$	0.788	-
COP	1.128	-	$\eta_{el,el}$	0.384	-
COP_{DH}	1.254	-	η_{RT}	0.427	-
COP_{DC}	0.302	-	$T_{max,charging}$	865.02	K
η_{RK}	0.341	-	W_{comp}	80.499	MW
Q_{DH}	4.850	MW	Q_{DC}	11.535	MW

6.5.2 Results EH-TES

Table 6.6 depicts the main results from the simulation of EH-TES configuration. The aim of this configuration is to provide a cheap and simple solution for the system examined. The charging process is performed by the electric heater which heats the air up to 923.5 K. This configuration does not need the heat exchanger between the charging unit and the storage, therefore the temperature of charge/discharge of the storage is considered 923.5 K as well. The Rankine cycle is operating with a temperature of 840.7 K at the turbine inlet, which is the maximum temperature globally achieved in this work for the Rankine cycle.

Because of the higher temperature of the storage, the temperature differences in the HRSG can be larger and therefore a smaller heating surface is required, resulting in a significant saving in terms of initial investment. This configuration nevertheless does not have the possibility to supply district heating or cooling, due to the lack of the heat pump. Moreover, while in the other two configurations the cold source for the condenser in the Rankine cycle can be provided by the cold side of the heat pump, the EH-TES requires an external cold source for this purpose.

Table 6.6. Main results for EH-TES simulation

Symbol	Value	Unit	Symbol	Value	Unit
A_{HRSG}	36276	m^2	η_{RK}	0.360	-
COP	1	-	$\eta_{is,st.turb}$	0.821	-
$T_{max,charging}$	923.5	K	$\eta_{el,el}$	0.360	-
W_{EH}	72.730	MW			

6.5.3 Results HPEH-TES

Option 1: High performance HPEH-TES

Table 6.7 shows the main results from the simulation of HPEH-TES configuration, option 1. The aim of this option is to provide the most efficient solution for the system analysed, combining the optimum operation conditions of the heat pump and the electric heater. The heat pump works until its limit of 873 K , after that the electric heater heats the air up until the maximum storage temperature of 923.5 K , at which the storage is charged and discharged as well. The Rankine cycle operates at its maximum temperature of 840.7 K as it is in the electric heater configuration, therefore the discharging unit performance are the same. The A_{HRSG} is smaller compared to the one required in HP-TES, due to the higher temperature difference available in the HRSG, which constitutes one of the major advantages of this combined configuration. The COP is slightly lower than the one with the heat pump alone, due to the presence of the electric heater, but the Rankine cycle is more efficient because of the higher temperature at the turbine inlet. This configuration results to have the highest round trip efficiency, according to the initial expectations.

Table 6.7. Main results for HPEH-TES (option 1) simulation

Symbol	Value	Unit	Symbol	Value	Unit
A_{HRSG}	36276	m^2	$\eta_{is,comp,stage}$	0.832/0.780	-
A_{Hex}	15000	m^2	$\eta_{is,st.turb}$	0.821	-
COP	1.114	-	$\eta_{el,el}$	0.401	-
COP_{DH}	1.229	-	η_{RT}	0.443	-
COP_{DC}	0.302	-	$T_{max,charging}$	923.5	K
η_{RK}	0.360	-	$W_{comp+EH}$	85.738	MW
Q_{DH}	4.850	MW	Q_{DC}	11.564	MW

Option 2: Balanced HPEH-TES

The main results for the balanced setup of the HPEH-TES are shown in table 6.8. The aim of this variant of HPEH-TES is to investigate a solution when the heat pump operates at lower temperatures, reducing the complexity and the cost of the charging unit. For the

same reason it has been decided to set less demanding conditions for the Rankine cycle as well, with the idea to have a system which does not imply any particularly complex components. The heat pump temperature limit is set now to 673 K , while the electric heater heats the air up to 888.5 K . The inlet temperature of the steam turbine is 801.5 K and results to have an isentropic efficiency of 78% .

Table 6.8. Main results for HPEH-TES (option 2) simulation

Symbol	Value	Unit	Symbol	Value	Unit
A_{HRSG}	37174	m^2	$\eta_{is,comp,stage}$	0.832/0.800	-
A_{Hex}	15000	m^2	$\eta_{is,st.turb}$	0.789	-
COP	1.073	-	$\eta_{el,el}$	0.367	-
COP_{DH}	1.207	-	η_{RT}	0.413	-
COP_{DC}	0.411	-	$T_{max,charging}$	888.5	K
η_{RK}	0.342	-	$W_{comp+EH}$	73.320	MW
Q_{DH}	4.850	MW	Q_{DC}	9.500	MW

Option 3: Quick-charging HPEH-TES

Table 6.9 illustrates the main results from the simulation of HPEH-TES configuration, option 3. The first objective of this configuration is to provide a solution which allows to charge and discharge the system in the same amount of hours. The second aim is to supply a consistently higher amount of cooling power to the district cooling circuit. Therefore the heating surface of the cold heat exchanger is set to 6000 m^2 . The COP of the cooling is increased to 40% , while the cooling power is 20.5 MW . At the same time, the system is still able to operate for power production purpose, since this variant does not show a significant drop in the other operating efficiencies, as it is possible to see from 6.9.

Table 6.9. Main results for HPEH-TES (option 3) simulation

Symbol	Value	Unit	Symbol	Value	Unit
A_{HRSG}	36276	m^2	$\eta_{is,comp,stage}$	0.832/0.780	-
A_{Hex}	15000	m^2	$\eta_{is,st.turb}$	0.821	-
COP	1.127	-	$\eta_{el,el}$	0.406	-
COP_{DH}	1.181	-	η_{RT}	0.425	-
COP_{DC}	0.410	-	$T_{max,charging}$	923.5	K
η_{RK}	0.360	-	$W_{comp+EH}$	146.476	MW
Q_{DH}	4.850	MW	Q_{DC}	20.473	MW

6.6 Summary of the results

In table 6.10 are collected the main results for all the investigated configurations.

Table 6.10. Summary of the main parameters of the different configurations

Configuration	I	II	IIIa	IIIb	IIIc
$T_{max, TES}$ [K]	865.02	923.5	923.5	888.5	923.5
$T_{min, TES}$	353.15	353.15	353.15	353.15	353.15
$T_{max, RK}$ [K]	799.6	840.7	840.7	801.5	840.7
$t_{charging}$ [h]	76.50	51.65	77.47	76.89	26.29
$t_{discharging}$ [h]	24	28.83	28.83	26.29	26.29
$\dot{m}_{charging}$ [kg/s]	80	120	80	80	215
$\dot{m}_{discharging}$ [kg/s]	255	215	215	242	215
$\eta_{is, turbine}$	0.788	0.821	0.821	0.789	0.821
η RK	0.34	0.36	0.36	0.35	0.35
η RT	0.427	0.360	0.443	0.413	0.425
η el-el	0.384	0.360	0.401	0.367	0.406
Q_{DH} [MW]	4.850	4.850	4.850	4.850	4.850
Q_{DC} [MW]	11.535	-	11.564	9.500	20.473
Area HRSG [m^2]	43404	36276	36276	37174	36276
Area Hot Hex [m^2]	15000	15000	15000	15000	15000
Area Cold Hex [m^2]	5000	-	6000	5000	6000
Volume TES [m^3]	14603	14603	14603	14603	14603
Energy stores TES [GWh]	3.31	3.75	3.75	3.48	3.48

7 Conclusions

This chapter sums up and concludes the main results of this thesis, which has investigated the feasibility of packed bed thermal energy storage with different charging strategies.

The concept of thermal energy storage is based on the possibility of using low cost materials and reliable technologies for the energy storage. The low thermodynamic energy conversion of heat to electricity represents a challenge for the system viability. In a hypothetical future energy scenario with low-cost and unpredictable renewable energy production, storage cost and reliability could be of greater importance than efficiency for the success of this technology.

Based on the obtained results from the system analysis, the influence of different parameters has been investigated.

In order to improve the performance of the system, it is crucial to maintain a constant temperature at the outlet of the TES, since it directly affects the Rankine cycle efficiency. It is important therefore to maintain the thermocline within the boundaries of the storage. To achieve this objective, the TES has to be designed with a longitudinal shape, increasing then the useful storage area.

The main drawback of increasing the length of the system is the linear increase of the pressure drop. From the obtained results it turned out to be a extremely limiting parameter for the feasibility of [Stiesdal, 2015a] original concept. In order to overcome this phenomena, different strategies can be adopted. One simple option could be to double the number of storage units connecting them in parallel, hence doubling the cross section area and dividing the mass flow between them.

The Sliding Flow Method could be an alternative solution for the pressure drop issue. It has proven to be a valid technique for the design of TES systems with high capacity due to the segmentation of the storage.

Regarding to continuous operation of the system, it has been determined that the cycling effect has a negative consequence on the TES performance. With an increasing number of cycles, the outlet temperature decrease is anticipated, reducing the bottoming cycle efficiency.

A significant advantage of the investigated technology is the possibility to provide district heating and cooling, leading to a higher system efficiency if this utilities can be complementary used. Therefore, this technology could be designed in order to operate in collaboration with different industries.

Based on the simple system architecture, several configurations can be implemented with different design criteria and objectives for the system. The main characteristics of the five investigated systems as exposed qualitatively in table 7.1 and discussed as follows.

The **HP-TES** configuration is limited by the maximum temperature achievable within the heat pump. The required heating surfaces is larger due to the smaller temperature differences between the storage and the charging/discharging unit. On the other hand, reducing too much the temperature in the Rankine cycle would affect significantly the overall efficiency of the plant. This configuration turned out to be promising in applications where it would be possible to take advantage of the district heating and district cooling supply.

The **EH-TES** configuration requires a lower investment, due to the simpler charging unit compared to the first case. This configuration is able to reach higher temperatures in the charging unit. On the contrary, the Rankine cycle is pushed to its technological limit, which leads to a higher efficiency. The main advantage is the fast installation period, due to its simplicity, especially in a brown field project. Nevertheless, this configuration is not able to supply any DH/DC.

The **High performance HPEH-TES** has the highest efficiency among the other studied configurations. The combination of the two charging units increases the initial cost, but the calculation has shown that the heating surface of the HRSG is significantly less compared to the HP-TES, which requires a more efficient heat exchange due to inferior temperature.

The **Balanced HPEH-TES** configuration target is to reduced the size of the heat pump, increasing therefore the electric heater power. The temperature reached are moderate compared to the other HPEH-TES configurations in order to avoid the necessity of any particularly complex component in the Rankine cycle. The performance of the charging unit is therefore lower than the other cases. With that configurations is still possible to supply district heating and cooling, with a reduced installation cost.

The **Quick-charging HPEH-TES** configuration has a charging time equal to the discharging process. The cost of the system, in particular the heat pump, is increased due to the larger required components. At the same time, this configuration seems particularly suitable for applications with strong district cooling requirements, since its power is almost double compared to the previous configurations.

Table 7.1. Qualitative comparison among the 5 TES configurations

Configuration	Cost	Efficiency	District Heating	District Cooling	Charging time
HP-TES	●●	●	●	●	●
EH-TES	●●	●●	-	-	●
High performance HPEH-TES	●	●●	●	●	●
Balanced HPEH-TES	●	●	●	●	●
Quick-charging HPEH-TES	●●	●	●	●●	●●

8 Future work

Throughout the development of this thesis, multiple ideas and for further analysis have been found. Due to the limited time frame of this thesis, it has not been possible to investigate all the different options that could yield interesting results. This chapter presents an overview about the possibilities for future work that could be implemented in order to extend and improve the findings.

One interesting direction to pursue is the investigation on the choice of the working fluid. The simulation tool developed in this thesis is able to handle different fluids thanks to the integration with the software REFPROP, which has a complete range of fluids in its database. A fluid with better characteristics could increase the performance of the TES itself, or perhaps the cold circuit. Regarding the discharge unit, an ORC instead of the traditional Rankine cycle would probably not increase the efficiency of the system, but could constitute an interesting option since it would allow the heat pump to operate in a lower range of temperatures. That could improve on the other hand the COP of the charging unit, which would result in a better round-trip efficiency.

In order to improve the system simulation, a completely dynamic model should be implemented. This leads to the integration of the the currently two independent models (system and TES model) in order to link completely the inputs and outputs of the system components. Furthermore, the Rankine cycle should be dynamically modelled, allowing to analyse properly the partial load operating conditions.

Due to the lack of information regarding the different cost functions, an economical analysis is not included in this thesis. The natural continuation of this work would be to carry it out, defining a cost for the initial installation and estimating a break-even point for the investment. A more accurate economical view would also permit to optimize the different configurations following a different approach.

The gradient of temperature in the solid particles within the packed bed has not been considered in the developed model. This assumption is completely justified by a $Bi < 1$, function of the particle diameter. It would require an upgrade in heat transfer model of the TES in order to take into account for the gradient temperature within the particle for larger particle size.

A Appendix:A

A.1 The Effectiveness–NTU Method

In order to evaluate and design the heat exchangers within the system, the Effectiveness–NTU Method, developed by Kays and London in 1955, has been applied due to the accuracy in spite of its simplicity. This method has been designed to determine the heat transfer rate and the outlet temperature when the size and type of heat exchanger is specified. For that purpose, it is necessary to define previously the temperature and mass flows of the inlets of the heat exchanger. The further equations are based on the method explained by [Y.A.Çengel and A.J.Ghajar, 2015].

This method is based on a dimensionless parameter called heat transfer effectiveness, ϵ , which determines the ratio of the maximum heat that can be exchanged and the actual heat transferred:

$$\epsilon = \frac{\dot{Q}}{\dot{Q}_{max}} = \frac{\text{Actual heat transfer rate}}{\text{Maximum available heat transfer rate}} \quad (\text{A.1})$$

Where the actual heat transfer rate can be determined from the energy balance:

$$\dot{Q} = C_c(T_{c, out} - T_{c, in}) = C_h(T_{h, in} - T_{h, out}) \quad (\text{A.2})$$

The heat capacity rates can be expressed as $C_c = \dot{m}_c c_{pc}$ and $C_h = \dot{m}_h c_{ph}$ for the cold and hot streams.

The heat exchange will get to its maximum when one of the streams reach the inlet/outlet of the other one (the cold fluid is heated to the inlet temperature of the hot fluid, or the hot fluid is cooled to the temperature of the inlet of the cold fluid). Therefore, it is needed to identify the stream that will first experience the maximum temperature at which the transfer will stop. Therefore, the maximum heat transfer is limited by the minimum heat capacity rate as shown in equation A.3, where C_{min} is the smaller of C_h and C_c .

$$\dot{Q}_{max} = C_{min}(T_{h, in} - T_{c, in}) \quad (\text{A.3})$$

The effectiveness of the heat exchanger enables the calculation of the heat transfer rate without knowing the outlet temperatures of the fluids. The effectiveness depends on the geometry as well as on the flow arrangement. Thus, the different types of exchangers have distinct heat effectiveness relations. The effectiveness of a heat exchanger can be expressed

as function of the number of transfer units (NTU) and the heat capacity ratio, as expressed in equation A.4:

$$\epsilon = f(NTU, C_r) \quad (\text{A.4})$$

Where the NTU is a dimensionless number expressed in equation A.5. Where U is the overall heat transfer coefficient and A_s is the heat transfer surface area.

$$NTU = \frac{UA_s}{C_{min}} = \frac{UA_s}{(\dot{m}c_p)_{min}} \quad (\text{A.5})$$

It is also necessary to determine another dimensionless quantity defined as capacity ratio, equation A.8, in order to be able to compute the effectiveness of the heat exchanger:

$$C_r = \frac{C_{min}}{C_{max}} \quad (\text{A.6})$$

For the different configurations and geometries of heat exchangers, the ϵ is determined by different expressions, for instance, the double pipe counter-flow is expressed by equation A.7:

$$\epsilon = \frac{1 - e^{-NTU(1-C_r)}}{1 - C_r e^{-NTU(1-C_r)}} \quad (\text{A.7})$$

The value of the heat capacity ratio ranges between 0 and 1. The effectiveness for a given NTU, will reach a maximum for $C = 0$ and a minimum for $C = 1$. The case where $C = C_{min}/C_{max} = 0$, corresponds to $C_{max} = \infty$, which occurs when a phase change takes place, such as in a condenser or a boiler. All effectiveness relations in that case reduces to equation

$$\epsilon = \epsilon_{max} = 1 - e^{-NTU} \quad (\text{A.8})$$

A.2 Steam Rankine Cycle

The Rankine cycle technology has been chosen to discharge the unit, mainly due to its reliability and flexibility. This technology has been deeply investigated since the 19th century, and nowadays constitutes one of the most well known technologies in the field of power production. Another reason for its selection is the large diffusion of this typology of power plants all over the world and therefore the possibility to make use of an already existing installation to build the storage system of analysis as a “brownfield” option. The storage unit could be placed into the former coal yard [H.Stiesdal, 2016], allowing a considerable space-saving.

The cycle shown in the T-s diagram is described by the following process:

- (1–2) Isentropic compression in a pump
- (2–3) Isobaric heat addition in a boiler
- (3–4) Isentropic expansion in a turbine
- (4–1) Isobaric heat rejection in a condenser

The feed water enters the pump (1) raises its pressure and temperature until point 2. Then within the boiler, it elevates its temperature leaving it as dry or superheated steam. Once in the turbine, the temperature and pressure of the steam decreases by the amount of heat converted into mechanical work (3 to 4), with a consequential enthalpy drop. The wet steam at low pressure and temperature leaves the turbine (4) and passes through the condenser, which carries out the condensation of the vapour bringing it back at the original condition as saturated water at point 1. The efficiency of the Rankine cycle is determined by the ratio between the mechanical power produced by the turbine and the heat power provided to the cycle into the boiler.

A.3 Balanced HPEH-TES configuration

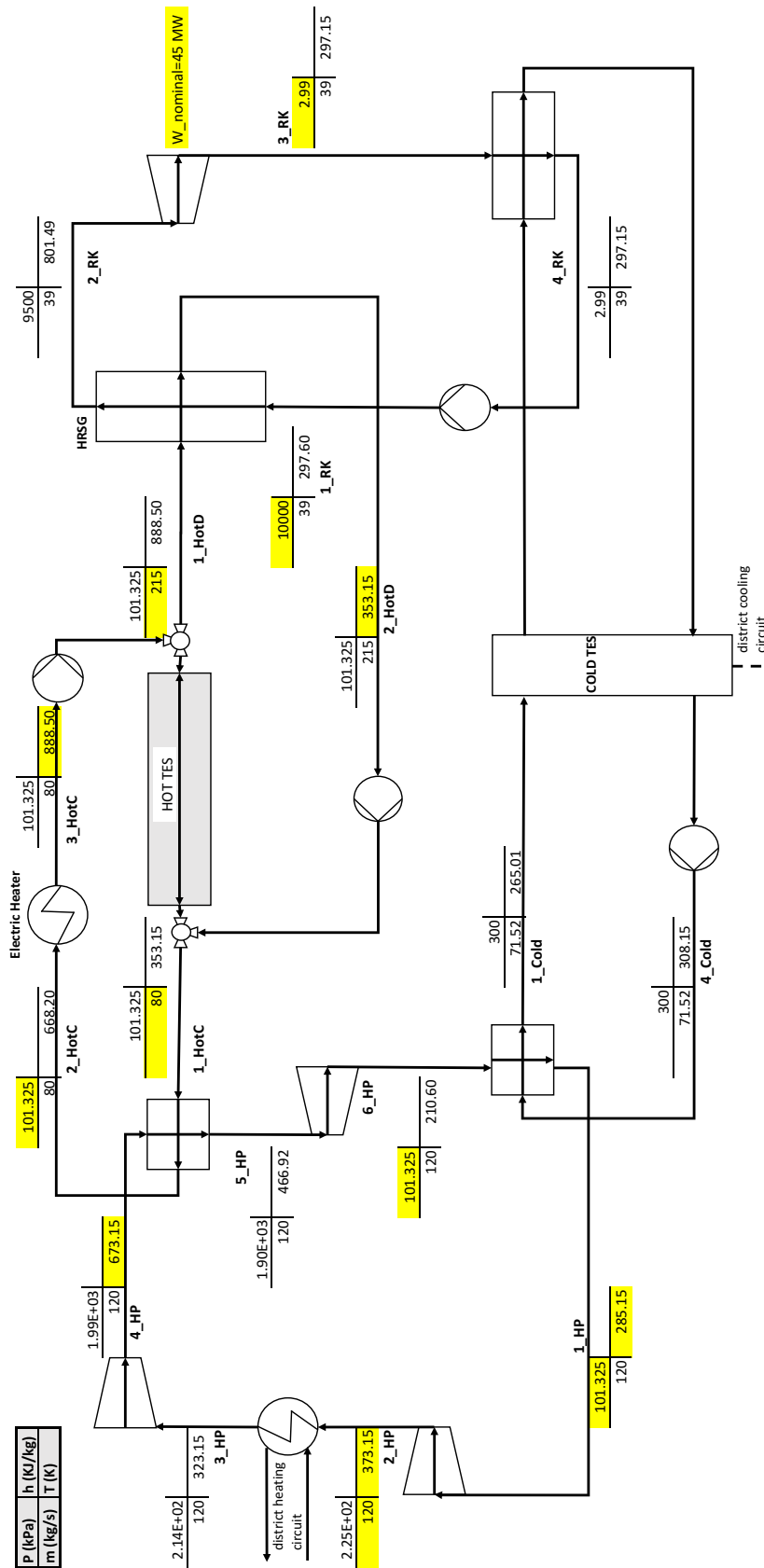


Figure A.1. Balanced HPEH-TES configuration diagram

A.4 Quick-charge HPEH-TES configuration

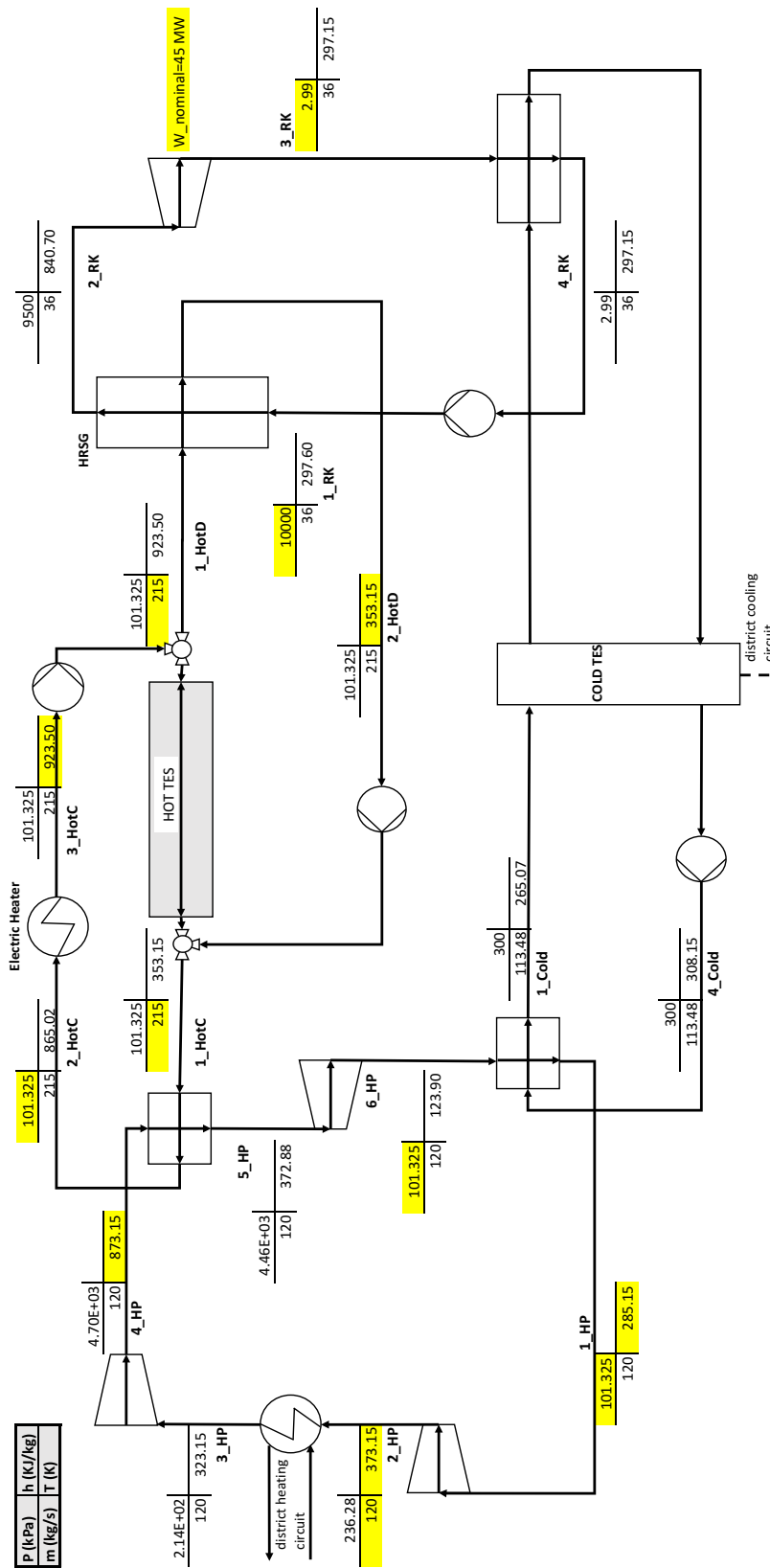


Figure A.2. Quick-charge HPEH-TES configuration diagram

Bibliography

- A.Castillo and D. Gayme. Grid-scale energy storage applications in renewable energy integration: A survey. *Energy Conversion and Management*, 87:885–894, 2014.
- A.Evans, V.Strezov, and T.J.Evans. Assessment of utility energy storage options for increased renewable energy penetration. *Renewable and Sustainable Energy Reviews*, 2012.
- H. Agalit, N. Zari, M. Maalmi, and M. Maaroufi. Numerical investigations of high temperature packed bed tes systems used in hybrid solar tower power plants. *Solar Energy*, 2015.
- K. Allen, T. von Backstrom, D. Kroger, and A. Kisters. Rock bed storage for solar thermal power plants: Rock characteristics, suitability, and availability. *Solar Energy Materials & Solar Cells*, 126:170–183, 2015.
- Al.S.Pedersen, B.Elmegaard, C.H.Christensen, C.Kjoller, and F.Elefsen. Status and recommendations for rd&d on energy storage technologies in a danish context. Technical report, Danish Energy Research Programme, 2014.
- J. Beek. Design of packed cathalytic reactors. *Adv. Chem. Eng*, 3:203–271, 1962.
- R. Courant, K. Friedrichs, and H. Lewy. Über die partiellen differenzgleichungen der mathematischen physik.pdf. *Mathematische Annalen* 100, pages 32–74, 1928.
- J. Coutier and E. Farber. Two applications of a numerical approach of heat transfer process within rock beds. *Solar Energy* 29, 451-462, 1982.
- V. Dreißigacker, H. Muller-Steinhagen, and H. Zunft. Thermo-mechanical analysis of packed beds for large-scale storage of high temperature heat. *Heat Mass Transfer* 46, 1199–1207, 2010.
- E.Larsson, J.Leymann, B.Danielssen, M.Vik, and M.Nora. Nordic market report 2014: Development in the nordic electricity market. Technical report, NordREG: Nordic Energy Regulators, 2014.
- EMD international A/S. URL <http://www.emd.dk/windpro/>.
- S. Ergun. Fluid flow through packed columns. *Chemical Engineering and Process* 48, 89-94, 1952.
- E.Simioni. Analysis of a new thermal electricity storage concept. Master’s thesis, DTU Mechanical Engineering, 2016.
- K. Hall and M. Andre. New insights into rock weathering from high-frequency rock temperature data: an antarctic study of weathering by thermal stress. *Geomorphology*, 41:23–35, 2001.

- M. Hanchen, S. Bruckner, and A. Steinfeld. High-temperature thermal storage using packed bed for rocks- heat transfer analysis and experimental validation. *Applied Thermal Engineering*, 2011.
- H.Bindra, P.Bueno, and J.F.Morris. Sliding flow method for exergetically efficient packed bed thermal storage. *Applied Thermal Engineering*, 64:201–208, 2014.
- H.Stiesdal. High-temperature thermal energy storage. slides, 2016.
- K. A. R. Ismail and R. Stuginski. Analysis of possible models for fixed bed thermal storage. *Congresso brasileiro de engenharia mecânica*, 1991.
- J.D.J.Anderson. *Computational Fluid Dynamics*. McGraw-Hill, 1995.
- J.Eyer and G.Corey. Energy storage for the electricity grid: Benefits and market potential assessment guide. Technical report, Sandia National Laboratories, 2010.
- Kehlhofer. *Combined-Cycle Gas & Steam Turbine Power Plants*. PennWell Corporation, 2009.
- K. Kelley. Contributions to the data on theoretical metallurgy: XlII high-temperature heat-content, heat-capacity, and entropy data for the elements and inorganic compounds. Technical Report U.S Bur. Mines Bull. No. 584, U.S. Government Printing Office, 1960.
- D. Kunii and J. Smith. Heat transfer characteristics of porous rocks. *A.I.Ch.E Journal* 6, 71-78, 1960.
- A. Meier, C. Winkler, and D.wuillemin. Experiment for modelling high temperature rock bed storage. *Sol. Energy Mater*, 24:255–264, 1991.
- M.Morandin, S.Henchoz, and M.Mercangöz. Thermo-electrical energy storage: a new type of large scale energy storage based on thermodynamic cycles. In *World Engineers' Convention*, 2011.
- R. Panton. *Incompressible Flow*. third ed. John Wiley & Sons, Hoboken, New Jersey, 2005.
- P.Denholm, E.Ela, B.Kirby, and M.Milligan. The role of energy storage with renewable electricity generation. Technical report, National Renewable Energy Laboratory, 2010.
- P.Taylor, R.Bolton, D.Stone, X. Zhang, C.Martin, and P.Upham. Pathways for energy storage in the uk. Technical report, Centre for low carbon futures, 2012.
- Renewable Energy Policy Network for the 21st Century (REN21). Renewables 2015: global status report. Technical report, Renewable Energy Policy Network for the 21st Century (REN21), 2015.
- R.Pfeffer. Heat and mass transport in multiparticle systems. *I&EC Fundamentals* 3, 380-383, 1964.
- G. Schneider and H. Maier. Status of the development of a new high temperature thermal energy storage system (httess) for csp-power plants. *Energy Procedia*, 49:965 – 972, 2014.

- T. E. W. Schumann. Heat transfer: A liquid flowing through a porous prism. *Combustion Utilities Corporation*, 1929.
- R. Serth and T. Lestina. Process heat transfer: Principles, applications and rules of thumb. Academic press, 2014.
- Siemens AG. Press realised, 07 2016. URL <https://www.siemens.com/customer-magazine/en/home/energy/renewable-energy/shaping-the-future.html>.
- Siemens AG. Siemens presents thermal storage solution for wind energy. Press, 2016. URL [http://www.siemens.com/press/en/pressrelease/?press=/en/pressrelease/2016/windpower-renewables/pr2016090419wpen.htm&content\[\]=WP](http://www.siemens.com/press/en/pressrelease/?press=/en/pressrelease/2016/windpower-renewables/pr2016090419wpen.htm&content[]=WP).
- W. Somerton. Thermal properties and temperature-related behaviour of rock/fluid systems. *Elsevier, New York, NY*, 1992.
- H. Stiesdal. Thermal energy storage and recovery with a heat exchanger arrangement having an extended thermal interaction region, 2013a.
- H. Stiesdal. Modification of a spatial temperature profile along a heat exchanging arrangement of a thermal energy storage and recovery device, 2013b.
- H. Stiesdal. Storage and recovery of thermal energy based on counter current principle of heat transfer medium transportation, 2015a.
- H. Stiesdal. High-temperature energy storage system and operating method therefor, 2015b.
- A. L. T.L Bergman, F.P Incropera. *Fundamentals of heat and mass transfer*. John Wiley & Sons, 2011.
- T.N.Cong, W.Yang, C.Tan, Y.Li, and Y.Ding. Progress in electrical energy storage system: A critical review. *Progress in Natural Science*, 19:291–312, 2009.
- US Energy Information Administration. Annual energy outlooks 2010 with projections to 2035. Technical report, US Department of Energy, 2010.
- H. Versteeg and W. Malalasekera. *An introduction to computational fluid dynamics, the finite volume method*. Pearson, Prentice Hall, 2007.
- J. Wu, Y.Boming, and Y.Meijuan. A resistance model for flow through porous media. *Transport in Porous Media*, 71(3):331–343, 2008. ISSN 1573-1634. doi: 10.1007/s11242-007-9129-0. URL <http://dx.doi.org/10.1007/s11242-007-9129-0>.
- S. Yagi and D.Kunii. Studies on effective thermal conductivities in packed beds. *A.I.Ch.E Journal* 3, 373-381, 1957.
- Y.A.Çengel and A.J.Ghajar. *Heat and mass transfer: fundamentals & applications*. McGraw-Hill Education, 2 Penn Plaza, New York, NY 10121, 5th edition, 2015.
- Y.Zhang, K.Yang, X.Li, and J.Xu. The thermodynamic effect of thermal energy storage on compressed air energy storage system. *Renewable Energy*, 50:227–235, 2013.

G. Zanganeh, A. Pedretti, S. Zavattoni, M. Barbato, and A. Steinfield. Packed-bed thermal storage for concentrated solar power-pilot-scale demonstration and industrial scale design. *Solar Energy*, 2012.

List of Figures

1.1	Renewable energy production variation within 15 days [EMD international A/S]	3
1.2	Energy storage technologies comparison (modified) [P.Taylor et al., 2012]	6
1.3	HT-TES system presented by Siemens [Siemens AG, 2016]	10
2.1	HT-TES subsystems: charging unit, thermal storage and discharging unit	13
2.2	Charging unit configurations: A) Heat pump B) High temperature electric heater	14
2.3	Combination of a heat pump and a electric heater as charging unit	15
2.4	Discharging unit configuration	15
2.5	Thermocline profile change with increasing charging cycles [Stiesdal, 2015a]	17
2.6	Thermocline profile change with increasing charging cycles [Hanchen et al., 2011]	17
2.7	Schematic traditional packed bed thermal storage (a) and siding flow method (b,c,d). [H.Bindra et al., 2014]	19
2.8	Sectioned storage presented by Stiesdal [Stiesdal, 2015a]	20
2.9	Temperature profile along the storage [Stiesdal, 2015a]	20
2.10	HT-TES with a heat pump as charging unit and Rankine cycle as discharging unit	21
2.11	HT-TES with a high temperature electric heater as charging unit and simple Rankine as discharging unit	23
2.12	HPEH-TES with a high temperature electric heater + heat pump as charging unit	24
3.1	Graphic representation of the models boundaries(modified)[Siemens AG, 2016]	27
3.2	h-s diagram for the steam turbine	31
3.3	Diagram of the HP-TES configuration	34
3.4	Diagram of the EH-TES configuration	36
3.5	Diagram of the HPEH-TES configuration	38
3.6	Schematic representation of the charging/discharging model	39
4.1	Storage finite volume method representation	44
4.2	Storage discretization	45
4.3	Specific enthalpy of the fluid and specific internal energy of the solid as function of the temperature	47
4.4	Density of the air	48
4.5	Dynamic viscosity of the air	48
4.6	Heat capacity and thermal conductivity of the air	49
4.7	Heat capacity and thermal conductivity of the solid	50
4.8	Effective thermal conductivity coefficient and	52

4.9	Schematic representation of the TES model	57
4.10	Inputs and outputs of the simulation tool	58
4.11	TES model validation	59
4.12	Comparison of the temperature profiles with different number of grid points . .	61
4.13	Normalised average RMS deviation	61
5.1	Pressure drop over time evaluated with [Ergun, 1952] and [Wu et al., 2008] . .	67
5.2	Pressure drop as function of the particle size	68
5.3	Pressure drop as function of the TES radius and the void fraction	69
5.4	Pressure drop as function of the TES radius with $\varepsilon = 0.342$	69
5.5	COP and COP_{dh} as function of the maximum temperature of the heat pump .	71
5.6	COP and Efficiencies simple case vs Temperature max heat pump	72
5.7	COP and Efficiencies with district heating vs Temperature max heat pump . .	72
5.8	Heating surface of the heat pump hot heat exchanger vs Temperature max within the Heat pump	73
5.9	Rankine efficiency vs Temperature max rankine cycle	74
5.10	HRSG heating surface vs Temperature max Rankine cycle	74
5.11	Effects on isentropic efficiency of the variation of the steam quality	75
6.1	Temperature profile of the fluid phase over time for the charging process	78
6.2	Temperature profile of the solid and fluid phases over the length	79
6.3	Temperature and energy over time for the charging process	80
6.4	Charging efficiency and loss fraction for the charging process	81
6.5	Pressure drop and accumulated fan energy consumption for the charging process	82
6.6	Sequential temperature profiles of the charging process	82
6.7	Temperature profile at the end of the 76 hours simulation	83
6.8	Temperature outlet of the fluid over time	83
6.9	Temperature profile of the fluid phase over time for the discharging process . .	84
6.10	Temperature profile of the solid and fluid phases over the length	85
6.11	Temperature and energy over time for the discharging process	86
6.12	Charging efficiency and loss fraction for the discharging process	87
6.13	Pressure drop and fans energy consumption for the discharging process	87
6.14	Sequential temperature profiles of the discharging process	88
6.15	Temperature profile at the end of the 24 hours simulation	89
6.16	Temperature outlet of the fluid over time	89
6.17	Charging temperature profile at the end of the charging for 10 cycles with 12 hours charging/discharging cycles	90
6.18	Temperature outlet after each charging and discharging process for 10 cycles . .	90
6.19	Temperature profiles of the TES segments during charging	92
6.20	Energy stored in the TES segments during charging	93
6.21	Pressure drop and energy consumed by the fans in the segmented TES	93
A.1	Balanced HPEH-TES configuration diagram	107

A.2 Quick-charge HPEH-TES configuration diagram	109
---	-----

List of Tables

1.1 HT-TES compared with known storage technologies [H.Stiesdal, 2016]	11
2.1 HT-TES configurations comparison	25
3.1 Input parameters of the system model HP-TES	28
3.2 Input parameters of the system model EH-TES	35
3.3 Input parameters of the system model HP-TES	37
4.1 Numeric assumptions [Zanganeh et al., 2012]	55
4.2 Validation parameters comparison	59
4.3 Dimensions and operating parameters of the TES system [Zanganeh et al., 2012],[Agalit et al., 2015]	60
5.1 Operating parameters of the different configurations	70
6.1 TES simulation parameters	77
6.2 Comparison of the charging conditions for the three different configurations . .	78
6.3 Comparison of the discharging conditions for the three different configurations .	84
6.4 Comparison of the main parameters of the segmented TES	91
6.5 Main results for HP-TES simulation	95
6.6 Main results for EH-TES simulation	96
6.7 Main results for HPEH-TES (option 1) simulation	96
6.8 Main results for HPEH-TES (option 2) simulation	97
6.9 Main results for HPEH-TES (option 3) simulation	97
6.10 Summary of the main parameters of the different configurations	98
7.1 Qualitative comparison among the 5 TES configurations	100